IEA INTERNATIONAL ENERGY AGENCY

Review on Infrared and Electroluminescence Imaging for PV Field Applications

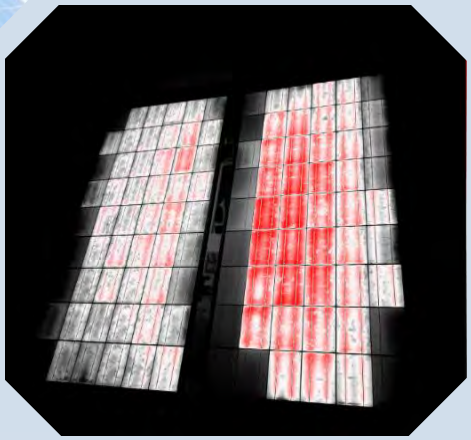

PVPS

PHOTOVOLTAIC POWER SYSTEMS PROGRAMME

Report IEA-PVPS T13-10:2018

Cover Photos:

Left: Outdoor infrared inspection using a drone for IR failure detection of PV power plants. Photo curtesy of TÜV Rheinland Energy, 2017.

Right: Night-time electroluminescence image using a consumer digital single-lens reflex camera of PID affected PV modules, in a black-white-red colour scheme. Photo curtesy of B. Kubicek, AIT, 2017.

INTERNATIONAL ENERGY AGENCY
PHOTOVOLTAIC POWER SYSTEMS PROGRAMME

Review on Infrared and Electroluminescence Imaging for PV Field Applications

IEA PVPS Task 13, Subtask 3.3
Report IEA-PVPS T13-10:2018
March 2018

ISBN 978-3-906042-53-4

Primary authors:

Ulrike Jahn, Magnus Herz
TÜV Rheinland, Cologne, Germany

Marc Köntges,
Institute for Solar Energy Research Hamelin, Emmerthal (ISFH), Germany

David Parlevliet
Murdoch University, Perth, Australia

Marco Paggi
IMT School for Advanced Studies Lucca, Italy

Ioannis Tsanakas
Interuniversity Microelectronics Centre (IMEC), Leuven, Belgium

Joshua S. Stein
SANDIA National Laboratory (SNL), Albuquerque, NM., USA

Karl A. Berger,
Austrian Institute of Technology GmbH, Center for Energy (AIT), Austria

Samuli Ranta
Turku University of Applied Sciences, Finland

Roger H. French
Case Western Reserve University, Cleveland, Ohio, USA

Mauricio Richter
3E, Belgium

Tadanori Tanahashi
National Institute of Advanced Industrial Science and Technology (AIST), Japan

Contributing authors:

Erin Ndrio, Gerhard Mathiak
TÜV Rheinland, Cologne, Germany

Bernhard Weinreich
HaWe Engineering GmbH, Germany

David Hottenrott
Fraunhofer ISE, Germany

Justin S. Fada
Case Western Reserve University, Cleveland, Ohio, USA

Bernhard Kubicek
Austrian Institute of Technology GmbH, Center for Energy (AIT), Austria

Claudia Buerhop-Lutz
ZAE Bayern, Erlangen, Germany

Vasco Medici
SUPSI ISAAC, Canobbio, Switzerland

This report is supported by

Austrian government, by means of the Austrian Federal Ministry for Transport, Innovation and Technology (bmvit), represented by the Austrian Research Promotion Agency (FFG), under contract No. 853028

European Research Council under the European Union's Seventh Framework Programme (FP/2007-2013) to the ERC Starting Grant "Multi-field and multi-scale Computational Approach to Design and Durability of PhotoVoltaic Modules" - CA2PVM (Grant Agreement n. 306622)

German Federal Ministry for Economic Affairs and Energy (BMWi)
under contract no. FKZ 0325786 A_B_C

Swiss Federal Office of Energy (SFOE)

U.S. Department of Energy (DoE)

Table of Contents

Foreword

The International Energy Agency (IEA), founded in November 1974, is an autonomous body within the framework of the Organization for Economic Co-operation and Development (OECD) which carries out a comprehensive programme of energy co-operation among its member countries. The European Union also participates in the work of the IEA. Collaboration in research, development and demonstration of new technologies has been an important part of the Agency's Programme.

The IEA Photovoltaic Power Systems Programme (PVPS) is one of the collaborative R&D Agreements established within the IEA. Since 1993, the PVPS participants have been conducting a variety of joint projects in the application of photovoltaic conversion of solar energy into electricity.

The mission of the IEA PVPS Technology Collaboration Programme is: To enhance the international collaborative efforts which facilitate the role of photovoltaic solar energy as a cornerstone in the transition to sustainable energy systems. The underlying assumption is that the market for PV systems is rapidly expanding to significant penetrations in grid-connected markets in an increasing number of countries, connected to both the distribution network and the central transmission network.

This strong market expansion requires the availability of and access to reliable information on the performance and sustainability of PV systems, technical and design guidelines, planning methods, financing, etc., to be shared with the various actors. In particular, the high penetration of PV into main grids requires the development of new grid and PV inverter management strategies, greater focus on solar forecasting and storage, as well as investigations of the economic and technological impact on the whole energy system. New PV business models need to be developed, as the decentralised character of photovoltaics shifts the responsibility for energy generation more into the hands of private owners, municipalities, cities and regions.

IEA PVPS Task 13 engages in focusing the international collaboration in improving the reliability of photovoltaic systems and subsystems by collecting, analyzing and disseminating information on their technical performance and failures, providing a basis for their technical assessment, and developing practical recommendations for improving their electrical and economic output.

The current members of the IEA PVPS Task 13 include:

Australia, Austria, Belgium, Canada, China, Denmark, Finland, France, Germany, Israel, Italy, Japan, Malaysia, Netherlands, Norway, SolarPower Europe, Spain, Sweden, Switzerland, Thailand and the United States of America.

This report focusses on test requirements, recording procedures, analysis methods and guidelines of infrared (IR) and electroluminescence (EL) imaging for PV field applications. This document shall help to identify, record and assess the most common failures of PV modules and components in the field.

The editors of the document are Ulrike Jahn and Magnus Herz, TÜV Rheinland, Germany (DEU).

The report expresses, as nearly as possible, the international consensus of opinion of the Task 13 experts on the subject dealt with. Further information on the activities and results of the Task can be found at: http://www.iea-pvps.org.

Acknowledgements

This paper received valuable contributions from several IEA-PVPS Task 13 members and other international experts, all of whom are listed as primary and contributing authors. In addition, we thank the following individuals for their careful reviews and suggestions:

- David Parlevliet — Murdoch University, Perth, Australia
- Karl. A. Berger — Austrian Institute of Technology GmbH, Center for Energy, Austria
- Samuli Ranta — Turku University of Applied Sciences, Finland
- Marco Paggi — IMT School for Advanced Studies Lucca, Italy
- Werner Knaupp — PV-plan, Stuttgart, Germany
- Bengt Jäckel — UL International Germany GmbH, Neu-Isenburg, Germany

Furthermore, we like to thank Ms. Barbara Schiffer and Ms. Cathy Zhou, TÜV Rheinland, for their efficient coordination and editing work to prepare this report.

List of Abbreviations

BOS	Balance of system
CCD	Charge coupled devices
CdTe	Cadmium telluride
CIGS	Copper indium gallium selenide
CMOS	Complementary metal oxide semiconductor
DSLR (camera)	Digital single-lens reflex (camera)
EL	Electroluminescence
FEM	Finite element analysis
FOV	Field of view
IFOV	Instantaneous field of view
InGaAs	Indium gallium arsenide
IRT	Infrared thermography
IS	International standards
MFOV	Measurement field of view
MILC (camera)	Mirrorless interchangeable lens (camera)
MPP	Maximum power point
MPPT	Maximum power point tracking
NETD	Noise equivalent temperature difference
PID	Potential induced degradation
PID-s	Potential induced degradation by shunts
PVP	Photovoltaic plant
ROI	Regions of interest
TS	Technical specifications
UASs	Unmanned aerial systems
UAV	Unmanned aerial vehicle

Executive Summary

In this report, we present the current practices for infrared (IR) and electroluminescence (EL) imaging of PV modules and systems, looking at environmental and device requirements on one hand, and on the interpretation of sample patterns with abnormalities on the other hand. The goal is to provide recommendations and guidelines for using IR and EL imaging techniques to identify and assess specific failure modes of PV modules and systems in field applications.

Currently, two Technical Specifications for IR Imaging are developed within the IEC Technical Committee TC 82. They describe a test procedure, and are not intended to have pass/fail criteria for the PV modules being investigated. While IEC/TS 60904-12 (draft) describes general methods of thermographic imaging for laboratory or production line purposes, focusing on the infrared imaging techniques of the PV module itself, IEC/TS 62446-3 describes investigations of PV modules and the entire plant in operation under natural sunlight. This document gives guidance for preventive maintenance and fault diagnostics of PV plants by means of infrared imaging techniques while the plant is operating under natural sunlight. The subjects of the investigation include PV modules, as part of the array, as well as balance of system (BOS) components such as cables, fuses, switches and inverters.

There are two different types of infrared or thermographic cameras, having cooled or uncooled detectors. The sensors of cooled thermographic cameras are made from narrow band gap semiconductors and while having very high sensitivity, are not commonly used in PV applications due to the cost and complexity of the associated cooling system. More commonly used thermographic cameras are those based on uncooled sensors that can work at ambient temperatures. These styles of sensors can be produced from a range of materials, however a common architecture is the micro-bolometer. This style of uncooled sensor is an appropriate thermographic camera type for PV applications due to its simplicity and affordability.

There is a broad variety of infrared cameras with a range of specifications on the market. The most suitable type of camera will depend on the application at hand. For example, handheld cameras are suitable for field inspection of PV modules. However, the same range of specifications may not be available for other applications such as airborne (UAV) surveys of PV plants due to the different lenses and distances in use. An appropriate selection of an adequate class of IR camera for use or purchase depends on the various possible use cases and detailed inspection tasks for that camera. It is impossible to give a straightforward decision matrix. While high end IR cameras will allow more possibilities for the analysis of detected thermal abnormalities, we acknowledge that for a number of IR inspection cases, medium class cameras are fully sufficient. In this report, Section 2.1.2 describes the types of cameras used for IR imaging.

Stable environmental conditions are a pre-requisite for high quality outdoor IR imaging of PV modules and arrays. Weather fluctuations must be much slower than the thermal time constant of the PV module. A typical PV module takes 5 to 15 minutes to thermally stabilize for new environmental conditions such as change of global irradiation intensity, temperature, or wind speed. Furthermore, thermal reflections of clouds, buildings, trees, or other objects on the PV modules must be avoided or minimized as they may distort the

evaluation of the IR image. This is usually done by either waiting for more stable conditions or moving the position of the IR camera to avoid specific reflections.

One important parameter derived from IR images is the temperature difference between different parts of the module or between modules and/or strings of modules. Inactive areas of a module or string usually appear hotter than surrounding active areas. When a PV module or string is not functioning, this energy is not converted to DC power and therefore remains as excess heat, which raises the temperature of the module or string. Inactive modules often suffer from one of the following defect types: disconnected PV modules or strings, PID effects or shunted cells, and short-circuited bypass diodes. These types of failures cause only a slight temperature increase between active and inactive parts, and this difference is often proportional to the irradiance. Thus it is more difficult or even impossible to detect these types of failures under low irradiance conditions. Hot spots that arise from poor electrical connections or severe mismatch within a module are another important type of failure that is usually easily detectable using IR.

The aim of thermographic inspections is to detect failures before yield reduction or serious material damage will occur. Because outlined damages often have not developed yet, the objective interpretation of thermographic scans is not trivial. However, these defects have the potential to cause power degradation in subsequent years. Hot spots with strong local heat gradients can affect the performance of the PV modules significantly and even, in extreme cases, lead to smouldering fires. IR imaging is a valuable tool to detect power relevant, malfunctioning PV modules, module strings, and certain devices in a PV array if the presence of artefacts, like partial shading, dirt, can be excluded. For high quality images it is recommended to take the IR images at high solar irradiance (> 600 W/m²) and constant ambient conditions (no clouds, low wind speed, stable ambient temperature).

The International Technical Specification IEC/TS 60904-13 (draft) specifies methods to capture electroluminescence images of photovoltaic modules, process images to obtain quantitative descriptors, and provide guidance to qualitatively interpret the EL images. EL images are obtained with camera detectors that are typically charge coupled devices (CCD) or complementary metal oxide semiconductor (CMOS). They may be cooled, usually with thermoelectric cooling, to achieve better signal to noise ratio by means of reducing device dark current originating from thermally generated charges. Relevant parameters in choosing detectors include number of pixels, noise, quantum efficiency at the wavelength of interest, and dynamic range. Silicon detectors are very often used and, for special applications, InGaAs detectors are employed.

High quality images are best taken in darkened environment for a better signal to noise ratio. Precautions should be taken to eliminate stray light entering the imaging studio, such as with use of hard walls, curtains, baffles, and sealing of any gaps with material that are of light absorbing nature (black). Fixed mounting of the camera and a mounting rack for PV module(s) to be imaged are used so that the camera and the module positions are stable. In the field, an option is to use curtains supported by a frame to cover the camera and the photovoltaic module. Alternatively, images have to be taken at sunset or during night.

There are a range of manufacturers in the market that produce cameras suitable for EL applications. The key specification for EL camera systems is derived from the need for the camera to be sensitive to the emission spectra of the material being tested. For a crystalline silicon solar module the emission spectra has a peak at 1150 nm, while for other

technologies such as organic PV the emission peak resides at a longer wavelength (1200 nm – 1400 nm) as described by T. Fuyuki et. al. in *Appl. Phys. Letters* in 2005.

While task specific EL camera can be prohibitively expensive for many users, it has been shown by K. Mertens that a relative simple modification enables consumer DSLRs to perform EL imaging. More recently non-reflex, mirrorless interchangeable lens cameras with large sensors can also be modified for EL application as demonstrated by J.S. Fada. The choice of the type of EL camera that is used when imaging PV modules is dependent on a range of factors. As with many types of camera equipment there is trade-off between cost, resolution and sensitivity. For example, silicon CCD cameras tend to have a higher resolution and lower cost than InGaAs CMOS sensors. While their high resolution makes silicon CCD sensors a popular choice, the InGaAs sensor would have a significantly greater sensitivity to crystalline silicon and some thin-film technologies. Despite the differing levels of sensitivity, with appropriate data collection intervals and methodologies, such as longer exposure times, filters and active cooling of the sensor, either camera type can be used for EL imaging of PV modules. This allows a great deal of flexibility in terms of the equipment used, but does make standardization of test images and measurements a challenge.

The EL technique can be profitably applied to detect and distinguish between different failures modes. This type of non-destructive inspection includes the possibility to observe defects and attribute them to the different stages of the PV module lifetime. For instance, defects can be caused by production problems not noticed after quality control, wrong handling of the PV module without enough care during transport or installation, or can be induced by environmental loading and degradation in the field after installation. Clearly, all of these causes might have different implications in terms of warranty claims and operation and maintenance actions. EL images taken on a set of PV modules before their installation can be very useful in case of legal actions against producers, since production defects can be clearly distinguished at that time. However, in many cases EL imaging is requested by customers at a much later stage, after detecting an unexpected low power output of their PV parks. However, the amount of time required to take a good quality EL image of a PV module, adjusting the focus and finding the right time of exposure depending on the module type, is often still a limiting factor for large-scale applications of EL imaging in the field.

In this report, Section 3.1.2 describes the types of cameras used for EL imaging and provides a discussion of sensors. Sensors with larger numbers of pixels per unit area typically yield better results for resolving image features, however, depending on the material, noise and quantum efficiency limitations can increase with higher resolution. Though with modern signal processing algorithms and image analysis software it is possible to mitigate a portion of the effects of noise on the resultant images.

This report provides a comparison of the relative merits of EL and IR imaging techniques in Chapter 4. These types of optical measurement provide fast, real-time and high resolution images with a two-dimensional distribution of the characteristic features of PV modules. IR imaging measurements of the thermal behaviour of cells in a module allows a number of defects to be easily and quickly identified. These include short circuits in solar cells, shunts, inactive cell parts and PID. However, not all the failures of PV modules lead to an increase in temperature. Taking this into consideration the IR measurements alone cannot identify all the types of failures. On the other hand, PV modules with clear EL-images sometimes provide IR-images with hot areas. A combination of both techniques quickly detects the

most common defects in a PV module with high accuracy and provides a good indication of the health and reliability of the PV modules with a plant.

1 Introduction

The quality assurance measures for PV modules are of fundamental importance for any PV power plant asset. The failure-free operation of the PV modules is a prerequisite for efficient energy production, long life, and a high return on the investment. During operation PV modules may develop defects which can be repaired if they are detected in time, but they can cause a severe drop in energy production and sometimes safety issues. To ensure the operation of the PV modules without significant losses, fast and reliable methods to evaluate the performance of the photovoltaic modules are required, both during the production process and after the installation of the PV modules. For that reason more and more EPC and O&M companies offer regular IR and EL imaging inspections of PV plants to ensure the safety and high performance of the PV array in addition to IV curve measurements and monitoring. IR and EL are two imaging techniques, which identify faults and problems developing with PV modules.

The use of infrared (IR) imaging for the evaluation of PV modules has many advantages. First of all, a great number of failures developed on PV modules can be detected using IR imaging, from hot-spots to mismatch losses or installation failures. Furthermore, IR imaging technique can be applied for non-destructive testing and used to scan installed PV modules during normal operation. Finally, thermal cameras also allow scanning large areas within a short time frame. In Figure 1-1 (bottom) the required time for the inspection of a PV plant is shown, according to its nominal power, using a hand-held IR camera. For instance, a PV plant of 4 MWp nominal power will require approximately 15 to 20 hours of IR inspection taking into consideration that all the other factors that might affect the inspection are ideal.

In Figure 1-1 (top) the required time for IR inspection using an IR camera attached to a drone, with respect to its nominal power, is shown. Due to the high resolution of IR cameras existing in the market today, such an inspection approach using drones, is possible. Using drones, for instance, a PV plant of 4 MWp nominal power will require approximately 5 to 10 hours of IR inspection taking into consideration that all the other factors that might influence the inspection are ideal.

The optimized operation of the PV cell is to absorb the light and convert it into electricity. However, due to reciprocity principle the opposite is also possible and offers the opportunity of Electroluminescence (EL) imaging. Electroluminescence is a phenomenon that has been used for a long time for other applications such as lightening, but recently has been introduced as an investigation procedure for PV modules and strings. It consists of applying a direct current to the PV module and measuring the photoemission by means of an infrared-sensitive camera. EL imaging provides insight into micro cracks and other defects within the cell material. This in turn helps identify faults and problems present or developing within the PV module.

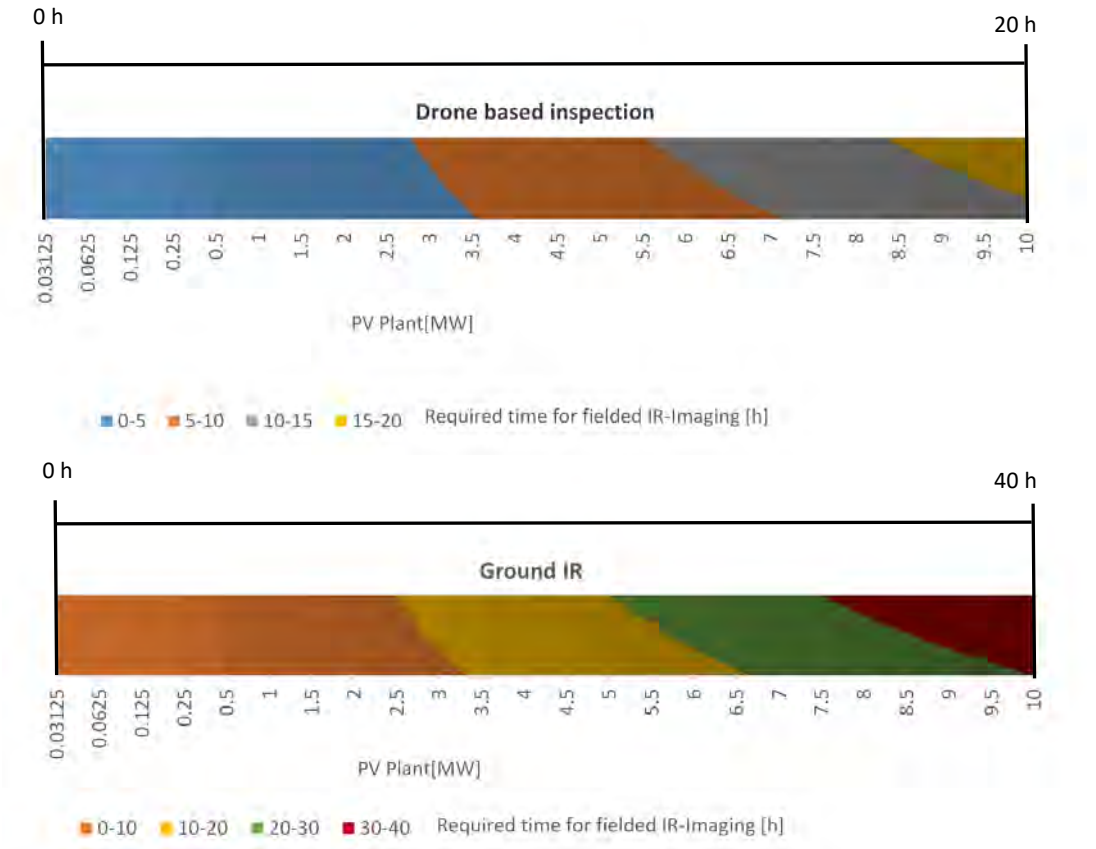

Figure 1-1 The required time for the inspection of PV modules using IR cameras, attached to a drone (top), and hand-held camera at the ground (bottom) with respect to the nominal power of the PV plant. The colours are used to identify the different time ranges for IR inspections.

In Figure 1-2 the required time for the inspection of a PV plant, with an EL camera attached to a drone, according to its nominal power is shown. In this case a PV plant of 4 MWp nominal power needs approximately 20 to 40 hours of EL inspection taking into consideration that all the other factors that might influence the inspection are ideal.

In Figure 1-2 (bottom) the required time for the inspection of a PV plant, with one EL camera, according to its nominal power is shown. For instance, a PV plant of 4 MWp nominal power requires approximately 100 - 150 hours inspection taking into consideration that all the other factors that might influence the inspection are ideal.

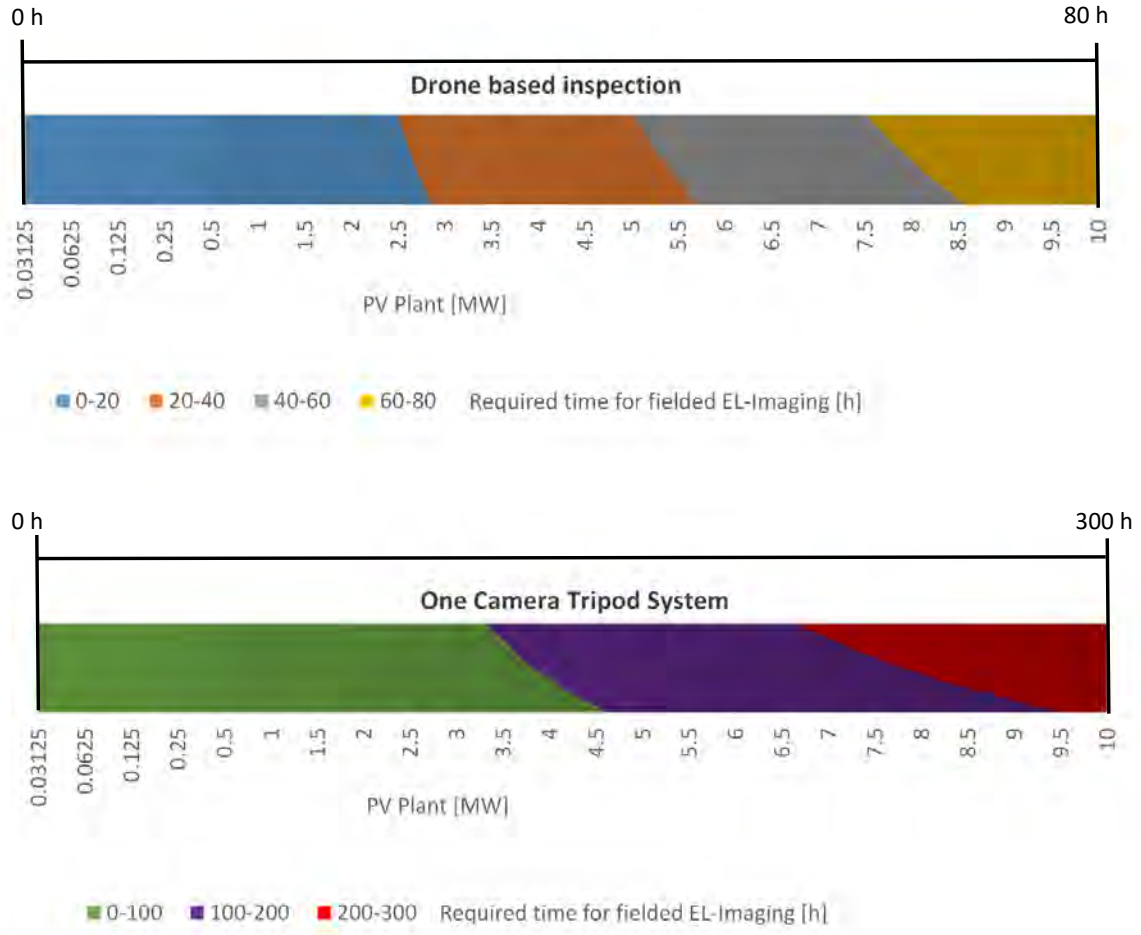

Figure 1-2 The required time for the inspection of PV modules with EL Imaging, attached to a drone (top), and hand-held camera at the ground (bottom) with respect to the nominal power of the PV plant. The colours are used to identify the different time ranges for EL inspections.

This report presents a review of current practices used in regarding IR and EL Imaging. In Chapter 2 an introduction in the IR Imaging is given as well as test requirements and examples. The-state-of-art technology and techniques are given. Chapter 3 deals with the EL Imaging and has the same structure as Chapter 2. For both inspection methods an overview is given to include information about the current market. In Chapter 4, the advantages and disadvantages of both methods are compared and discussed.

2 Infrared Imaging

2.1 State of the art of IR Imaging

2.1.1 Review of existing standards/guidelines

Within the IEC Technical Committee TC 82 (Photovoltaic), currently two Technical Specifications are developed: Technical Specifications (TS) approach International Standards (IS) in terms of detail and completeness, however, they usually describe a (test) procedure and do NOT include pass/fail criteria associated with the test results.

The TC 82 system working group (WG3) was working on a new TS embedded in the IEC 62446 series, dealing with system testing, documentation and maintenance of PV plants, IEC/TS 62446-3 “Photovoltaic modules and plants – Outdoor infrared thermography“ [1]. In this document guidance for preventive maintenance and fault diagnostics of PV plants by means of infrared imaging techniques is given, while the plant is operating under natural sunlight. The subjects of the investigation include the PV modules, as part of the array, and the Balance of System (BOS) components such as cables, fuses, switches, inverters. While IEC/TS 62446-3 describes investigations of PV modules under natural sunlight in operation, procedures that use external current sources - e.g. for indoor inspections in the dark - are also described. As mentioned above, it is a Technical Specification too, having an instructional purpose, and is not intended to have pass/fail criteria for the PV modules being investigated.

A chapter in IEC/TS 62446-3 deals with the principles of heated and cooled regions in PV modules operated with and without irradiation applied, and how quantitative metrics of the severity of module failures/damages can be achieved. The TS closes with reporting requirements, and with a Table for qualitative interpretation of IR images and failure modes (from [3], with some modifications). In an Appendix additional information about optics and optical calculations are summarized.

The TC 82 photovoltaic module working group (WG2) is - within the IEC 60904 “Photovoltaic Devices” series of standards, dealing with measurement procedures - also working on the proposed Part 12, IEC/TS 60904-12 “Infrared thermography of photovoltaic modules” [2]. It describes general methods of thermographic imaging for laboratory or production line purposes, focusing on the infrared imaging techniques of the photovoltaic module itself. Guidance will be given on how to capture thermal images of photovoltaic modules with sufficient quality, how these data can be processed to obtain quantitative metrics to gain further insight, and to provide guidance on how such images can be interpreted qualitatively.

In introducing the chapters terms, definitions and acronyms are assembled that have to do with the (electrical) operation of a photovoltaic module, as well as basics about thermal imaging cameras, its lenses, resolution and aberrations. Common helpful post processing features are also briefly summarized and hints for the useful range of the angle of view and precautions to minimize reflections are given.

For (indoor) dark thermography using external power supply under forward bias conditions, it is recommended not to take only a single image for (almost) equilibrium conditions, but to take images in (predefined) time intervals. Typical values for the time span from applying the forward bias are given in brackets for a standard module that is viewed from the back sheet side, to:

- have an initial thermal image including artefacts and reflections, useful for calculating differential images (0 s),
- see where possible extreme heating points occur during heating process, (20 s),
- image an equilibrium temperature distribution pattern, for e.g. the maximum power point current (2 min),
- better image the less severe heating effects (4 min), for two times the maximum power point current - if that can be safely applied, and
- list these points of time and the image numbers together with the current and voltage measurements in a tabulated form.

If a PV module is operated in steady state under illumination within a string, the operating point is normally set by the inverter close to the maximum power point of the string, depending on the actual irradiation and temperature. If the I-V curve of a (faulty) module investigated differs from the I-V curve of the other modules in a string, the resulting operating point will differ from the operating point of a single module if a resistive load is applied. The string behaviour can be reproduced by a controlled power source applied on a single module with the maximum power point current set point calculated from the data sheet values considering the measured in plane irradiation and module temperature. As described above for dark conditions, an analogue procedure is described for irradiated outdoor conditions or in steady state solar simulators.

2.1.2 Overview of camera types

Infrared thermography (IRT) has been used for detecting shunts in solar cells under reverse bias in the dark since 1990 [4]. However, lately uncooled infrared detectors have gained wide attention for infrared imaging applications, due to their advantages such as low cost, low weight, low power and large spectral response compared to those of photon detectors [5].

According to the black body radiation law any object above absolute zero will emit infrared radiation and its characteristics can be used to measure the temperature. Therefore, infrared measuring devices acquire infrared radiation emitted by an object and transform it into an electronic signal [6]. The detected radiation from the objects can be imaged from the IR camera and abnormalities in the temperature of the objects can be observed.

However, the IR camera does not receive only the radiation from the object but the reflection of surroundings as well. Emissivity, reflection radiation and absorption of the atmosphere are some parameters that influence the measurement of the temperature of the inspected object. Therefore, the following parameters have to be measured or/and entered into the camera software:

1. Emissivity, which qualifies how much radiation is emitted compared to a blackbody. Typical emissivity values are 0.85 for the glass and 0.95 for the polymer

back sheet, respectively, if the angle of view is within 90°- 60° (glass) and 90°- 45° (polymer)
2. Reflected temperature in order to compensate for the radiation reflected in the object
3. Atmospheric temperature and humidity.

There are infrared or thermographic cameras with cooled and uncooled detectors. The sensors of cooled thermographic cameras are made from narrow band gap semiconductors and while having very high sensitivity, are not commonly used in PV applications due to the cost and complexity of the associated cooling system.

Commonly used thermographic cameras are based on uncooled sensors that can work at ambient temperatures. The most common sensor architecture is the micro-bolometer. These styles of sensors can be produced from a range of materials, however a common architecture is the micro-bolometer. This is seen in a range of consumer handheld thermographic cameras. This style of uncooled sensor is an appropriate thermographic camera type for PV applications due to its simplicity and affordability. There are a broad range of these styles of cameras available on the market.

Some important characteristics for an IR camera system for PV applications are:

1. Detector resolution, the higher the resolution, the higher the cost of the camera. Pixels are the data acquisition points for thermal measurements, and the data are used to create a visual image from the thermal profile. The more pixels and data points per investigated area, the more accurate the thermal interpretation and the higher the resolution of the thermal image. High resolution is particularly important because it allows identification of smaller image details and therefore more accurate temperature measurements, for the same field of view [7].
2. Noise equivalent temperature difference (NETD) or thermal sensitivity is considered to be of great importance for the process of evaluating and comparing performances of thermal imagers which are essentially non-contact temperature measurement devices [8].
3. Accuracy, including tools for entering emissivity and reflected temperature values. Those parameters, when have been correctly inserted, can produce accurate temperature measurements.
4. Intercompatibility of the generated photos
5. Screen resolution
6. Ergonomic features:
    a. Weight
    b. Battery
    c. Interactive controls
7. User Interface:
    a. Report generation
    b. Connectivity
8. Warranty

Table 2.1.1: Overview of camera characteristics.

Manufacturer	Model	Detector Resolution (pixel)	Image Display (pixels)	Spectral range (μm)	Thermal Sensitivity (mK)	Accuracy % of reading	Battery	Weight	Focus Mode	Warranty (years)
Testo	875i-2DLX	160x120	320x240	8 to 14	50	2%	4 hours +	0.9kg	Manual	2
Flir	E6	160x120	320x240	NA	60	2%	4 hours	0.575kg	Auto	10
Satir	GN	160x120	640x480	8 to 14	80	2%	NA	0.5kg	Manual	NA
Fluke	TiS45	160x120	320x240	7.5 to 14	90	2%	4 hours +	0.72kg	Manual	2
Trotec	V Series	160x120	640x480	8 to 14	80	2%	2-3 hours	0.5kg	Manual	NA
Testo	882	320x240	320x240	8 to 14	50	2%	4 hours +	0.9kg	Manual & Motor	2
Flir	E8	320x240	320x240	NA	60	2%	4 hours	0.575kg	Auto	10
Fluke	Ti450	320x240	640x480	7.5 to 14	50	2%	3-4 hours	1.04kg	Manual & Auto	2
Satir	Hotfind	384x288	640x480	8 to 14	50	2%	NA	0.6kg	Manual & Motor	NA
Trotec	LV Series	384x288	640x480	7.5 to 14	50	2%	2-3 hours	0.65kg	Manual	NA
Infratec	Variocam HD 900	1024x768 @30Hz	1280x800	7.5 to 14	20	1%	2-3 hours	1.6kg	Manual & Auto	2

An overview of the range of characteristics and specifications for IR cameras used in PV applications is shown in

Table 2.1.1. As can be seen, there is a broad variety of infrared cameras with a range of specifications on the market. The most suitable type of camera will depend on the application at hand. For example, handheld cameras are suitable for field inspection of PV modules, however, there are recommendations on the minimum resolution required as described in section 2.2. However, the same range of specifications may not be available for other applications such as airborne (UAV) surveys of PV plants due to the different lenses and distances in use.

2.1.3 Evaluation of existing practice

A significant amount of published research studies have been reported in the literature through the last decade, reflecting the increasing interest in the application of infrared thermography (IRT) measurements and their potential for fault diagnosis of PV installations in the field [9].

In the early steps of such studies, [10] first investigated the applicability and practicality of IRT imaging of PV modules under outdoor conditions. For PV array-scale applications, [11] used IRT to assess the condition of a building integrated, grid-connected PV array. The investigated PV system presented abnormally low performance, which finally exhibited abnormal temperature profiles through the acquired thermal images. These abnormalities were due to either the panel material itself or the overall function. In terms of accuracy and practicality of IRT measurements of PV modules' materials, three different early studies [12], [13], [14] discussed the infrared reflection errors related to the glass covers as well as variations between the cell temperature and the measured modules' temperature for different back sheet materials. In addition, [15] presented a procedure for accurate measurement of IR emissivity of the glass surface, in the spectral range of the thermal cameras that were used, proposing a necessary correction (offset) of the temperatures measured by such bolometer detectors.

The importance of further interpretation of the thermal images and the correlation between performance degradation, fault types and thermal signatures of PV modules was introduced in [16], [17]. In particular, [16] showed that by the combination of several IRT

measurement methods typical defects in crystalline silicon (c-Si) PV modules and their influence on the I-V curve (e.g. the series resistance or the short- circuit current) can be explained. In particular, it was found that in the case of sun illuminated thermography several defects can be distinguished by varying the electrical load on the PV module. In another experimental study [17], daily profiles with one minute I-V field measurements were acquired from a range of defective PV modules. These were collected together with additional continuous IR imaging and meteorological data sampling. A direct relation between the power output (thus, energy yield) losses and the thermal differences was observed; however, in order to quantify the effective loss in kWh/kWp per year further evaluation is needed and is not published yet.

Focusing on more particular mechanisms of abnormal heat development in PV modules, in [18], [19], [20], the formation of hot spots and the early challenges upon their quantification and detection by means of IRT were addressed. Being focused on indoor IRT applications, the approach proposed by [18] shows that, through short-time illumination of c-Si PV modules at high irradiance (1000 W/m²), the location, the geometry and the area size of hot spots can be evaluated from raw IRT data. It was particularly concluded that hot spots with smaller area or higher leakage current densities, are more critical for a hot spot formation in a partially shaded PV module and present higher temperatures. On the other hand, in [19], [20] field IRT measurements and basic thermal image analyses were implemented toward the successful detection of hot spots corresponding to individual defective cells or group of cells. For such so-called regions of interest (ROIs) assigned to hot spot areas, the resultant increase of the operating temperatures was quantified in a fast and fairly accurate way.

As more and more PV plants are installed and the existing PV modules age further (and, thus, more faults evolve) there has been increased scientific interest in this research field through the last ten years. This is added by the fact that IRT measurement equipment is more readily available for PV inspection applications, in terms of cost and usability.

Recent studies focused not only on improving the already developed concepts, but also on:

- Better understanding of the degradation/ageing mechanisms and their impact on the thermal behaviour of PV modules.
- Classification of different fault types by correlating their thermal signature with the I-V characteristics.
- Implementation of wide-areas measurement applications of IRT for large-scale PV plants.
- Eliminating sources of measurement errors or uncertainties; understanding all characteristics of IRT measurements and developing standards and technical specifications).

Further experimental data and preliminary analysis techniques were added during recent studies [21], [22], [23], validating and/or improving already suggested concepts. In [21] IRT was proved to be a fitting way for fast detection of invisible defects that were experimentally investigated in their first stages of development. Such an early detection of occurring faults allows the time needed for assessing the risk of potential domino effects from the evolving defects to adjacent parts of the installations and, thus, for adopting preventive maintenance actions and planning for the whole PV installation. On the other hand, in [22], [23], the use of basic thermal image analysis tools, such as temperature line

profile and histogram-based statistical analysis of ROI, applied to both outdoor and indoor IRT measurements, were proved easily-implementable and efficient tools for qualitative analysis of hot spots under short-circuit conditions.

In particular, the thermal signatures of potential faults, such as hot spots, can be observed as bi- or multi-modal formed histograms, thus characterized by higher variance, standard deviation and skew values. Besides, line profiles have been proved useful to yield the temperature fluctuation across the abnormal thermal signatures of planar defects in PV module (Figure 2-1). Such simple techniques provide complementary qualitative information about the thermal signature of occurring faults in PV modules, which can be valuable for thermal modelling and classification of different failure modes in PV modules.

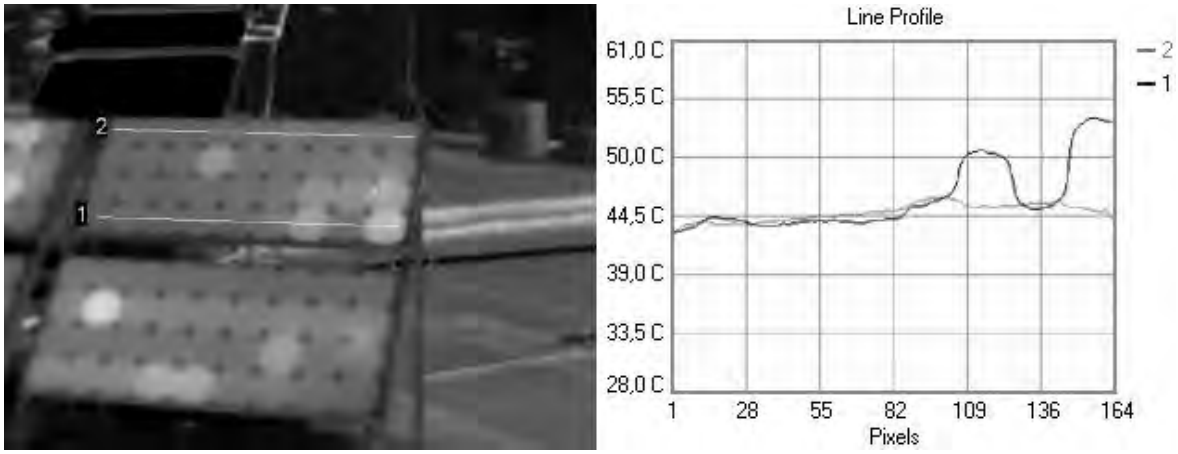

Figure 2-1: Example of a simple analysis based on temperature line profiles of ROIs corresponding to hot spots in a PV module under short circuit conditions.

Experimental results and observations presented in several recent studies focused on the need for better understanding of the degradation/ageing mechanisms and their interrelation with the resultant thermal signatures of PV modules, obtained by field IRT measurements. The degradation/ageing impact on the thermal signature can be investigated following either real-time exposure to field conditions [24], [25], [26] or accelerated-time ageing in an environmental chamber (e.g. thermal cycling) [26], [27]. Particularly, in [24], an IRT analysis was performed to study the degradation mechanisms in a 2 kWp c-Si PV installation after 12 years of exposure. One of the most significant findings following their analysis was the fact that all solar cells located close to the junction boxes typically feature operating temperatures about 3°C higher than the rest ones in the same cell matrix. Consequently, it can be assumed that the thermal degradation of these cells evolves at a higher rate. Besides, string-to-string mismatches were also observed in several modules with the help of IRT imaging. Surprisingly, despite the higher operating temperatures of some cells, no visible defects were observed, while modules with visible hot spot damage showed no abnormal thermal signatures. For such observations it was assumed that once the rupture of the cell occurs, the shunt resistance becomes sufficiently low for the temperature to increase significantly. Moreover, IRT observations of aged PV modules, after longer field exposure periods (18-22 years), were made in [25], [26]. IR thermography was proved an effective and reliable tool for diagnosis of occurring and propagating defects, particularly revealing the existence of hot cells, hot spots on the

busbars, and optical degradation in the form of colder bubbles (delamination). Accelerated ageing tests, by thermal cycling, were attempted in [27], in order to study the propagation of existing hot spots and the evolution of abnormal thermal signatures, through the module's lifetime. The IRT imaging results of this study might be assumed surprising, since the initial temperature differences (corresponding to hot spot areas) were decreased. It was concluded that such observations could be explained as a result of the expansion of the dissipated heat to the defective areas and the allocation of such areas to the whole surface of each defective module.

The classification of different fault types by correlating their thermal signature with the I-V characteristics is of utmost importance for assessing the expected power output losses and scheduling the needed maintenance actions to prevent further failure or even safety risks for the PV system. [28] proposed hot spot evaluation procedures and well defined acceptance/rejection criteria, on the basis of several observations (among them IRT inspections) of 200 field exposed and defective modules. These evaluation procedures address both the lifetime and the operational efficiency of the modules.

[29] presented an IRT-based temperature distribution analysis to analyse three different categories of faults in PV modules. The proposed methodology, which was validated by both simulation and experimental test results, was proved to be effective in establishing parameter-based electrical/thermal models and developing an optimized global maximum power point tracking (MPPT) algorithm. In their extensive experimental work, [14], [30], investigated numerous c-Si PV modules from 16 different PV plants with a range of field exposure times. The evaluated data from IRT measurements, together with electrical characterization and electroluminescence imaging, manifested various failure mechanisms, such as cell fracture, deficient solder joints, short-circuited cells and bypassed substrings. The impact of these frequently detected defects on the resulting temperature was discussed and differing defects could be diagnosed by characteristic temperature differences. Such different thermal "patterns" were then correlated with the current voltage (I-V) characteristics at STC, and the resultant power output losses. In both of these two studies, the high reliability and usefulness of IRT mapping for PV plants for fault classification, were the main conclusion.

Advances in the field of fault analysis and characterization for installed PV modules, based on IRT imaging, were recently reported in [31], [32]. The influence, in particular, of differing ambient conditions on the characteristics and the temperature profile of defects in PV modules is studied in [31]. All investigated faults were distinguished by the authors as three different types; areal/planar defects, cell defects (e.g. cell fracture and shunted cells) where an individual cell is heated up, and point-shaped defects which are considered much smaller (e.g. solder joints).

Finite element analysis (FEM) and experimental measurements were evaluated. As a result areal cell defects behave linearly with the solar irradiance, while the temperature development in point-shaped defects exhibits a less predictable behaviour due to the glass cell temperature difference, the limited resolution and possible material changes.

The demonstrated reliability and effectiveness of IRT imaging also encourages the implementation of wide area measurements (WAMs) for large-scale PV plants, by means of aerial IRT [33], [34], [35], [36], [37], [38]. The general potential of aerial thermographic inspections for operating PV installations are briefly addressed in [34]. In early though

significant steps of such large-scale applications, in [35], an experimental set-up was implemented, based on a remote-controlled drone, to investigate 60 different PV plants of up to 1 MWp. With the proposed set-up, the performed aerial IRT inspections had a typical duration (net flight time) ranging from just few minutes to up to 1 hour, depending on the size of the PV plant. As it was concluded in the same paper, defects like disconnected strings, substrings, shunted cells, faulty soldering and cell fracture could be visualized and distinguished. Moreover, the impact of such faults was further studied and understood by means of electrical simulations. Furthermore, in [36], a novel concept was proposed for monitoring PV plants by using light unmanned aerial vehicles (UAVs) or systems (UASs) during their operation and maintenance, providing additional experience and solutions in the field of large-scale IRT.

More recently, in [33], the preliminary results of an ongoing study were presented on an application for detection, diagnosis and classification of faults in large-scale PV plants, by means of both aerial IRT mapping and auxiliary diagnosis/characterization on the ground (i.e. IRT, I-V characterization and EL). The developed IRT mapping technique was proven to be efficient though practically limited to provide diagnosis only in qualitative terms and for small-scale plants. As the authors noticed, the advantage of large-scale applicability of aerial IRT, should be evidently exploited in a more efficient way. This can be achieved by implementing less complex qualitative diagnosis and by quantifying the radiometric data of each fault's thermal signature in terms of the electrical power output loss of the impacted module. On the basis of this "strategy", a novel methodology of both qualitative and quantitative fault diagnosis for PV plants is under development by the authors.

Towards the same research direction, in the field of UAV-based IRT mapping of PV plants, another two in-progress studies were also recently published [37], [38]. In the study of [37], several diagnosed faults in a PV plant of more than ten thousand modules, were quantitatively correlated with the generated currents of the associated strings, by means of aerial IRT imaging and monitoring data respectively. The correlation analyses indicated that one or more inactive submodules as well as severe cell defects with significant ΔT ($>15^{o}C$) strongly correlate with a reduced current in the associated modules' string. In the same study, the authors also attempted a preliminary techno-economic analysis in order to quantify the impact of such diagnosed module defects, in terms of energy yield and consequential financial losses, which could be balanced or even avoided by proper inspection/maintenance. As a general conclusion, coming out from all these preliminary studies and results, within such recently opened research field, the strategy of utilizing thermographic UAVs can be a cost-effective and much less time-consuming option for fault diagnosis of large-scale PV plants.

Considering that IRT is a relatively new method, especially for fault diagnosis of PV modules, the need of reliable measurements and accurate interpretation of the inspected thermal signatures becomes increasingly important, especially when dealing with large-scale PV plants and, thus, high PV investments. A missed fault diagnosis, either as non-detected fault or as "false alarm" may lead to wrong performance assessment and maintenance decisions. For these reasons, the upcoming international standards and technical specifications of IRT for PV applications (IEC 60904-12, IEC 60904-14 and IEC 62446-3) should be established and followed [39]. Moreover, sources of possible measurement uncertainties and incorrect interpretation of thermal image data should be further investigated, as in [40], and addressed in such technical specifications. Last but not

least, careful analysis and thermal image processing comprise key steps for efficient IRT-based diagnosis, especially for large-scale measurements.

2.2 Test requirements

2.2.1 Camera requirements

There is a broad variety of different IR cameras available on the market. As to provide a useful guidance in an appropriate selection of a specific IR camera product, we classified typical parameters of different IR cameras. Table 2.2.1 lists the main differences for each of the four camera classes we distinguished. No matter what camera class, a calibration certificate is a clear prerequisite. This prerequisite is therefore included in the overview given in Table 2.2.1 for completeness. The recalibration of the camera should be carried out on an annual basis.

The stated temperature ranges listed in Table 2.2.1 are kept in italic letters, since these values are not reflecting actual prerequisites of IR quality assurance services of PV applications directly: It is clear that listed temperature ranges of up to 2000 °C are not needed for any type of PV application. However, “Professional upper class” cameras have highly sensitive infrared detectors to allow for parameters “Thermal Sensitivity” and “Accuracy” to be as high as listed. In turn, this brings along this broad temperature range.

The following paragraphs briefly summarize each parameter that is relevant for IR imaging tasks of PV systems, listed in Table 2.2.1.

Table 2.2.1: General camera requirements.

Camera parameter	Lower class	Medium class	Professional class	Professional upper class
Calibration Certificate	Yes			
Temperature Range	*-20…+250 °C*	*-20…+650 °C*	*-20…+1200 °C*	*-40…+2000 °C*
Resolution (Super Resolution*)	160 x 120	320 x 240	320 x 240 (640 x 480)	640 x 480 (1280 x 960)
Thermal Sensitivity	<0.1 K	<0.05 K	<0.04 K	<0.002 K

Accuracy	+/- 2 °C			+/- 1 °C
Focus	Fix focus	Manual	Manual and auto	
Digital Camera	-	2 Megapixels	3 Megapixels	5 Megapixels
Adjustable Emissivity	0.01…1			
Voice Recording	-	Yes (short)	Yes	
Interchangeable Lens	-	Yes (telephoto and wide angle)	Yes (telephoto, wide angle, macro)	
GPS Recording	-	-	Yes	Yes
External Wireless Sensor** Function	-	-	Yes	Yes

** Some cameras are equipped with an additional function that will increase the available resolution by combining multiple images.*

*** Wireless current clamp, humidity or temperature sensor*

Resolution

Pictures taken with an infrared camera have a specific resolution. Depending on the thermal abnormality of a PV module, a higher resolution might be necessary. Higher resolution images also allow pictures to be taken from a further distance and thus capturing a greater number of modules per image.

Thermal Sensitivity

Infrared detectors have their intrinsic thermal sensitivity. This thermal sensitivity correlates with temperatures differences that can be detected. This parameter therefore directly reflects the ability of the camera to detect a particular minimum temperature difference.

Accuracy

This parameter includes all errors for the internal technical process and calculations performed within the camera to identify the temperature value listed for each pixel in the obtained IR images.

Focus

Each infrared camera is equipped with a focus unit, used to set the appropriate focus of the camera lenses, in order to obtain sharp images. In cheaper IR cameras, only a fixed or a manual focus mode may be available. For professional IR cameras, the auto-focus function is a given function.

Digital Camera

Many infrared cameras are often equipped with the feature of providing a regular, visible light, digital image, in addition to the IR image. Such "real" images provide further information, which can be highly valuable in case of abnormalities found in the IR images. This feature is greatly beneficial for documentation and reporting purposes.

Adjustable emissivity

For different applications, the emissivity of the infrared camera must be manually adjusted. Only a manual adjustment allows the exact determination of the temperature next to the thermal abnormality. It also may be possible to adjust effective emissivity in post processing using software provided by the manufacturer. This allows the operator to determine the sensitivity of the temperature readings to the emissivity used as input. The ability for manual adjustment of the emissivity is important for PV applications.

Voice Recording

Infrared cameras can be equipped with an additional function for the storage of audio comments. The option for technical personnel to append audio comments to every IR image can be greatly beneficial for hands-on work and can help to speed up the process of time needed per MWp of IR tested modules. These comments may include for example a short description of the abnormality, a serial number or any other information deemed relevant.

Interchangeable Lens

Different applications of infrared thermography require the usage of interchangeable lenses. These interchangeable lenses are used for the documentation process of the spotted abnormality. Typical interchangeable lenses are, for example, at wide angle or a telephoto lens.

GPS Recording

Another feature of the IR camera is the internal storage of geographical coordinates for each infrared image. These GPS coordinates will be used for the additional documentation regarding the position of the detected abnormalities.

External Wireless Sensor Function

IR cameras using this function can be connected to external sensors. These external sensors are used for the record of surrounding weather conditions or other important parameters like ambient temperature, relative humidity or current flow through the modules or string.

Some additional camera requirements can be defined as well. The additional requirements are listed in *Table 2.2.2*.

Table 2.2.2: Additional camera requirements.

Camera parameter	Lower class	Medium class	Professional class	Professional upper class
Viewfinder	-			Yes
Measurement modes	3	3	4	6
Camera Software for update and inspection reports	Yes			
Colour Palettes	4		6	6
Display	3,5”	3,5”	4,3” touch	4,3” touch
Operating Time	4h	4h	4h	4h
Battery Charging	Inside camera only	Inside and with external charging unit		
Additional Accumulators	-	Yes		

Viewfinder

Many infrared cameras are equipped with an externally mounted display. Installation sites often exhibit very bright environmental conditions, making it very hard to see what is displayed. The ‘good old viewfinder’ offers a clear view of the internal display of the camera.

Measurement Modes

Infrared cameras are equipped with different measurement methods, such as for example ‘isotherm’, ‘point measurement’ or ‘area’ functions. These functions provide various options to analyse the present abnormalities and temperature variations. The different modes control the image processing depending on the application. For example, the ‘point measurement’ mode allows the user to select on a single point in the field of view. This mode allows the user to measure the temperature at a particular point in the field of view of the camera or image. The ‘area’ function allows the user to define an area of interest and the camera calculates the temperature statistics for the area. Typically, this includes the calculation of maximum, minimum and average temperature within the selected area.

In addition to these two measurement modes the colour palette used to display the image can be user selected. This is often based on user preference but can be useful in visualising regions of the image within a narrow temperature range. The 'isotherm' measurement mode displays areas of the image with the same temperature in the same colour.

Colour Palettes

Each infrared camera is equipped with various colour palettes. These palettes are used for the easier visualization of the present abnormality. Selecting different colour palettes can allow the use of isothermal measurements as mentioned above.

Camera Software for update and inspection reports

For the evaluation and presentation of infrared images, evaluation software is usually provided by the manufacturer of cameras. In addition to the evaluation of IR images, this software is typically also used for the preparation of an inspection report and to perform software updates on the camera.

Display

Each infrared camera is equipped with a display. This display is used for the presentation of the taken IR image. Depending on the class of camera, this screen is larger and is equipped with a touchable human interface.

Operating Time

Estimated time for the usage of the infrared camera before the accumulator has to be changed.

Battery Charging and Additional Accumulators

Batteries of each camera need to be recharged. An external charging unit is highly advisable, because otherwise the camera itself needs to be connected to a recharging unit and thus cannot be used during the time of the recharge for any inspection task. Additional accumulators can be very helpful for inspection tasks that last all day long.

Which class of camera to use or purchase?

An appropriate selection of an adequate class of IR camera for use or purchase depends on the various possible use cases for that camera. It is impossible to give a straightforward decision matrix (above paragraphs highlighted that it depends very much on the specific project case, the camera is used in).

On a general note, one may distinguish a tendency of smaller PV power plants (e.g. <100kWp) and their related DC and AC zones and medium-sized PV power plants (e.g. multiple 100 kWp) and their related DC and AC zones to fit the medium and professional class cameras, respectively.

Despite higher initial costs, the reasons for the selection of a professional class camera may outweigh the purchase of a medium class IR camera:

- The auto focus functionality
- The GPS recording function
- The possible higher resolution of the IR picture

- The feature to connect external wireless sensors.

In case of many thermal abnormalities during the IR inspection, manual focusing of IR pictures can impose large time penalties, which is both inconvenient for the technical personnel and costly in terms of labour costs. The GPS recording function will assist to identify the exact location of the spotted thermal abnormity, which eases the creation of detailed inspection reports once the on-site part of the PV plant inspection routines are finished. Since reports include GPS coordinates processed by machines and software, there is also little risk of errors induced by manual interaction. Last but not least, some thermal abnormalities demand a more detailed analysis. The super resolution function will help to get the required, more detailed IR pictures. The possibility to connect specific external wireless sensors to the IR camera will provide more possibilities for the analysis of detected thermal abnormalities. With these aspects considered, we would in principle advice the professional class over the medium class, however, with acknowledging at the same time that for a number of IR inspection cases medium class cameras are fully sufficient.

Finally, the 'upper professional class' cameras offer the top-functions the present time. However, the high cost for such cameras is significant. So the decision of choosing the 'upper' professional class of IR cameras depends on the detailed inspection task (and potential supplementary tasks) and, last but not least, the available budget.

2.2.2 Environmental conditions

Stable environmental conditions are crucial for high quality outdoor IR imaging of PV modules and arrays. Weather fluctuations must be much slower than the thermal time constant of the PV module. The thermal time constant of the module is a function of its thermal resistance and capacitance. A typical PV module takes 5 to 15 minutes to thermally stabilize for new environmental conditions such as change of global irradiation intensity, temperature, or wind speed [41]. A common environmental change that affects IR imaging of PV arrays are clouds passing in front of the sun, which results in rapid changes of irradiance. Clouds also can produce thermal reflections on the PV modules which may distort the evaluation of the IR image. For this reason, thermal reflections of clouds, buildings, trees, or other objects should be avoided or minimized. This is usually done by either waiting for more stable conditions or moving the position of the IR camera to avoid specific reflections, if possible.

One important parameter derived from IR images is the temperature difference between different parts of the module or between modules and/or strings of modules. Inactive areas of a module or string usually appear hotter than surrounding active areas. This occurs because a portion of the radiation hitting a functioning PV module is converted to DC power, which flows to the inverter and loads on the grid. When a PV module or string is not functioning, this energy is not converted to DC power and therefore remains as excess heat, which raises the temperature of the module or string. Inactive modules often suffer from one of the following defect types: disconnected PV modules or strings, PID effects or shunted cells, and short-circuited bypass diodes. These types of failures cause only a slight temperature increase between active and inactive parts, and this difference is often proportional to the irradiance. Thus it is more difficult or even impossible to detect these

types of failures under low irradiance conditions. Hot spots that arise from poor electrical connections or severe mismatch within a module are another important type of failure that is usually easily detectable using IR.

The temperature differences of these failures define the minimum requirements for the weather condition, where a module failure can still be detected. The difference can be calculated if the electrical conversion efficiency of the module is known as shown in Figure 2-2. The radiation power flux I_{irr} heats up the PV module. A part of I_{irr} is converted by the PV module efficiency into electrical energy and conveyed away from the PV module. The ambient temperature T_{amb} and the wind speed v_{wind} cause further heat flux to the surrounding environment. Other heat fluxes (frame conduction, radiation flux to the sky and ground) are neglected in this simplified energy flux diagram of Figure 2-2. A more detailed heat flux diagram is given in the review of Skoplaki [42].

The electrical conversion efficiency of a module $\eta_{25ºC}$ can be taken from the datasheet of the PV module or calculated by the Area A (m^2) and the peak power P_{MPP} (W_p) of the module:

$$\eta_{25ºC} = P_{MPP} / (1000 W/m^2 \times A) \qquad \text{(ETA25)}$$

The electrical conversion efficiency $\eta_{25ºC}$ is given for standard test conditions at 25 °C. To calculate the efficiency η for another PV module temperature T_{mod} the following equation is applicable:

$$\eta = (1 - (T_{mod} - 25\ ºC) \bullet c_T) \bullet \eta_{25ºC} \qquad \text{(ETA)}$$

The power temperature coefficient c_T can be found in the module data sheet. The value c_T is the same for the module power and efficiency. However, one should be aware of deviating definitions for c_T.

Figure 2-2: Heat flux scheme of a PV module outdoors.

For various module mounting conditions and module types [42] collected module temperature models. The easiest equation to calculate the module temperature (T_{mod}) for practical use is:

$$T_{mod} = T_a + (G_T / G_{NOCT})(T_{NOCT} - T_{a;NOCT})(1 - \eta) - f(v_{Wind}). \qquad \text{(MODT)}$$

With T_a represent the ambient temperature in °C, G_T the global irradiation intensity on the module plane, G_{NOCT} the global irradiation intensity on the module plane used to measure the nominal operating cell temperature T_{NOCT} at the ambient temperature $T_{a;NOCT}$.

All parameters should be available from the PV module data sheet and the weather forecast, except for the function f of wind speed v_{Wind}. PV module datasheets typically provide the standardized value G_{NOCT} for 800 W/m² and $T_{a;NOCT}$=20 °C. Eq. (MODT) is together with Eq. (ETA) an implicit equation, which can easily be solved e.g. by a data calculation sheet.

For PV modules certified according to the new standard IEC61215-2:2016 the temperature is given in terms of the Faiman model for a module working at the maximum power point. For the parameters of the new standard, equation (MODT) cannot be applied.

An active PV module behaves exactly like an inactive module except that a portion of the irradiation is converted into electrical power. Therefore, the difference in module temperature ΔT for active and inactive module parts is:

$$\Delta T = (G_T/G_{NOCT})(T_{NOCT}-T_{a;NOCT})\eta\,. \qquad \text{(TDIFF)}$$

The parameter TNOCT is typically given in the datasheet for a free standing PV module. For other installation situation the TNOCT has to be exchanged by the NOCT temperature of a built-in solar module TINNOCT. The TINNOCT can be estimated by the values given in

Table 2.2.3.

Table 2.2.3: Estimation of T_{INOCT} based on T_{NOCT} [43]. *h* is standoff, entrance, or exit height/width, whichever is minimum. If channelled, 4 °C is added.*

PV array mount type	TINOCT [°C]
Rack mount	NOCT + 3°C
Direct mount	NOCT + 18°C
Standoff/integral	NOCT + X
h* [cm]	X [°C]
2.5	+11
7.5	+2
15	-1

Figure 2-3 shows the temperature difference for a typical multi crystalline silicon module with an efficiency of 15 % for various mounting situations given in

Table 2.2.3. Eq. TDIFF can be used to estimate the expected temperature difference for a given PV module, mounting situation and weather conditions. Modules of high module efficiency such as 20 % will have a 1 K higher temperature difference for active and inactive parts compared to 15 % efficiency and are therefore easier to detect. It is recommended to use weather conditions which lead to temperature differences Δ*T* higher than 2.5 K. Temperature differences of up to 8 K may be found in a PV module caused by natural inhomogeneous temperature fields [44]. These natural inhomogeneities are almost seen as a gradient on the module. Defect features can be distinguished from these effects by showing cell or string or module wise temperature steps. The temperature gradients on modules and arrays increase linearly with the global irradiation. So the temperature gradients at 1000 W/m² global irradiation are higher than at 600 W/m². The natural temperature gradients are highest at the edges of the array.

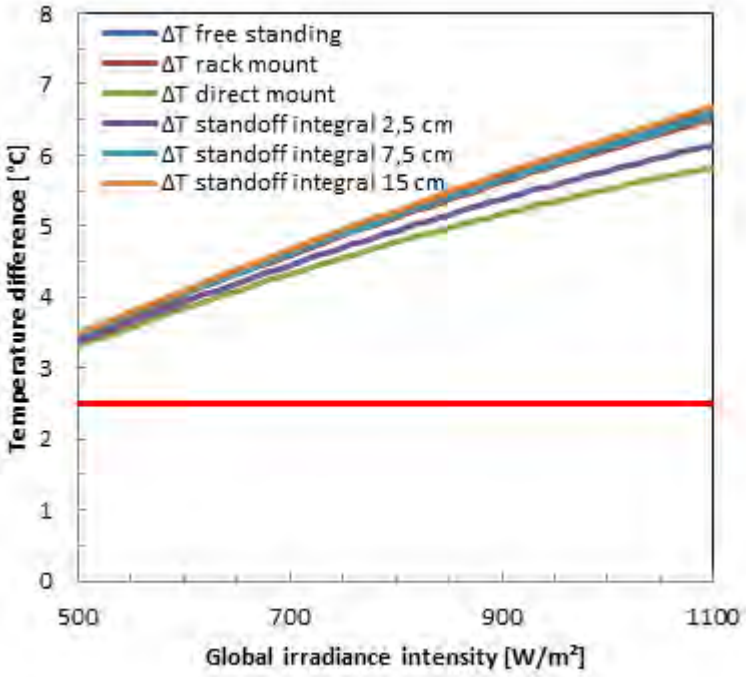

Figure 2-3: Example of temperature difference ΔT calculated with Eq. (TDIFF) for a 15 % efficient PV module with T_{NOCT}=60 °C, an ambient temperature T_a of 20 °C, for various installation situations and no wind having an active and an inactive part of the module. The red line represents a minimum temperature difference needed to assure that it is not an artificial effect.

Actually, the estimation of temperature difference Δ*T* for an inactive module part is a rough approximation. However, the estimation for practical use only is based on easily accessible parameters, such as datasheet values. The temperature difference helps assessing the

observed temperature variation and gives a decision support for taking IR images for a given weather forecast. For most practical cases an irradiance of 600 W/m² is enough to detect failures in PV modules with inactive module parts. Equation (TDIFF) shows no dependence of the temperature difference of active and inactive parts in the module on the wind. However, wind should be avoided because the wind adds inhomogeneous temperature fields to the PV array which makes it more difficult to identify the temperature differences caused by inactive module parts. Cell cracks, hot spots or other additional heat sources in the module can also be identified at lower irradiance levels, because they generate local heat accumulations. With these kinds of defects the temperature is higher compared to normal active module parts.

2.2.3 Recording procedures

PV fields, especially large-scale ones, comprise a complicated target for monitoring and performance evaluation [28], [45], [46]. With the aim of establishing reliable and efficient IRT-based inspection services for PV installations in the near future, recording procedures should feature large-scale applicability and/or provide complete and accurate diagnosis (i.e. qualitative and quantitative) of occurring failure modes.

Recent ideas on how to accelerate IRT inspection of PV plants and recording processes are focused on open-source flying platforms, known as micro UAV or, more simple, “drones” [47], [48]. Indeed, given the development of new, safer platforms and effective sensors, as well as the improvement of data acquisition devices and automatic flight control systems, advanced aerial inspections are becoming sensationally easy, fast and feasible nowadays. Such rapidly growing technological trends, consequently widens the employment of UAVs for proximal sensing for both quantitative and qualitative imaging investigations [49]. Based on early studies and recent feedback from experience, net inspection times (raw aerial IRT imaging) can reach an impressive rate of 2 MWp or even 3 MWp (typically up to ~12000 modules) per hour, depending on the desired detail in the recorded data [38], [33], [30].

On the other hand, conventional IRT recording procedures on the ground, although being time-consuming compared can provide auxiliary information on the thermal signature of operating PV modules, especially when combined with geo-referencing techniques [50].

All IRT recordings, either aerial or terrestrial, which are taken into account for qualitative and quantitative analysis of operating PV modules, should be ideally performed in compliance with recommended specifications. Such recommendations, in experimental (e.g. hardware features, distance to target, angle of view) and environmental conditions (e.g. irradiance, cloud coverage, wind speed) are set to optimize the quality of acquired thermal signatures, minimize misinterpretations (“false alarms”) of abnormal temperature profiles and, ultimately, maximize the reliability of the recorded data. Further details on recommended experimental and environmental conditions for IR recording procedures, based on forthcoming IEC standards, are given in Subsections 2.2.1 and 2.2.2. Figure 2-4 gives a brief overview of involved actions before, during and after the IR inspection of a PV plant.

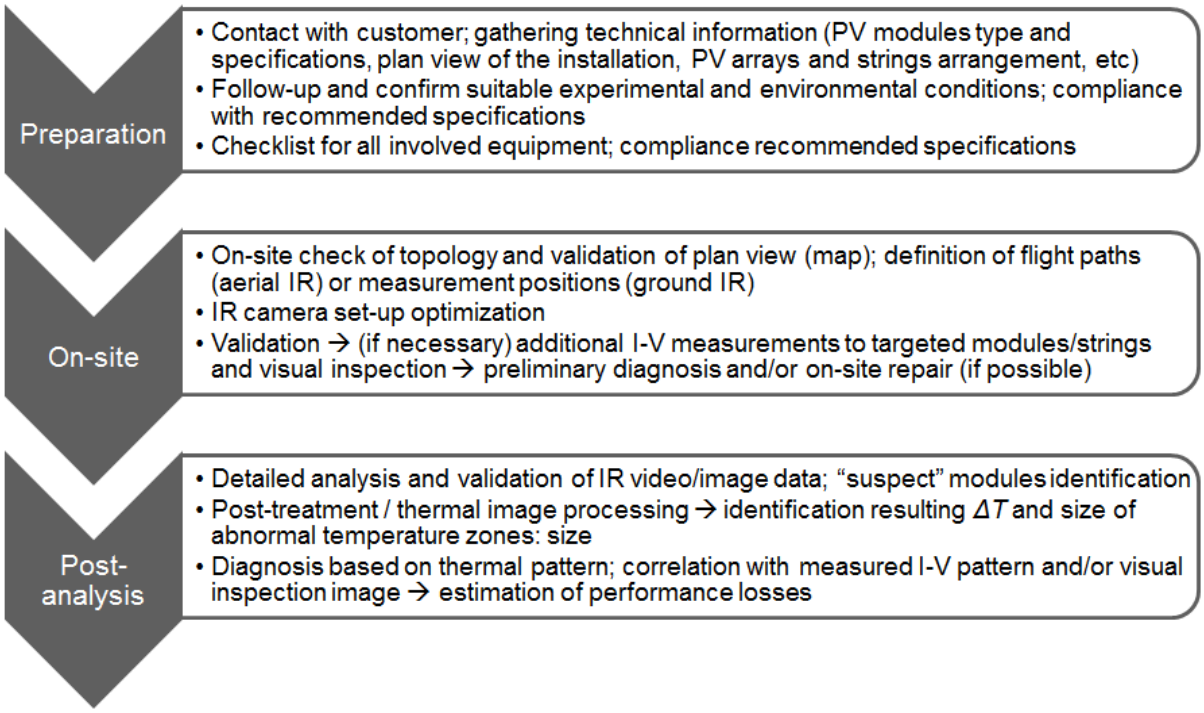

Figure 2-4: Overview of involved actions before, during and after IR inspection of a PV plant.

An important factor for any outdoor IRT recording procedure, is the distance between the camera lens and the target (surface of PV module or array). In principle, long-distance measurements involve unwanted variations of the atmospheric transmission and directional emissivity [40]. The latter and, most importantly, the limited spatial and lateral resolution at long-distance measurements have a negative impact on the accuracy and, thus, the reliability of quantitative results, compared to short-distance measurements. In both aerial and ground measurements, the future IEC 60904-3 standard is oriented to recommend a distance-to-target limit where the thermal signature of a single cell of an inspected module is depicted with ideally 5 × 5 pixels.

In order to respect this empirical rule and to find the allowed maximum distance-to-target (d_{max}), a simple lens calculation should be performed, prior to recording and interpreting thermal images. For such analysis, the most important parameters to consider, are: i) the optical resolution of the output thermal image, ii) the field-of-view (FOV) of the thermal camera, as well as the instantaneous FOV (IFOV or spatial resolution) and the measurement FOV (MFOV) and iii) the physical surface dimensions of the target. For instance, we assume a typical thermal camera with a lens of FOV = 62°× 49°, optical (radiometric) resolution of 382 × 288 pixels and temperature resolution of 0.04 °C; and a PV module with solar cell size of 160 × 160 mm, to be inspected. In this case, the 5 × 5 pixels/cell recommendation, is respected when the pixel size (i.e. the IFOV) is not more than 160/5 = 32 mm. Such cell size and resulting IFOV correspond to typical 60-cell PV module dimensions (i.e. ~1600 x 1000 mm). Given these, Figure 2-5, presents a lens calculation example [51] where the allowed d_{max} is identified, for optimum IR recordings of operating PV modules. Thus, on the basis of the recommended IEC specifications, a distance d_{max} = 10.19 m is calculated for the mentioned module and camera parameters, as shown in Figure 2-5. Similar lens calculator example can be also found in [52].

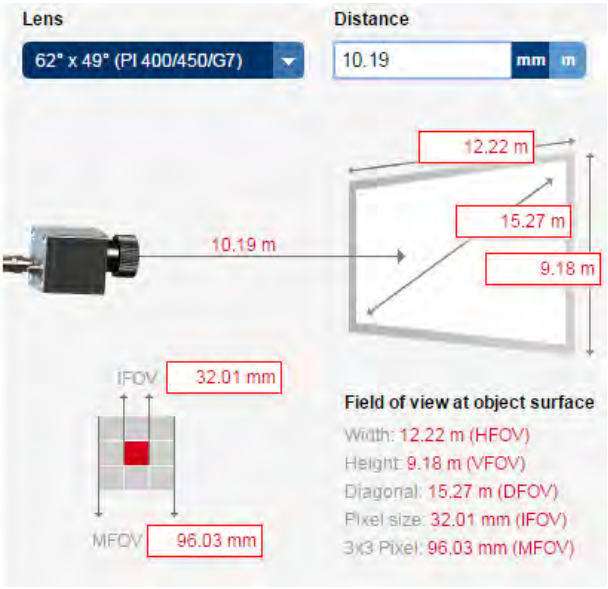

Figure 2-5: Example of lens calculation [51] *and identification of d_{max} for an example case where IFOV ≤32 mm.*

However, recording of thermal images at d>d_{max} can be efficient as well, at least for "rough" detection of abnormal temperatures (possibly defective modules); especially where preliminary measurements could identify priority "areas of interest" in large PV plants. In fact, it is highly recommended to obtain so-called "IR overviews" of a PV installation, even under lower image resolution, for a good orientation and visualization of large extended defects on string level, which might otherwise be undetected.

Another significant issue to be considered, during a recording procedure in real field, is to accurately identify the exact location of each thermal signature. Such task can be very challenging, especially when dealing with numerous measurements and post-treatment of thermal imagery of large-scale PV plants, which consist of thousands of strings and modules. Towards tackling this challenge, IR recordings of PV plants may involve mapping techniques based on geographical information and/or photogrammetry, depending on the application (ground or aerial inspection).

Two typical examples of IRT recording procedures, i.e. aerial triangulation and geo-referencing, were presented in a recent work [50].

2.2.4 Comments and recommendations

Infrared thermography as an analysis method enables the detection of hot spots and other defects that cannot be detected by visual inspection due to the absence of optical effects. Thermography displays temperature differences that, depending on their intensity, indicate acute defects or cause performance degradation over the operating period.

The aim of a thermographic inspection is to detect errors before yield reduction or serious material damage will occur. Because outlined damages often have not developed yet, the objective interpretation of thermographic scans is not trivial. Furthermore, defects found during a thermographic investigation do not inevitably lead to performance degradation.

However, these defects have the potential to cause power degradations in subsequent years. Hot spots with strong local heat gradients can affect the performance of the PV modules significantly and even, in extreme cases, lead to smouldering fires.

IR imaging is a valuable method to detect power relevant, malfunctioning PV modules, module strings, and certain devices in a PV array if the presence of artefacts, like partial shading, dirt, can be excluded. It is recommended to take the IR images at high solar irradiance (> 600 W/m²), constant ambient conditions (no clouds, low wind speed, stable ambient temperature). The knowledge of the PV array data (inclination of the modules, orientation, string configuration, variations within the generator) is obligatory of evaluation of IR images. If monitoring data are available, they can be helpful for data interpretation within the accuracy of the inverter. However, when the installations are rather complex, e. g. on factory roofs with different roof installations, varying string lengths, different orientation, different inclination angle, the monitoring data tend to scatter and do not prevent clear indications for defective devices. IR images do. Modules with high local temperatures are visible clearly and indicate strong power losses and technical risks. In general, high temperature differences indicate strong power loss and low ones correspond to low power losses.

IR images provide an overview of the solar park quality during operating conditions by checking easily 100 percent of the PV modules with respect to the presence of defects that can reduce the power output.

2.3 Classification and evaluation

2.3.1 Sample patterns with abnormalities

PV modules can be tested using a thermal imaging camera without any operational interruption of the PV power plant. Using the InfraRed (IR) image gathering method, temperature sequences within a module or within a larger module field can be made visible. Damaged modules, such as for example hot spot effects on crystalline silicon modules, can be easily identified. Also other phenomena can be detected, such as active bypass diodes in the module junction box, inactive strings and similar effects.

The main thermal abnormalities in PV power plants are:

1. Hot cells formally named as hot spots by
    a. Breakage of front glazing
    b. External shading
    c. Internal cell problems
2. Heated bypass diodes inside the PV module junction box
3. Heated string fuses in combiner box
4. Heated DC and AC cables and connections points.

The IR patterns presented in the following section include examples for specific thermal abnormalities of PV power plants. For a better understanding, some of the IR images are shown together with the corresponding digital pictures.

2.3.1.1 Breakage of PV module front glazing

Figure 2-6 through Figure 2-9 show breakages of the front glass, caused by heavy impacts such as hail or other extreme mechanical stress onto the module frame, causing the front glass of the PV module to be damaged. The damage of the front glass often creates broken hot cells in the damaged PV module.

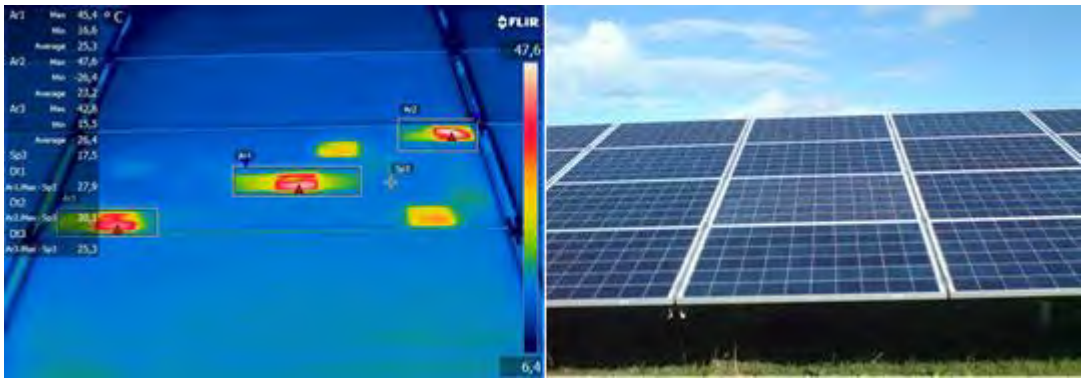

Figure 2-6: Breakage of front glass.

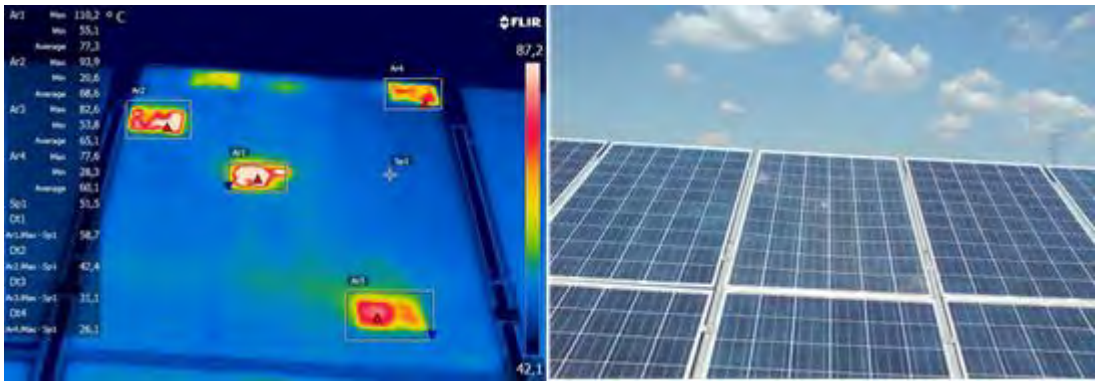

Figure 2-7: Breakage of front glass.

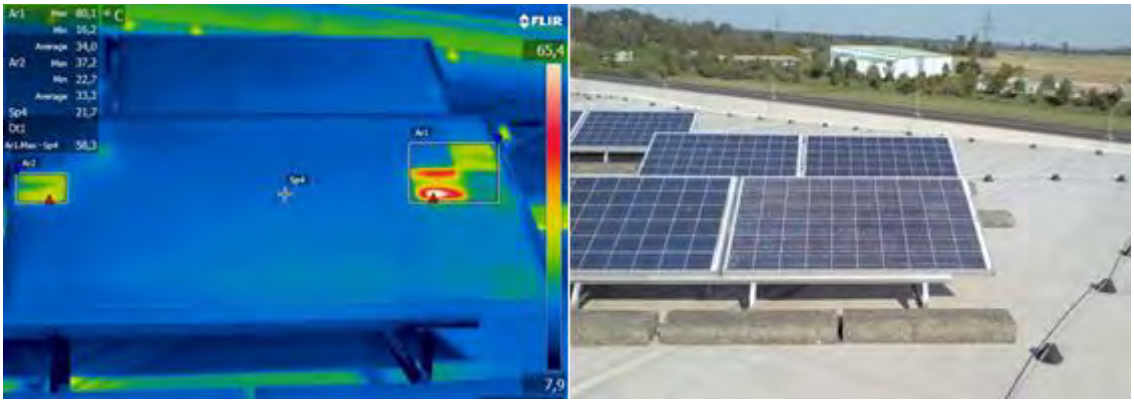

Figure 2-8: Breakage of front glass.

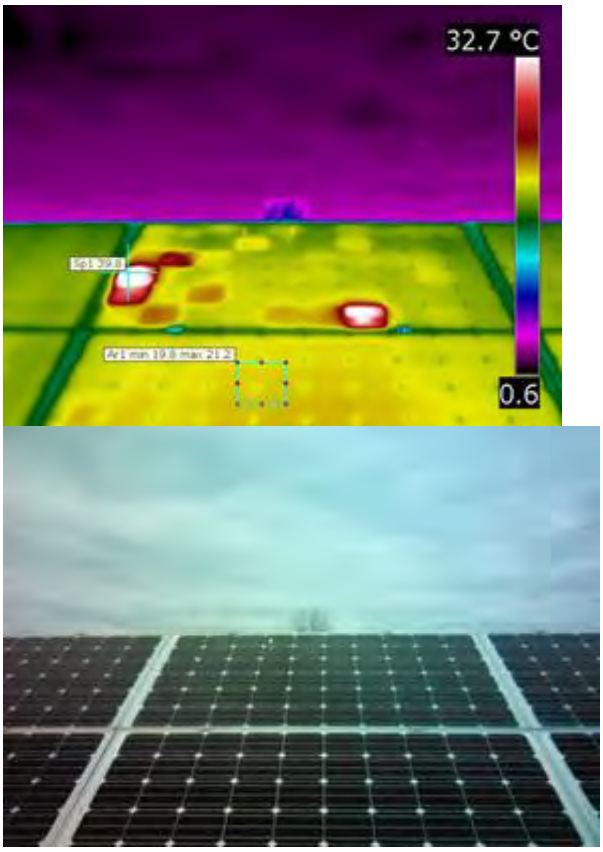

Figure 2-9: Breakage of front glass.

2.3.1.2 PV module with overheated cells (hot spots) by internal cell problems

The sample pictures presented in this category depict PV modules with overheated cells. These cells are overheated due to failures in the cell and module manufacturing process. Some examples for failures during these production processes are inaccurate cell sorting, local short circuits within the solar cell or an insufficient electrical contact. Most of the overheated cells derive from internal cell problems.

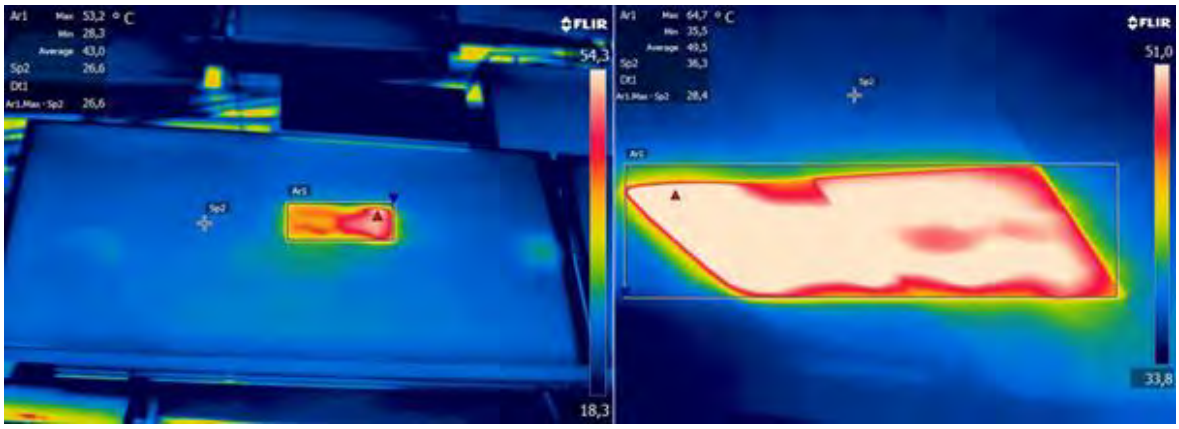

Figure 2-10: On the left side front view and on the right hand side rear side view of a PV module with overheated cell caused by internal cell problems.

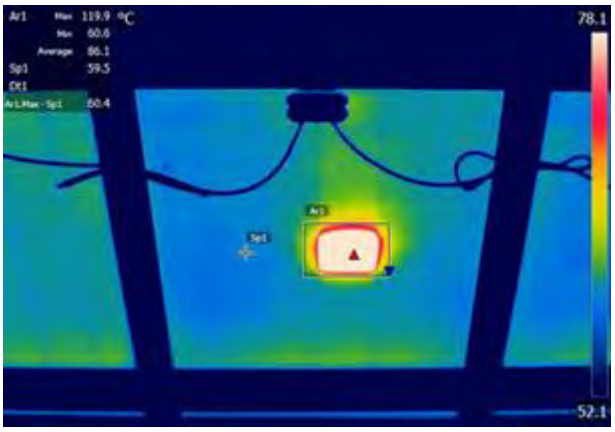

Figure 2-11: Rear side view of PV module with overheated cell caused by internal cell problems.

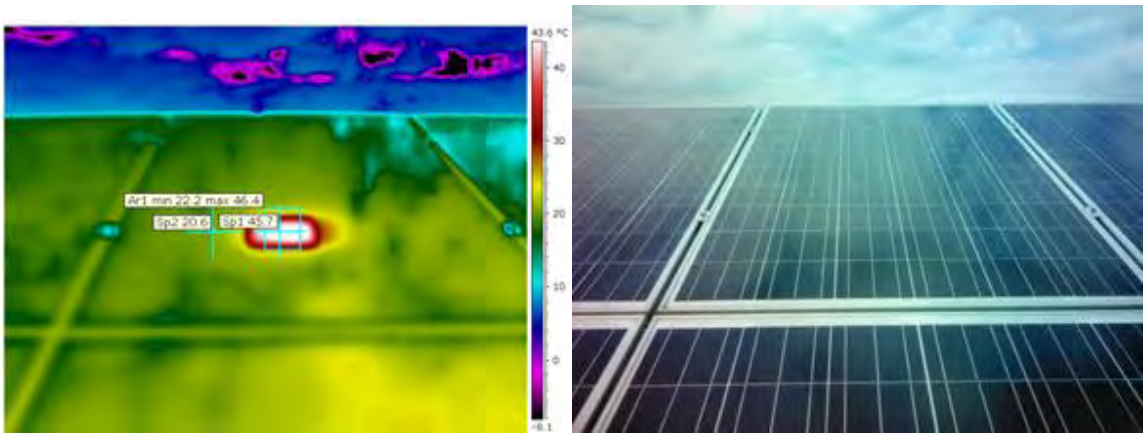

Figure 2-12: Hot Spot > 20 K.

2.3.1.3 PV modules shows overheated cells (hot spots) due to external shading

The previous sub-chapter showed IR patterns of overheated cells due to internal cell problems. In this subchapter, similar patterns of overheated cells are shown, which are caused by external shading. The IR pattern that can be observed strongly depends on the exact external shading source, which is usually distinguished into local shading and large-scale shading. Local shading sources are for example bird droppings, small crops and small trees. Large-scale shading sources are high buildings, lightning rods, masts (pylons) or trees next to the PV power plant.

When the operating current of the overall series string of cells approaches the short circuit current of the shaded cell, the overall current of the string becomes limited by the shaded cell. The extra current produced by the good cells then forward biases the good solar cells. If the series string is short-circuited, then the forward bias across all of these cells reverse biases the shaded cell. Hot spot occurs when a number of series connected cells cause a reverse bias across the shaded cell, causing the dissipation of power in the shaded cell. Essentially the entire generating capacity of all the unshaded cells in the string cells is dissipated in the shaded cell.

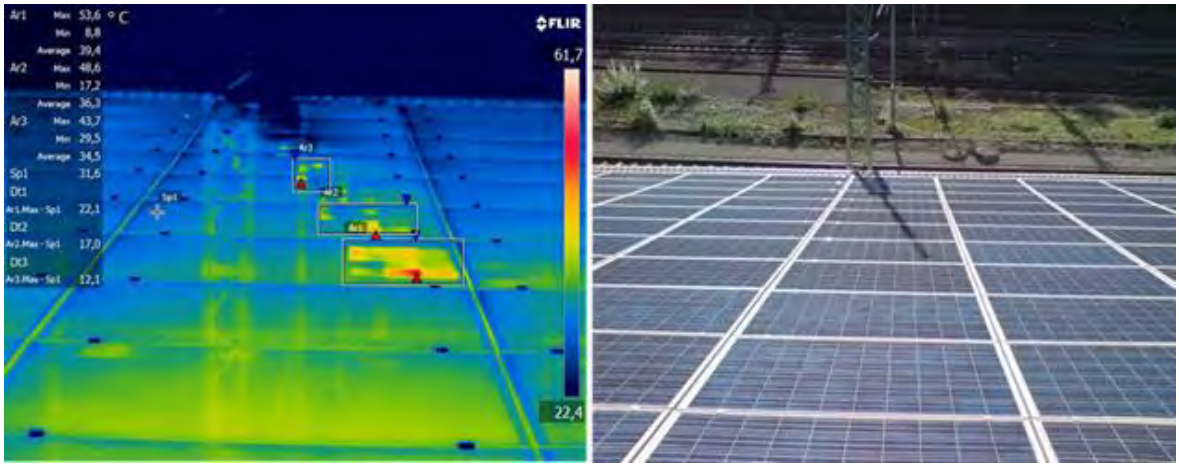

Figure 2-13: PV Module shows overheated cells due to shading by metal rod.

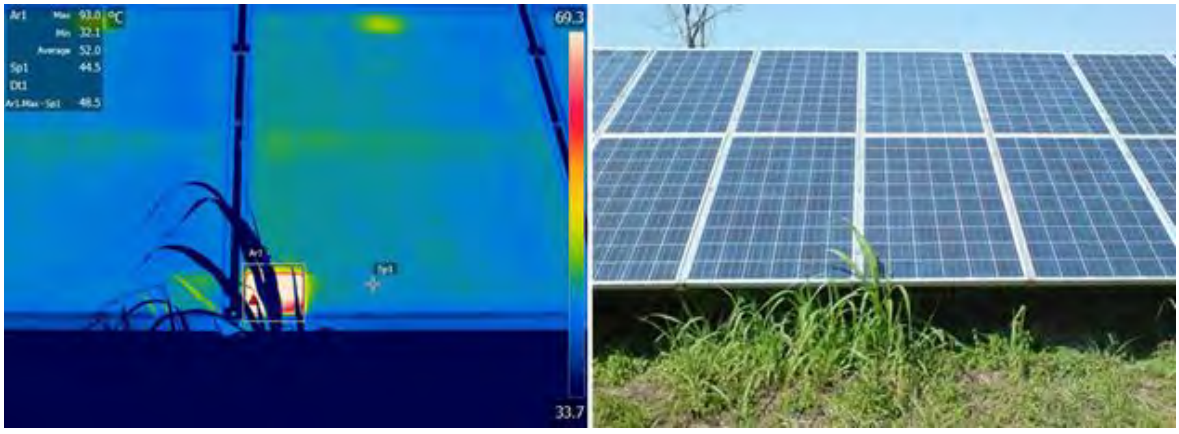

Figure 2-14: PV module shows overheated cells due to shading by plants.

Figure 2-15: PV module shows overheated cells due to shading by the medium voltage overhead lines and its pylon.

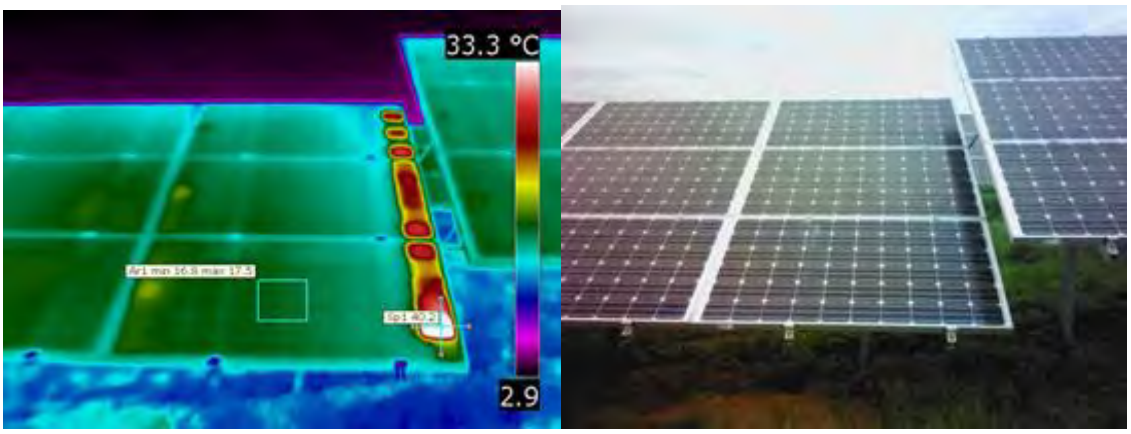

Figure 2-16: PV module shows overheated cells due to shading by neighbouring PV module row.

2.3.1.4 PV modules show overheated bypass diode

The area of the junction boxes of PV modules is slightly warmer than the rest of the module and sometimes includes thermal abnormalities, too. The main thermal abnormalities in that case are overheated bypass diodes, which are located inside the junction box.

To reduce the effects of hot spots, a bypass diode is connected in parallel and with opposite polarity to a string of solar cells. Under normal operational conditions of the cells, the bypass diode will be reverse biased thus inactive. Due to mismatches of the cells or partial shading of the string of cells, the bypass diode is forward biased, active-, allowing the current to flow through it and not the cell that is shaded for example. Thus, the temperature of the diode when is active is higher than the inactive diodes.

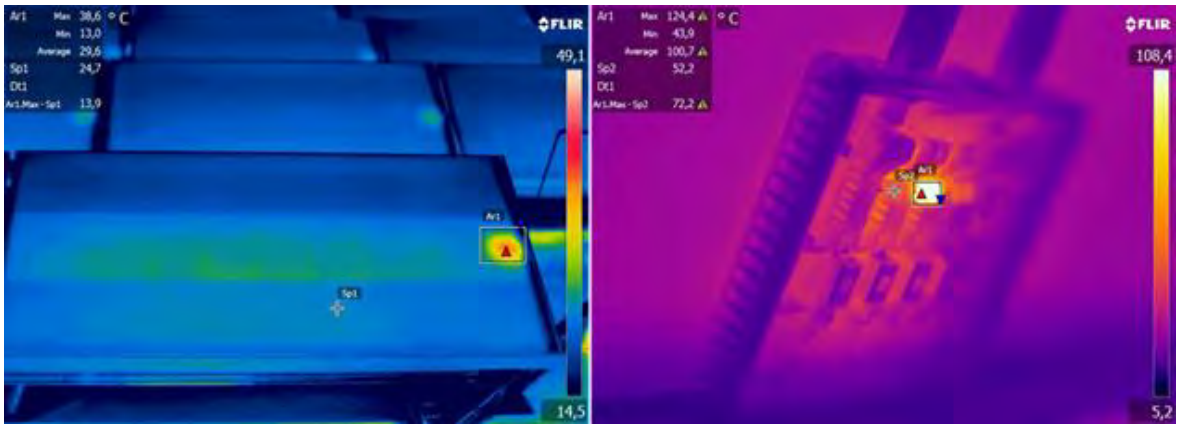

Figure 2-17: On the left side, front view PV module with overheated junction box and on the right hand side, rear side view with open junction box and overheated diode.

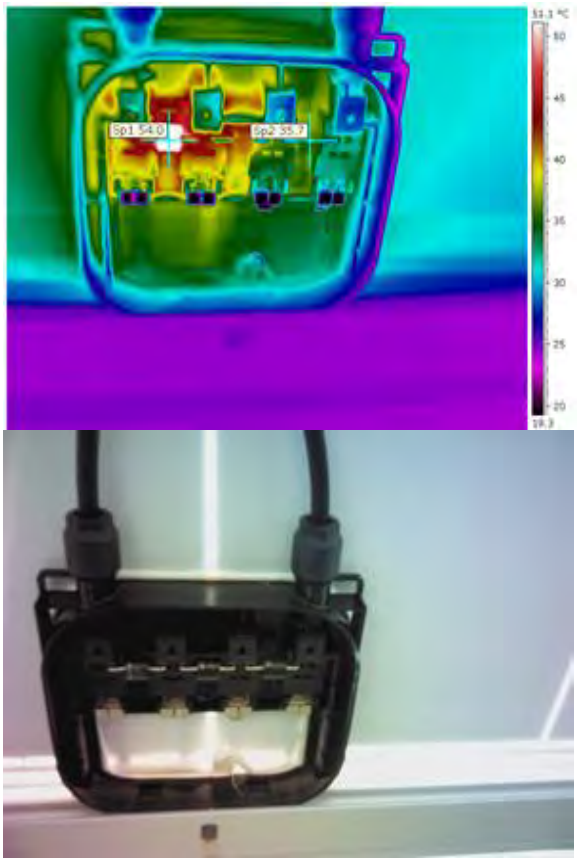

Figure 2-18: Overheated bypass diode because it is forward biased and active.

2.3.1.5 DC combiner box include overheated cable interconnection

Large-scale PV power plants are often equipped with large central inverters, with DC combiner boxes used to collect individual DC strings and connect them to one larger, single cable. These combiner boxes sometimes evolve thermal problems too, most often caused by improper cable connections, either a loose cable connection within the internal cross bar or an improper compressed connection between the DC cable and the cable lug.

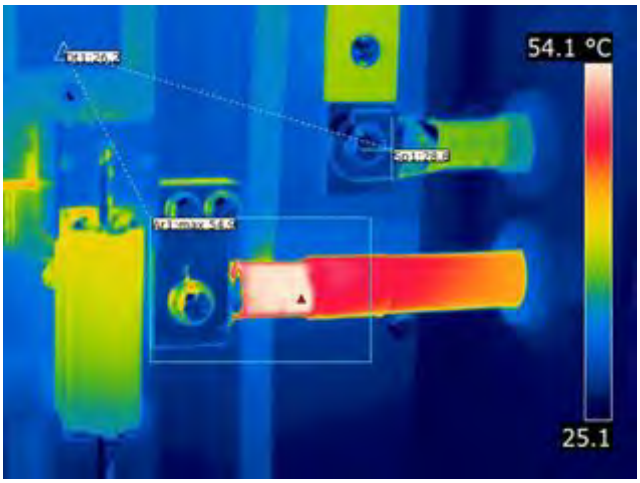

Figure 2-19: DC combiner box includes overheated interconnection with cross bar between cable and lug.

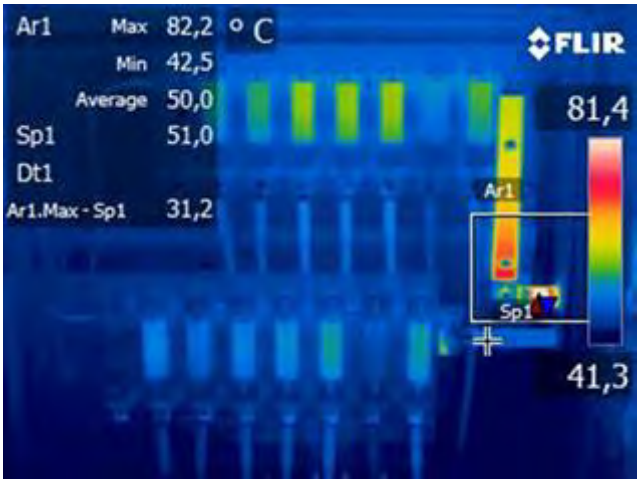

Figure 2-20: DC combiner box includes overheated interconnection with cross bar between cable and lug.

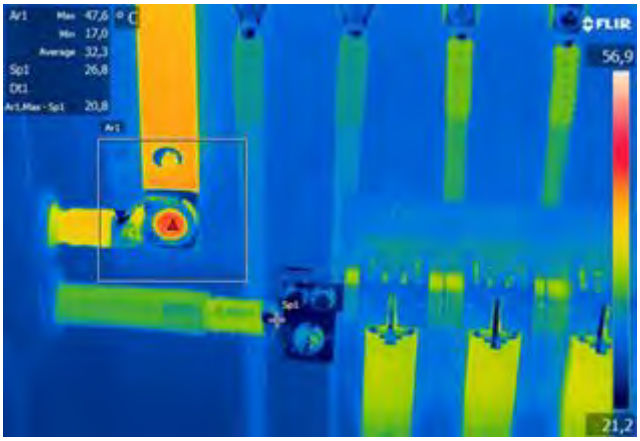

Figure 2-21: DC combiner box includes overheated cable interconnection with cross bar due to a loose screw.

2.3.1.6 Miscellaneous thermal abnormalities

In this last section on IR failure patterns, various different abnormalities that can be found during an IR inspection procedure of a PV power plant are shown.

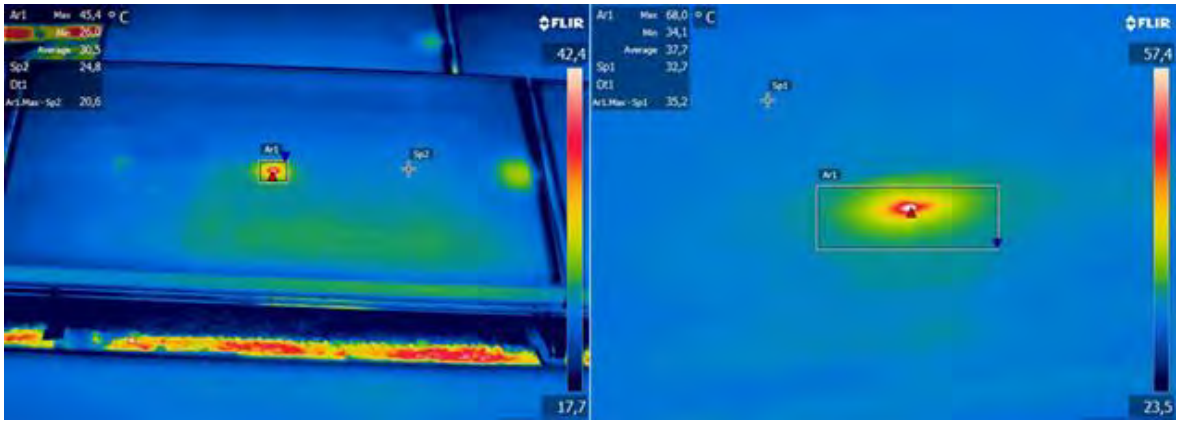

Figure 2-22: The left side IR image is derived from the front view of a PV module with heated cell interconnection. On the right hand side the rear side view of this heated cell interconnection is depicted.

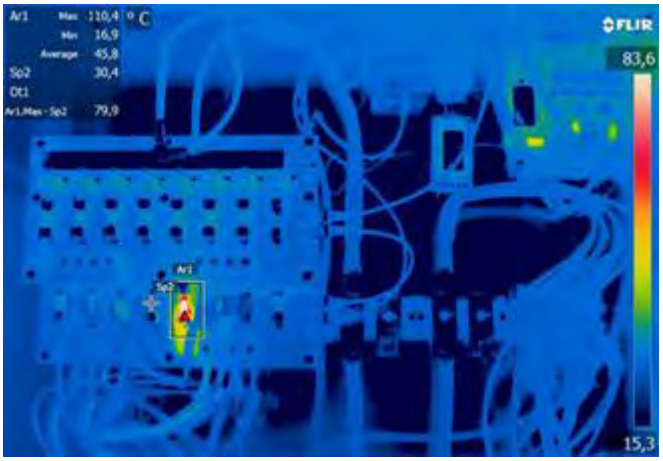

Figure 2-23: DC combiner box with overheated string fuse/spring clamp connection.

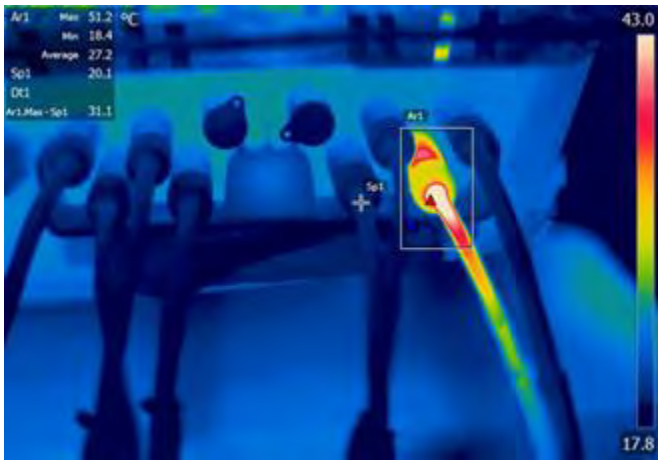

Figure 2-24: String inverter with overheated DC connector.

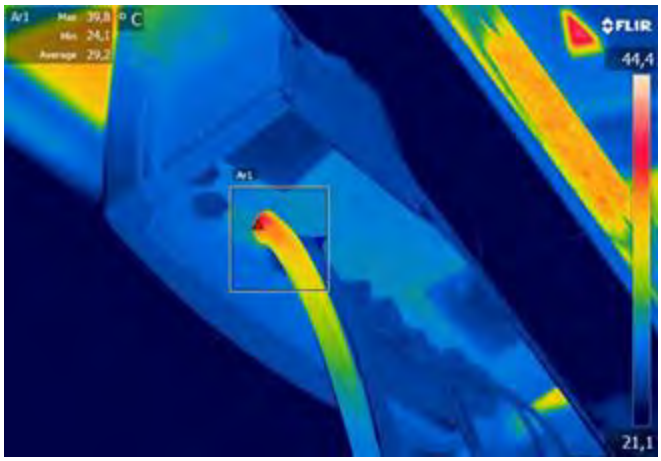

Figure 2-25: AC cable of string inverter shows overheating due to loose connection.

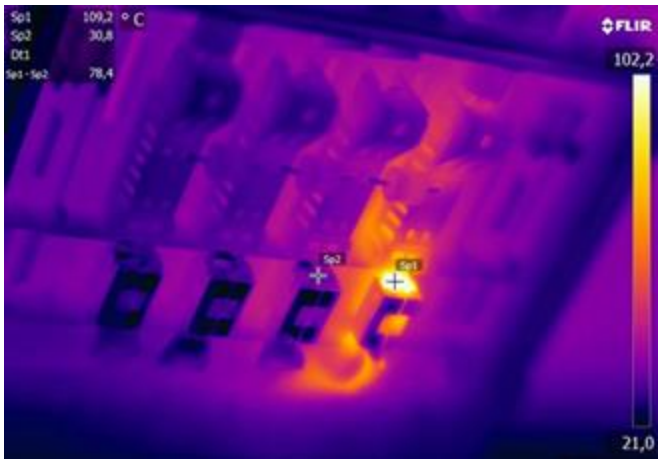

Figure 2-26: Open PV module junction box with overheated terminal.

2.3.2 Infrared thermography imaging of PID-s affected modules

Infrared thermography (IRT) imaging of PV modules in the direct sunlight is an efficient method for getting an estimation of the degree of PID degradation by shunts (PID-s) during the operation of modules in the PV plant. Typical PID-s IRT patterns (warmer cells close to

the bottom frame or patchwork patterns) and module positions close to the negative pole of the module string are strong indications for PID-s effects.

For infrared thermography (IRT) and electroluminescence (EL) imaging of the PID-s affected module in the laboratory, a test current of I_{sc} was applied (see *Figure 2-27*) in a dark room. Both images were in good agreement. The strongly PID-s affected cells were cooler in IRT image and darker in EL image.

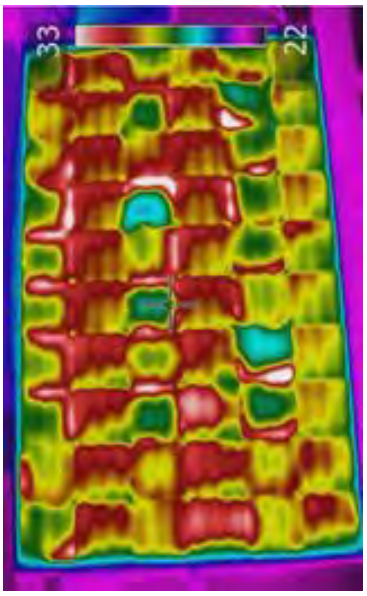

a) IRT at I_{sc}

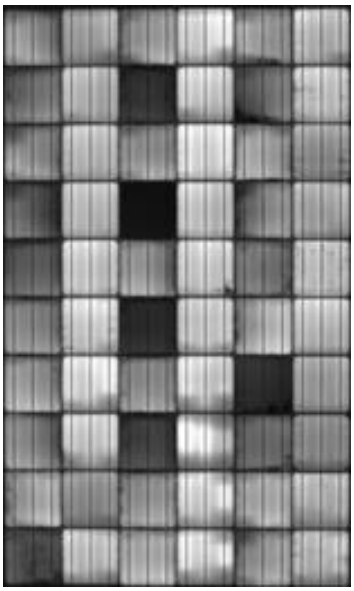

b) EL at I_{sc}

Figure 2-27: IR thermography and EL image of a PID-s affected module at the same applied test current (I_{test} = I_{sc}) in the dark. a) The IRT image shows that the strongly affected cells are cooler than the rest. b) The EL image shows that the affected cells are darker [53].

To simulate operating conditions, the PID-s affected module was mounted at 30° tilt angle in natural sunlight. A variable resistive load was used to set module current and voltage. IR imaging (see Figure 2-28b) with the module operating close to maximum power (MPP) condition is in good accordance with EL imaging Figure 2-29b, but with the PID-s affected cells warmer instead of darker in the EL image. At open circuit conditions (Figure 2-28c) no pattern appears and at short circuit (Figure 2-28a) reverse bias operation of cells dominates the pattern. IRT patterns may differ if - instead of a resistive load - an active power source is applied, as it is also the case in string connected modules under string MPP operation (Figure 2-29), because the modules are never affected homogeneously by PID-s, and therefore have different IV-curves and operating points.

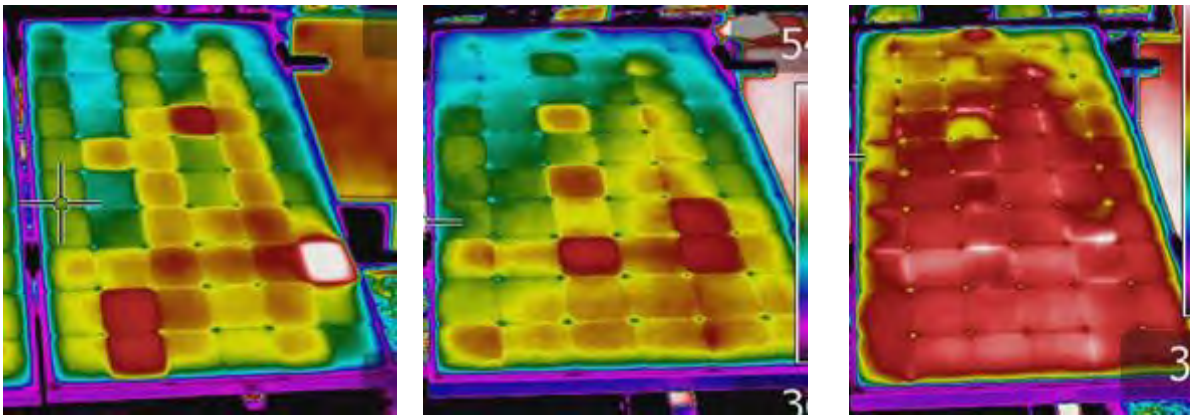

a) I = 7.3 A; V = 0 V *b) I = 6.6 A; V = 22 V* *c) I = 0 A; V = 30 V*

Figure 2-28: IR thermography of a PID affected module (same as in Figure 2-27) under sunlight conditions (approx. 900 W/m²):
a) Short circuit: one hot cell (white) in the right column is not PID-s affected, the cell is overheated by reverse biasing due to lower I_{sc}. b) Close to MPP: the IR image is in good agreement with the EL image. c) Open circuit, the cell temperature distribution is homogeneous and PID-s is not detectable [53].

Degraded cells are cooler in the IR image, if a current is injected in the dark. But they are warmer in the IR image, if the module is operating in the sunlight close to maximum power point conditions. In the first case (dark IR image) the cells are heated by the applied current with the heating power $P = I\,V$. The higher the voltage at each cell, the warmer the cell is. The PID-s affected cell has a lower voltage and is cooler. In the second case (sunlight IRT image), the cells are heated homogeneously by the sunlight and, due to the photovoltaic conversion, the power $P = I\,V$ is absorbed by the load. This cooling effect is lower for PID-s affected cells so that these cells are warmer in the IRT image of the module.

The main field method to detect PID-s affected modules is to prepare IRT images under clear sky conditions during operation [54], [55], [56]. In Figure 2-29, a PID-s affected PV array is shown. For the modules close to the negative pole, power loss and number of warm cells in the IRT image are in good agreement. The string-position depending IRT patterns are a clear indication for PID-s affection of the system.

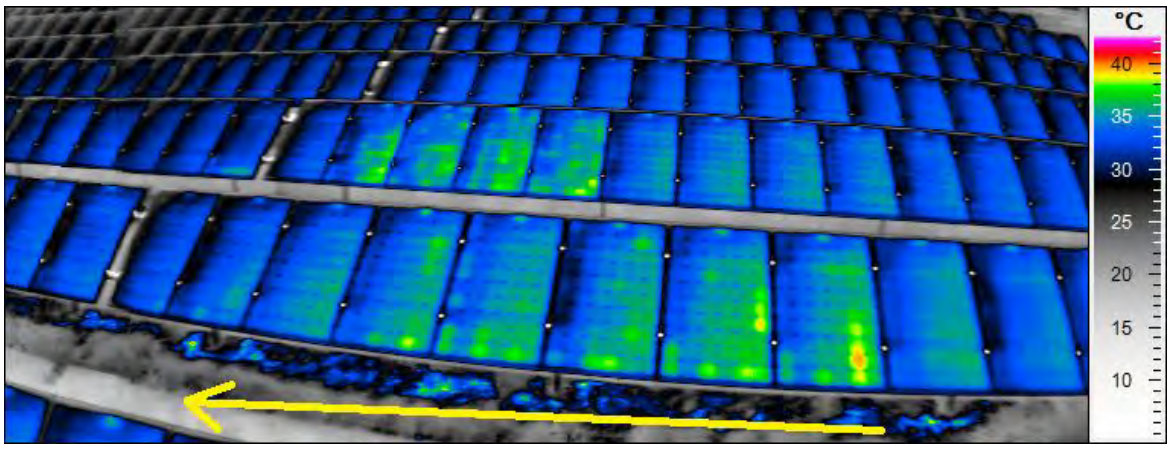

Figure 2-29: IRT image of a PID affected system under sunlight conditions. The modules in the foreground show PID patterns with warmer cells close to the bottom frame. The power

of the modules (nominal power 225 Wp) from the negative pole is (see arrow from right to left): 188 Wp, 187 Wp, 190 Wp, 181 Wp, 199 Wp, 207 Wp, 212 Wp, 220 Wp [57].

Another IR thermography field method is to apply a current into one string at night (see Figure 2-30). As described in Figure 2-27, the PID-s affected cells are cooler than the non-affected cells. No reflections and shadows due to sunlight disturb the measurements. The effort is the same as for outdoor EL imaging, and both methods can be done simultaneously.

Figure 2-30: IRT image of a PID-s affected rooftop system with applied current during the night. In this case, the cooler cells are the PID-s affected cells [58].

2.3.3 Recommendation for analysis

The analysis of the IR images should be done by qualified personnel using special IR analysis software. As orientation for personal qualification, the ISO 9712 Level 2 can be named, as also described in IEC 62446-3 TS Ed.1 – Part 3. In any case the personal should have detailed knowledge of thermal imaging techniques as well as of PV system behaviour and module design.

IR software

In small PV systems or as a sample, a quick analysis can also be done in the field using the firmware installed in professional IR cameras. For efficient IR inspections of larger PV installations with a higher number of modules (above 100 kWp) the application of IR software for PC in the office is recommended. In most cases, the software is strictly linked

to the camera's manufacturer and its unique IR file format. Only a few versions of IR software can be used to open all IR file formats.

Most basic IR software already provides the sufficient features for image analysis, which are:

- Altering of emissivity and reflected temperature
- Altering the colour scale by type, level and span
- Setting spot, linear and area measuring fields with mean, cold and hot spot temperature values.

IR image analysis procedure

The analysis procedure can be divided into three parts. Firstly, IRT images and digital pictures must be sorted and matched to the location, especially according to the string plan. If every module can clearly be identified from the IR image and from the digital picture at the string plan, the qualitative analysis can start. Within the qualitative analysis, the images are scanned for thermal patterns showing known system or module defects such as substrings in open circuit condition. If further abnormalities are detected, which cannot clearly be identified and evaluated on the basis of their quantitative thermal patterns, a qualitative analysis is necessary. The quantitative analysis cannot exactly be separated from the qualitative analysis. Also, the qualitative analysis has a quantitative aspect as during the qualitative analysis the span of the colour scale should be linearly altered with the efficiency of the module and the irradiance. In most cases, a scaling of the relevant colours of around 20-30 K temperature difference (span) for a module efficiency of 15 % at 1000 W/m² is useful. For a module efficiency of 10 % at 750 W/m², a span of about 10-15 K is recommended.

Quantitative interpretation of abnormal thermal pattern

If the colour scale itself does not provide sufficiently clear information about a thermal pattern, the temperature measuring functions of the software should be used to better identify temperature rises and differences. Functions such as the spot measuring tools can be set on local abnormal connection sockets or idling points, for example. Polygon measuring fields can be set on cells, modules or up to whole module strings. The correct setting of the measuring fields on abnormalities and reference areas needs some experience of the IR camera user. In skilled hands these tools can show many complex module or system defects down to just about 1 K of temperature rise. And it can be used for plausibility checks of potentially known defects, as shown in the following example (see Figure 2-31). In any case, the measuring of temperature differences of just about 1-2 K should be interpreted with good care as there are many misleading effects within PV array, such as different convective cooling or emissivity effects that may significantly exceed a signal of 1 K.

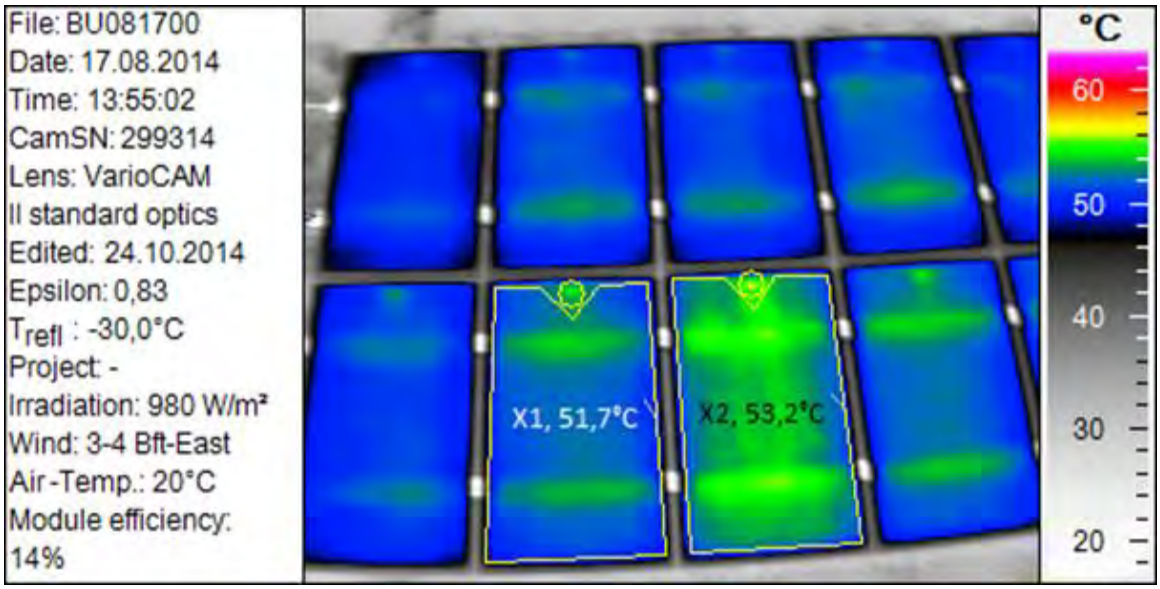

Figure 2-31: Example of plausibility check by determining the mean value of the temperature over the entire module excluding the junction box. In this example, the small temperature rise of 1.5 K was due to a different emissivity of the back sheet used for the two modules.

In Figure 2-31, a module is shown with a measured temperature rise of 1.5 K compared to the neighbouring PV module. As the module efficiency is 14 % and the IRT image was taken at an irradiance of nearly 1000 W/m², a temperature rise of a disconnected module of around 5 K would have been expected, see [44]. Therefore, the temperature measurement as plausibility check proofs that the module cannot be in open circuit conditions. In this case, a different back sheet material with lower emissivity was responsible for the temperature rise on the front side.

2.3.4 Recommendations for action

After detection and evaluation of thermal abnormalities (s. also Chapter 2.3.3) the following basic actions are recommended:

Normal temperature behaviour

- A temperature gradient of a single solar cell smaller than 10 °C is normally considered as unproblematic and will not be listed separately.

Heated cells

- The temperature gradients in a range of 10°C to 20°C are unproblematic in the current stage, although they may increase during the operation of the PV power plant.
- The modules should therefore be observed closely in regular thermographic inspections.

Hot spots

- Temperature gradients above 20 °C are expected to cause degradations of panel output; in extreme cases, the material compound may even degrade, resulting in a safety issue during maintenance work. Further increase in temperature gradient is expected during the operation phase of the PV power plant if the modules are not replaced.
- The modules should therefore be replaced.

Activated bypass diodes (modules)

- A permanent activated bypass diode leads to a minimized power output of the affected solar cell string and thus to a reduction of the total power output of the plant. Modules with active bypass diodes should be substituted.

Pattern

- If one module or several modules connected in series have a higher temperature, the modules may not be connected to the system and the wiring should be checked.
- Warmer cells close to the bottom frame patchwork pattern are strong indicators for PID-effects. The root cause for this pattern should be further investigated as described in chapter 2.3.2.

Due to normal tolerances in cell sorting and module production, thermal abnormalities of less than 10 % of the recorded modules do not indicate a special quality issue regarding the used modules.

If more than 10 % modules show thermal abnormalities, the reason for that behaviour should be evaluated. The behaviour could be caused by quality problems of the modules as well as planning, installation, maintenance or operation faults of the PV plant.

Critical thermal abnormalities should be followed up as soon as possible.

For warranty claim of the supplied modules the first IRT should be conducted when commissioning the PV plant. If the PV modules of the system are not cleaned and maintained at a suitable frequency, high temperatures of some cells or modules could occur due to bird droppings or power mismatch for a long time which may lead to module damage. At a later stage it might be difficult to evaluate whether the damage was caused by quality problems or by missing cleaning and maintenance procedures.

3 Electroluminescence Imaging

3.1 State-of-the-art of electroluminescence imaging

3.1.1 Review of existing standards/guidelines

Investigations of PV modules benefit from infrared (IR) and electroluminescence (EL) imaging techniques, and both are widely used indoors and outdoors. So far, no international standards exist for their quantitative interpretation within the International Electrotechnical Commission (IEC), only draft versions are currently under development.

The IEC technical specification [59] specifies methods to capture electroluminescence images of PV modules, process images to obtain quantitative descriptors, and provide guidance to qualitatively interpret the obtained images. The standard is applicable to PV modules measured indoors in forward bias condition, i.e., by forcing current flow with a power supply where the leads are connected to those of the same polarity on the sample. However, similar technical issues do arise also in the field, where EL imaging of strings of PV modules could nowadays be performed using special tripods or drones.

Camera detectors are typically charge coupled devices (CCD) or complementary metal oxide semiconductor (CMOS). They may be cooled, usually with thermoelectric cooling, to achieve better signal to noise ratio by means of reducing device dark current originating from thermally generated charges. Relevant parameters in choosing detectors include number of pixels, noise, quantum efficiency at the wavelength of interest, and dynamic range. Silicon detectors are very often used and, for special applications, InGaAs detectors are employed. The following three resolutions for are defined for application in practice to compare EL images:

(A) Less than or equal to 0.2 mm
(B) Less than or equal to 2.0 mm
(C) Less than or equal to 5.0 mm.

To obtain maximum image resolution and illumination level, the optical axis of the camera shall be placed perpendicularly and as close as possible to the module face to image the solar cell or module area. This is easy to be achieved in the laboratory, see e.g. Figure 3-1 for a photo of a typical experimental setup, but it is quite problematic in the field. To overcome this issue, some companies have developed tripods to be anchored to the frame of photovoltaic strings that can support the EL camera almost perpendicular to the photovoltaic modules. In the case of drones, on the other hand, orthogonality is almost impossible and this might affect the focus and the sharpness of the acquired image.

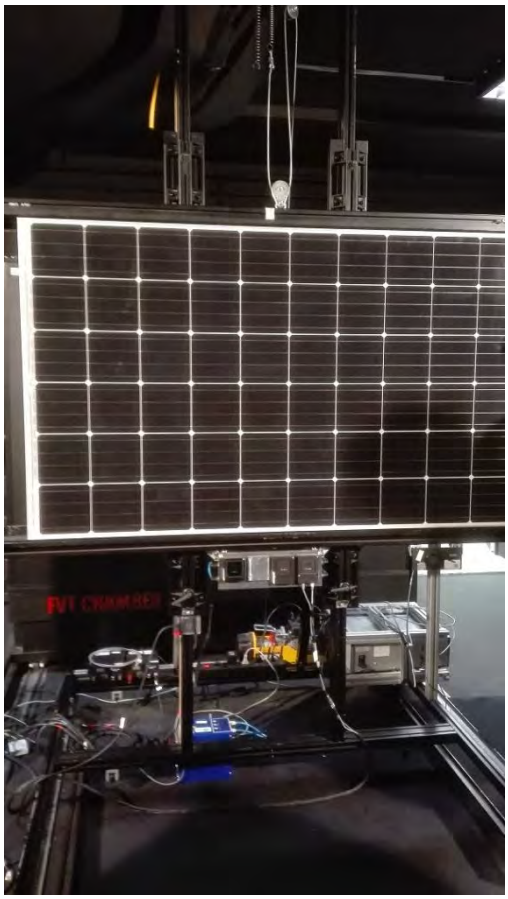

Figure 3-1: Photo of a typical experimental setup for EL tests in the laboratory, taken in the PV lab at SUPSI, Lugano, Switzerland.

Lenses must be free of absorption filters or coatings that remove the infrared near the band-gap of the semiconductor material to be examined. Filters on the camera lens may be used to help cut light of extraneous wavelengths from being detected. In such a case, 850 nm to 950 nm long-pass filters may be used when imaging near band-edge EL from silicon.

High quality images favour darkened environment. Precautions should be taken to eliminate stray light entering the imaging studio, such as with use of hard walls, curtains, baffles, and sealing of any gaps with material that are of light absorbing nature (black). Fixed mounting of the camera and a mounting rack for PV module(s) to be imaged are used so that the camera and the module positions are stable, with a pre-selected distance between each other, see Fig. 3-1. In the field, an option is to use curtains supported by a frame to cover the camera and the photovoltaic module. Alternatively, images have to be taken at sunset or during night.

An electric DC power supply capable of applying I_{sc} of the module or a series string of modules of interest is required. The power supply must be able to provide sufficient voltage to achieve I_{SC}. Depending on the module technology, the required voltage may be approximately equal to the open circuit voltage V_{OC} of the module. Computer control of power supply and camera so that pre-programmed currents can be quickly achieved and coordinated with image capture are optional equipment that will provide speed and

improve accuracy of the imaging of module EL. In the field, this operation has to be done by technicians, or using wireless control methods, if the installations have been equipped with such a facility. The image is transferred electronically from the camera to a computer for display and image post-processing.

A first, rough focus, may be performed by viewing in the visible light regime, but fine focus shall be optimized to the wavelength of the EL signal to be imaged. The usage of a strong diffuse IR light source in the 950 nm -1000 nm wavelength for the initial focusing is highly recommendable, however, care must be taken that there are no direct light source reflections towards the camera. Focusing in the field can be very problematic if fixed supports or tripods able to maintain the distance of the camera from the PV module are not used, as in the case of drones. Moreover, in the latter case, vibrations due to the imprecision of the global positioning system could affect the sharpness of the taken images.

The imaging laboratory temperature shall range from 20°C up to 25°C. Temperature, for reporting purposes, should be obtained with a thermocouple adhesively attached to the module rear. For measurements performed in environments outside this temperature range, the measurement temperature shall be additionally noted as being performed outside of the standard testing condition. This complexity should be considered in the field, where the control of ambient temperature is not possible, perhaps by measuring also the temperature via an IR camera. Uniform temperature conditions, for instance by night, should be preferred.

An EL image can be quantitatively interpreted by evaluating the voltage between two points (x_1 and x_2) associated with a series resistance. This voltage is equal to the logarithm of the EL intensities $I(x_1)$ and $I(x_2)$ at those points, multiplied by the Boltzmann constant k and the temperature T measured in Kelvin:

$$dV(x_1,x_2) = kT \cdot (\ln(I(x_1)) - \ln(I(x_2)))$$

While defects such as cracks are seen in EL with an easily recognizable signature pattern, it is not always possible to identify a specific physical phenomenon using EL images taken at a unique forward bias current and temperature. Signals taken at two bias currents and combined with other techniques such as infrared thermography, photoluminescence, or laser-beam induced current methods can be used to further elucidate on EL signal variation across module surfaces.

Statistical processing of EL data can be made by computing the histograms counting the number of pixels having an EL intensity within a certain range. Further processing of those data can be made to determine a probability density function vs. EL intensity plot as in *Figure 3-2 t*aken from [60]. As a general trend, the shift of the probability density function towards lower EL intensities is noticed for PV modules with higher power losses. However, so far it was not possible to establish a clear correlation between frequency distributions of intensities and specific forms of defects or damage in the solar cells. Further research is in progress [61].

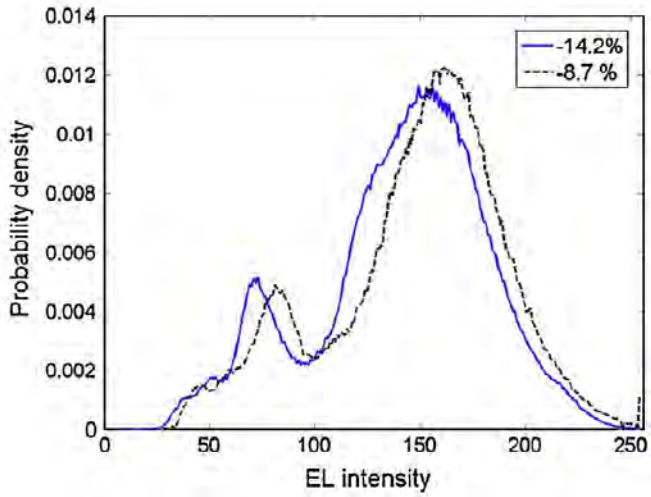

Figure 3-2: probability density functions of the EL intensity derived from EL images of two PV modules with 8.7 % and 14.2 % of power losses, respectively (from [60]*). As a general trend, the probability density function of EL intensities shifts to the right in the case of higher power losses.*

According to [62], EL intensities can also be converted to the current flowing through the solar cells, using a multiplicative factor. Hence, EL images can also be used to extract those current data along the finger directions and correlate them to the predictions of simplified electric models of a mono-dimensional grid line, provided that additional losses at the interface between the silicon cell and metallization are neglected. Examples, also in the presence of cracks crossing the grid line, are reported in [63], [64].

3.1.2 Overview of electroluminescence camera types

Electroluminescence testing, brought to the attention of the PV community by Fuyuki and co-workers in 2005, has become a very popular technique for inspecting PV modules for minority carrier lifetime [65], micro cracks, shunts, and voltage differences [66]. For these measurements a PV module is typically supplied with a DC current in a dark environment and imaged with a camera sensitive to the emission spectra of the material being analysed. There are a number of cameras and products available on the market that are suitable for EL measurements of PV modules ranging from modified DSLR or the closely related “mirrorless” MILC cameras through to dedicated EL systems with a corresponding broad range of specifications.

There are a range of manufacturers in the market that produce cameras suitable for EL applications including thermal imaging, machine vision, spectroscopy and silicon wafer inspection. These are not necessarily specific to the PV industry but consist of cameras and sensor arrays produced for a broad range of end uses. There are two general styles of camera, the line scan camera consisting of a 1D line of pixels and an area camera consisting of a 2D array which is similar to the sensor within modern consumer digital cameras (see Figure 3-3). The line scan camera lends itself to inspection applications whereby the camera moves relative to the module allowing a high resolution image to be built up from consecutive scans. The area camera functions similarly to a standard digital camera and can take a single image of a module or cell.

Figure 3-3: Linescan (left) and area (right) cameras produced by UTC Aerospace Systems [67].

Within these cameras will reside a sensor of a particular variety. There are two varieties of sensors that are commonly used for EL applications which can be made from a range of materials. These are the Charge Coupled Device (CCD) and the Complementary Metal Oxide Semiconductor (CMOS). Variations of sensor type and optimisation have resulted in a number of sensors and products with differing resolution, sensitivity, spectral response and cost. It should be highlighted that the CMOS and CCD are differing designs used in imaging sensors, but are not directly responsible for absorbing the incident photons.

The key specification for EL camera systems is derived from the need for the camera to be sensitive to the emission spectra of the material being tested. For a crystalline silicon solar module the emission spectra has a peak at 1150 nm [65], while for other technologies such as organic PV the emission peak resides at a longer wavelength (1200 nm – 1400 nm) [68]. Figure 3-4 shows a range of emission spectra for different technologies with crystalline silicon modules showing a distinct peak at 1150 nm. Of the thin-film technologies, CIGS is fairly similar to crystalline silicon, amorphous silicon and micro-morph tandem cells tend to have a broad EL emission spectra, while CdTe has a emission peak at a much shorter wavelength of 830 nm [69].

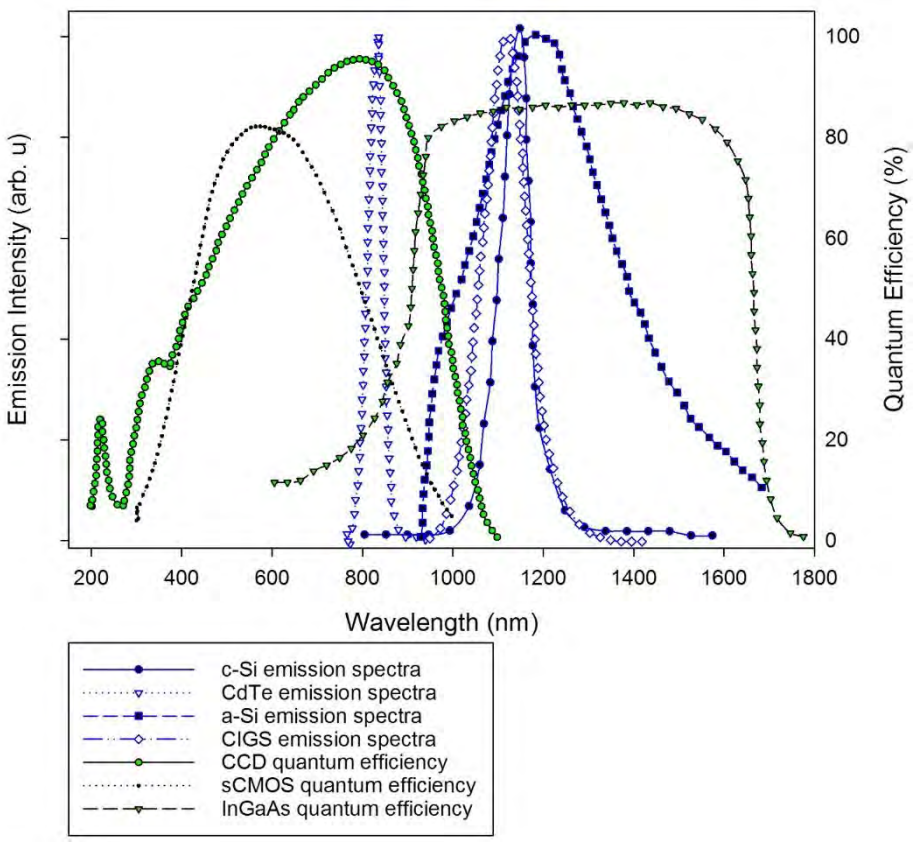

Figure 3-4: Emission spectra from a range of solar cell technologies and the quantum efficiency of silicon CCD, CMOS and InGaAs CMOS cameras.

Figure 3-4 also shows the quantum efficiency curves of several styles of sensor from ANDOR's range of cameras used for EL measurements [70]. Silicon based CCD and sCMOS cameras response curves only partially overlap the silicon and CIGS emission peaks and would have a low response to emission in this part of the spectrum. However, InGaAs has greater quantum efficiency in the long wavelength portion of the spectrum and is more sensitive in this region. Regardless of the sensor type being used, the sensors in most of these systems are thermally insulated from the environment or actively cooled to reduce thermal noise.

The silicon CCD was the sensor first used when EL was brought to the attention of the PV community [65], tends to be very popular and are is used [65], [66], [68], [69], [71], [62] due to their relatively low cost and high resolution. For experimental systems with high resolution and reduced cost, modified DSLR cameras have been used by removing the inbuilt IR filter [69]. These sensors have multi megapixel resolution sensors which allow fine detail to be captured and the entire module to be photographed in one picture. As described earlier, the three resolutions for intercomparison of EL images that are defined for application in practice are:

(A) Less than or equal to 0.2 mm
(B) Less than or equal to 2.0 mm
(C) Less than or equal to 5.0 mm.

The high pixel count of the silicon CCD combined with good optics helps enable a finer spatial resolution in the image. The downside of the silicon CCD for EL measurements of crystalline silicon, amorphous silicon and CIGS based PV modules is that the silicon CCD has poor quantum efficiency beyond 100 nm as shown in Figure 3-4.

A smaller bandgap semiconductor material such as InGaAs has greater quantum efficiency in the longer wavelength part of the spectrum when compared to silicon and covers the full emission spectra from silicon [72]. This makes it a good candidate for EL imaging of crystalline silicon with reduced noise and greater sensitivity. InGaAs semiconductors are typically used within CMOS style sensor and sensor arrays. With this increased sensitivity, InGaAs CMOS sensors allow much faster data acquisition but tend to have much lower pixel counts and a correspondingly smaller resolution. While InGaAs are the most common variety of CMOS sensor used, there are conventional silicon CMOS sensors and modified waveband sCMOS sensors which have also found application in EL imaging and are produced by several manufacturers. Particularly low cost EL imaging systems have been built based on a RaspberryPi single board computer and its accompanying NoIR camera board which includes a Sony silicon CMOS 8 megapixel sensor.

It has been shown [73] that a relative simple modification enables consumer DSLRs to perform EL imaging and more recently [74] non-Reflex, mirrorless interchangeable lens cameras with large sensors can also be modified for EL application. These systems feature resolutions of ~20 Megapixel at a cost of less than 2k€, while having a typical exposure time of 15 to 30 seconds per image. The modification consists of the removal of a UV-IR filter adjacent to the camera sensor, and is regularly performed by specialized companies, as these cameras can also be used for astro and art photography. And these modified MILC EL cameras can achieve comparable signal to noise ratio images, albeit with longer exposure times [74].

The type of sensor within the camera determines many of the other specifications such as the spectral band, sensitivity and resolution. A representative, but not exhaustive, list of EL cameras currently available are shown in Table 3.1.1.

Table 3.1.1: An example list of cameras on the market that are suitable for use in EL imaging of PV modules.

Manufacturer	Model	Camera Type	Sensor Type	Resolution	Dynamic Range	Type of Cooling	Target Size (mm)	Size (mm)	Weight
Andor	DU491A	Linescan	InGaAs CMOS	1024		Thermoelectric		155x101x100	2kg
Hamamatsu	C10633-13	Area	InGaAs CMOS	320x256		None		50x50x50	0.23kg
Hamamatsu	C12741-11	Area	InGaAs CMOS	640x512		Thermoelectric w/ forced water		189x108x110	3.4kg
NPC group	EPTiF	Area	InGaAs CMOS	320x256					
UTS Aerospace systems - Sensors Unlimited	320KTS	Area	InGaAs CMOS	320x256	2500:1	Room Temperature		65x53x53	0.27kg
UTS Aerospace systems - Sensors Unlimited	GA1280IS	Area	InGaAs CMOS	1280x1024	1500:1	Room Temperature		42x41x41	0.235kg
UTS Aerospace systems - Sensors Unlimited	1024-LDM	Linescan	InGaAs CMOS	1024	4500:1	Room Temperature		76x74x61	0.45kg
Xenics	Bobcat-320-Gated	Area	InGaAs CMOS	320x256		Thermoelectric		72x55x55	0.285kg
Andor	Clara Interline CCD Series	Area	Si CCD	1392x1040	6500:1	Thermoelectric		127x112x96	2.2kg
Andor	PV Inspector	Area	Si CCD	1024x1024		Thermoelectric		208x105x64	2.2kg
Camels	MT-EL-H1709M	Area	Si CCD	1392x1040		Thermoelectric w/ forced air	2,000x1,100 / 1,700x1,000	730x465x465	150kg
Camels	MT-EL-H1708M	Area	Si CCD	1392x1040		Thermoelectric w/ forced air	200x200	Custom	
Camels	MT-EL-H1708I	Area	Si CCD	1392x1040		Thermoelectric w/ forced air	200x200	130x125x55	
Camels	MT-EL-H1709I	Area	Si CCD	1392x1040		Thermoelectric w/ forced air	2,000x1,100 / 1,700x1,000	130x125x55	
Chinup technology	EL-MT01M	Area	Si CCD	1640x1130					
Greateyes	LumiSolarCell	Area	Si CCD	2048x2048			200x200	1120x715x600	60kg
Greateyes	LumiSolarProfessional Inline	Area	Si CCD				2000x1000	2200x2200x1400	
Greateyes	LumiSolarProfessional	Area	Si CCD	up to 12,000x20,000			2000x1000	2460x1400x1200	250kg
Greateyes	LumiSolarOutdoor	Area	Si CCD	2048x2048					40kg
Hamamatsu	ORCA II	Area	Si CCD	1024x1024		Air or water cooled		215x110x76	
PCO	Sensicam qe	Area	Si CCD	1376x1040		Thermoelectric w/ forced air		210x93x78	1.6kg
PCO	pco.4000	Area	Si CCD	4008x2672	5455:1	Thermoelectric		195x135x51	1.9kg
Various	Modified SLR	Area	Si CCD	Various		None		Various	Various
Andor	Zyla 4.2 PLUS	Area	Si CMOS	2048x2048	33,000:2	Air or water cooled		133x82x80	1kg
Sony	Raspberry Pi NoiIR Camera	Area	Si CMOS	3296x2512		None		25x23x9	0.003kg

The choice of the type of EL camera that is used when imaging PV modules is dependent on a range of factors. As with many types of camera equipment there is trade-off between cost, resolution and sensitivity. For example, silicon CCD cameras tend to have a higher resolution and lower cost than InGaAs CMOS sensors, but are not as sensitive to the crystalline silicon emission spectra. While their high resolution makes silicon CCD sensors a popular choice, the InGaAs sensor would have a significantly greater sensitivity to crystalline silicon and some thin film technologies. A silicon CCD however, does match very well to the CdTe emission spectra and would be the recommended camera type for this application. Despite the differing levels of sensitivity, with appropriate data collection intervals and methodologies, such as longer exposure times, filters and active cooling of the sensor, either camera type can be used for EL imaging of PV modules. This allows a great deal of flexibility in terms of the equipment used, but does make standardization of test images and measurements a challenge.

3.1.3 Evaluation of existing practice

The typical camera for EL imaging features multiple settings for imaging, e.g. the focus, aperture, zoom, ISO, exposure time, and storage file bit depth.

If the aperture value is very low (e.g. f/2.4), the iris of the lens is fully open, allowing a lot of light to pass through. This fact lowers the required exposure time and when, the non-ideal parts of the lens system are participating, the image is less than ideal: a radial decrease of the image brightness will occur (vignetting). The focus plane will change in distance with the radius from the image centre. Furthermore, small deviations from the ideal distance of the object will cause a visible blurriness (“Depth of field”). These issues are very important in the field, where the PV modules are often not perpendicular to the EL camera.

To improve camera focusing, as a small deviation of the ideal focus setting is recognizable visually or algorithmically. However, for performing the actual image acquisition, it is recommendable to increase the aperture value by one or two set points (“stops”), to increase the depth of field and sharpness [75].

The focus should be at a distance that averages the minimum and maximum distance of the camera from the object, in order to centre the depth of field. While this is hardly a challenge for ideally positioned modules in the laboratory, typically, multiple modules are imaged at slanted angles in the field, see *Figure 3*-.

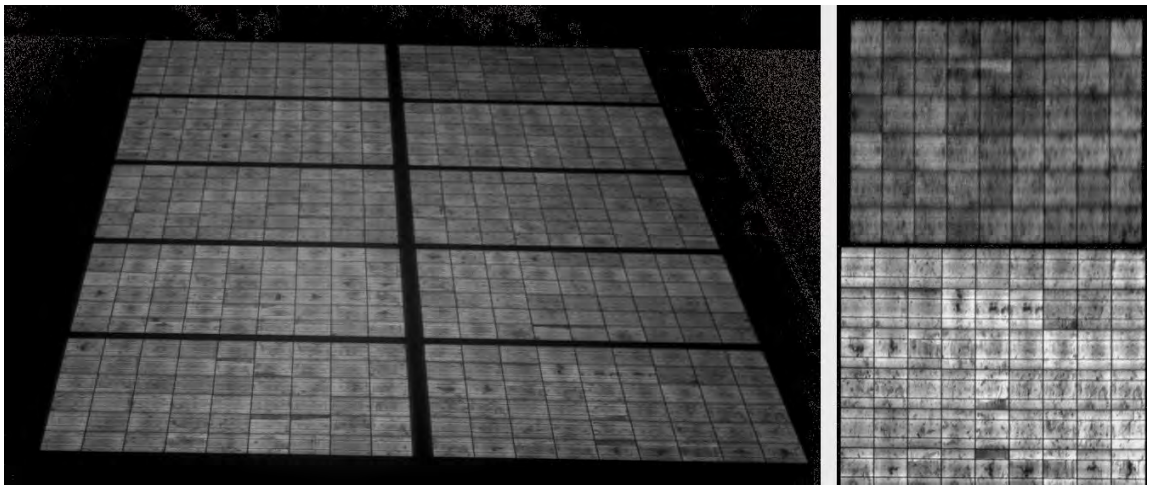

Figure 3-5: An outdoor EL performed with a consumer DSLR. The focus was performed on the front modules. Hence, as depicted to the right, only the front row can be imaged correctly, while one of the upper modules (right, top) is very blurry.

The ISO value is an amplification level between the pixels photon created charge and the pixel brightness. For low large amplifications, the statistical deviation of photons captured (Poisson distribution) is visible as noise in the image. To improve the time required to focus it is useful to decrease exposure time to e.g. 5-10 seconds with a very high ISO. For final image acquisition, a value should not be larger than 400 typically.

It is highly recommendable to store pictures with a format of more than 8 bit per colour channel. Typical cooled system feature 16 bit resolution, while consumer DSLRs or MILCs are typically limited to 14 bit in RAW files. The main benefit is that brightness corrections can be done without decreasing essentially the quality in the post processing. Additionally, local overexposures (e.g. at cracked cells where the current density is very high) can be often resolved. By acquiring multiple pictures and averaging them, the effective noise can be decreased [76]. Additionally, the removal of dark frames is common practice in digital astrophotography or lock-in thermography.

With DSLR or MILC EL measurements, the ambient brightness plays an important role, however humans are badly equipped to measure absolute brightness, due to the partially chemical compensation within the retina [77]. A good rule of thumb is that proper EL exposures start at a brightness where reading a book gets difficult (approximately ~50 mW/m^2). These conditions are often met one hour after typical sunset.

3.2 Test requirements

3.2.1 Camera requirements

While there are a broad range of different EL cameras and camera styles, three main classes and the related typical parameters are defined in

Table 3.2.1.

Table 3.2.1: General camera requirements.

Camera parameter	**Lower class**	**Medium class**	**Professional class**
Type of sensor	CDD	CMOS/CDD	CMOS/CDD
Resolution (CDD) (CMOS)	<1 megapixel	1-5 megapixel 320 x 256	>5 megapixel 640 x 512
Sensitivity (dynamic range) (exposure time)	2500 : 1 >10 s	5000 : 1 1-10 s	10000 : 1 <1 s
Spectral band	Si (0.3-1.1)	Si (0.3-1.1) InGaAs (0.7-2.6)	Si (0.3-1.1) InGaAs (0.7-2.6)
Test conditions	twilight/night	twilight/night	lowlight/night

Type of sensor

CCD (charge coupled device) and CMOS (complementary metal oxide semiconductor) image sensors are two different technologies for recording EL images. Each has its own strengths and weaknesses, e.g. exposure time, resolution. The CDD sensors are usually made of silicon materials, the CMOS sensors consist of silicon or InGaAs materials as described in chapter 3.1.2. Depending on the material, the Quantum Efficiency of the sensor is defined (Spectral band).

Resolution or number of pixels

Images recorded with an EL camera have a specific resolution. Depending on the detected EL abnormality of a PV module, a higher resolution might be necessary in order to identify the failure cause. Higher resolution images also allow pictures to be taken from a further distance and thus capturing a greater number of modules per image.

Sensitivity

The sensitivity represents the performance of the camera. This includes the capacity to differentiate between the signal and the surrounding noise. The Signal-to-Noise Ratio can be improved by increasing the Quantum Efficiency of the sensor (Spectral band) or/and by reducing the sources of noise (Cooling).

Spectral band

The camera sensor has to be sensitive to the emission spectra of the material being tested, e.g. c-Si, CdTe, CIGS, etc. The Quantum Efficiency is related to the ability of the sensor to response to the signal. Only with overlapping bands the sensor is suitable for the material to test. The Quantum Efficiency can be further improved by applying additional coating or lenses.

Type of cooling

In order to reduce the noise, which increases with longer exposure times, the camera should be cooled. Deep-cooling is required for longer exposure times of more than 10 s. Exposure times of less than 1 s reduce the demand of cooling.

Test conditions

The most EL systems can only be used during the night or low light conditions. Day-light systems have the advantages of higher service availability, but require advanced equipment and image processing.

Size and weight

Depending on the application the size and in particularly the weight of the camera are decisive. Larger and heavier cameras are not appropriate for UAVs, but also for ground-systems should be considered that the handling is feasible with only one person.

3.2.2 Recording procedures

The camera is one part of the complete EL system which can be designed for use in the lab environment with controlled conditions or for outdoor field measurements. For indoor lab based measurements the cameras are used in a range of configurations for small scale measurements through to turnkey EL imaging solutions such as the GreatEyes LumiSolar Professional Inline System [78]. These turnkey systems consist of the power supplies, cameras, enclosures and software required for high throughput inspection of PV modules. Alternatively EL turnkey systems have been designed for use outdoors for field inspections and tests of PV modules. These systems typically include a camera, portable power supply (battery) and computer. To remove background illumination the measurements using these portable systems are usually conducted at night or with a shroud for the module. The advantage of these styles of systems is they can be deployed in the field to enable in-situ inspection of PV modules without having to relocate them to a test facility. These manual

systems might lead to a productivity of about 0.2 MWp of inspected PV installations per night.

It can be differentiated between two main approaches for the recording:

1. The ground-level inspection and
2. The aerial inspection.

The ground-level inspection includes fixed EL cameras on portable constructions or smaller hand-held systems. Depending on the size of the power supply single modules or whole strings can be imaged. In order to increase the recording rate the power supply and the string should be interconnected to a multi-box with several inputs and a remote-controlled switch. Thereby the time between each recording can be reduced significantly, increasing the productivity of inspection. For roof-mounted systems a telescopic tripod is recommend with a remote-controlled pivot arm. Due to the not-working autofocus of the EL cameras during night time the distance between camera and modules needs to be measured with a distance sensor, so that the focal length of the camera can be adjusted based on the recorded distance. One example of a ground-level system is the LumiSolarOutdoor produced by GreatEyes [78] and pictured in Figure 3-6.

Figure 3-6: GreatEyes LumiSolar outdoor measurement system for field tests of PV modules.

The aerial inspections can be conducted by the means of EL cameras mounted on UAVs (Figure 3-7). Not all of the EL cameras are appropriate for the aerial operation, since higher sensitivities and lower exposure time are required. Mirrorless full-format cameras are most

recommended for this application. As already mentioned for the ground-level inspections the UAV should be equipped with distance sensor and remote-controlled focal length. A power supply combined with a multi-box is also highly recommended due to the battery-limited flight duration. Furthermore, the angle of the camera should be adjustable and the UAV should include a GPS guided system to determine the position. For these systems, the productivity can increase up to 1 MWp of inspected PV installations per night.

Figure 3-7: EL camera mounted on octocopter [79].

3.2.3 Comments and recommendations

The voltage at one cell can be calculate by the equation derived by Fujuki [62]

$$U = V_T \cdot ln\left(\frac{I}{C}\right), \quad \text{(U)}$$

where VT is the thermal voltage is the EL intensity in counts of the camera detector. Without knowing the calibration constant C it is possible to calculate the voltage difference between two cell parts in a broken cell with lateral homogeneous recombination pattern by the equation

$$\Delta U = V_T \cdot ln\left(\frac{I_1}{I_2}\right), \quad \text{(DU)}$$

where I_1 and I_2 is the EL intensity in counts of the camera detector of part 1 and part 2 of a cell or two cells. If two cell parts show a distinct voltage difference than the maximum voltage difference which could be measure is restricted on the lower level by the noise level of the CCD detector and on the higher level on the maximum counts of the CCD sensor. For a 12 bit camera with a very low noise level the lowest practical noise level is typically higher than 10 counts for typical EL images. For checking the voltage difference the image information at the intensity image part has to be above the noise level. The maximum usable counts of a 12 bit CCD camera are not higher than 3500 counts (85% of 4096). At higher count level the sensor might become non-linear.

Using these numbers (I_1 = 3500 counts, I_2 = 10 counts) at room temperature (V_T = 25.85 mV at 300 K) in Eq. (DU) results in a maximal detectable voltage difference in an EL image of approximately 150 mV. For a 14 bit camera (I_1 = 14000 counts) under the same optimum conditions you might be able to detect a voltage difference of approximately 185 mV. In both cases you must use the full dynamic range the camera at very low noise conditions to

generate the image. If for example the noise level of the camera reaches 30 counts even then a 14 bit camera cannot resolve more than approximately 160 mV. In most practical outdoor cases the noise level is even higher and the initial assumption of homogeneous recombination pattern for multi-crystalline silicon materials is mostly not true.

In the following we discuss how much voltage difference is needed to identify cell cracks with a relevant break resistance causing a power loss. To assess this question we use a electrical SPICE simulation described by Köntges in [80] of a 60 cell module with 230 W_p. The electrical power of the 60 cell module is simulated under STC conditions including one cracked cell with varying cracked cell area and crack resistance. Furthermore, the voltage drop across the crack resistance is simulated under dark forward current conditions as it is done for El imaging. The simulation results are shown in Figure 3-8 for a forward current corresponding to the nominal current I = I_{sc} = 8 A and in Figure 3-9 for a forward current of I = I_{sc}/10 = 0.8 A.

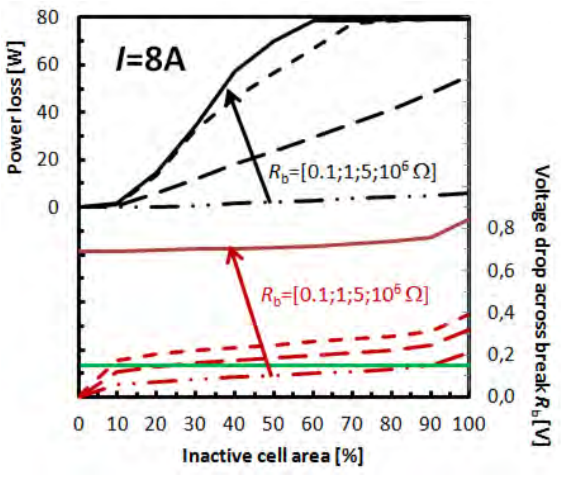

Figure 3-8: Simulated voltage drop across the break resistance of a separated cell part for a 230 Wp PV module at a forward current of 8 A (nominal current of the module). The green line marks 150 mV being able to detect with a low noise 12 bit CCD camera.

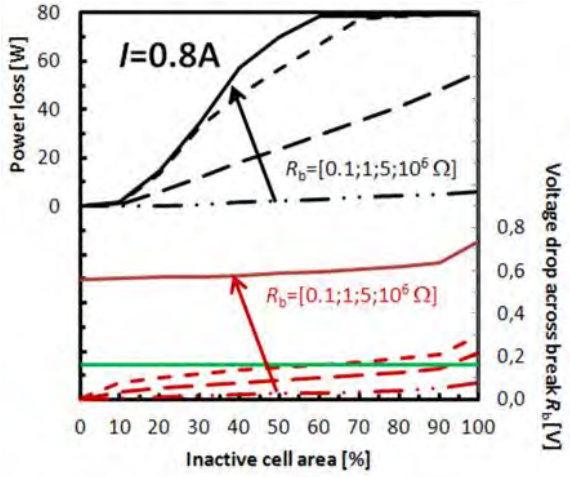

Figure 3-9: Results of same simulation as depicted in Figure 3-8, but calculated for 0.8 A (1/10th of nominal current of the module).

In Figures 3-8 and 3-9, a green line marks the maximum voltage difference being detectable with a 12 bit EL camera. For the 8 A forward current the voltage drop across the break resistance is higher than the detectable voltage drop for all relevant power losses. That means that one detects only noise for a cracked cell part not been able to assess if the broken cell part is power relevant or not. The situation changes for a forward current of I_{sc}/10. Cell parts being below the noise level are in any case relevant for the power loss of the module. These results show why often EL images with putative isolated cell parts do not show the expected power loss in a power measurement.

3.3 Classification and evaluation

3.3.1 Methods of analysis

The EL technique can be profitably applied to detect and distinguish between different failures modes according to the classification proposed in the report [3], Sec. 5.4. The relevance for this type of non-destructive inspection regards the possibility to observe defects and attribute them to the different stages of the PV module lifetime. For instance, defects can be caused by production problems not noticed after quality control, wrong handling of the PV module without enough care during transport or installation, or can be induced by environmental loading and degradation in the field after installation. Clearly, all of these causes might have different implications in terms of warranty claims and operation and maintenance actions.

Although EL images taken on a set of PV modules before their installation could be very useful in case of legal actions against producers, since production defects can be clearly distinguished at that time, EL imaging is usually requested by customers at a much later stage, after detecting an unexpected low power output of their PV parks. In such a case, IR monitoring should be used first to localize PV modules with anomalies that can be unmounted and then shipped to a lab for EL measurements. Alternatively, EL measurements on site without unmounting the module in nearly dark conditions and using a specific instrumentation such as those outlined in the previous section is an option possible with the advent of new EL technologies on the market. However, the amount of time required to take a good quality EL image of a PV module, adjusting the focus and finding the right time of exposure depending on the module type, is often still a limiting factor for large-scale applications of EL imaging in the field.

As an example of analysis of EL images, some results reported in [60] from the inspection of sets of monocrystalline and polycrystalline Silicon PV modules unmounted after three years and a half of installation on a roof and tested in the laboratory using EL imaging are herein summarized. Very often, the complex situation of having the simultaneous presence of different types of cracks and defects in the solar cells makes it difficult to quantify the impact of each abnormality on the overall power losses of the module that can be ascertained from the I-V curves.

This is for instance the case in Figure 3-10, where various defects are simultaneously present. Three cells in the second row from the top of the module present very bright and dark areas, and are caused by temperature dishomogeneities during firing of the solar cells in the production stage, giving rise to a gradient of the contact resistance of the cell-finger metallization from the cell centre to its border. This production problem can also lead to chain patterns, as the one observable in the last solar cell on the right of the fourth row from the top. The fifth solar cell from the left in the second row has a much dimmer EL signal than the others and it is caused by an imperfect connection of the busbars to the solar cell.

In the same image, we also notice a series of other defects. In some cases, defective solar cells with few interrupted fingers are observed. They can be present without cracks (see the last row of solar cells from the top), or can be induced by cracks that have a sufficient crack opening (see the second solar cell from the left on the third row from the top). The

former type of finger disconnection has in general a marginal impact on power losses and it does not substantially degrade with time. Finger disconnections induced by cracks are on the other hand potentially much more harmful. This is for instance the case of cracks almost parallel to busbars that can isolate significant portions of the solar cell (see the fourth solar cell from the left in the last row on the bottom). In other cases, cracks are still partially conductive and, although they are crossing the whole cell, their impact on power losses is almost negligible at the moment the picture was taken (see the first cell on the left in the second row from the top). However, such cracks can propagate and further open after exposure to environmental loading, increasing the power loss by provoking wear out failure modes. Some of those cracks are presumably caused by wrong assembly operations of the PV module, for instance during soldering, with crack tips emanating from points near busbars (see the fifth cell from the left in the third row from the top). In other cases, they are caused by mechanical loads during transportation or installation (see the fourth solar cell from the left in the fourth row from the top).

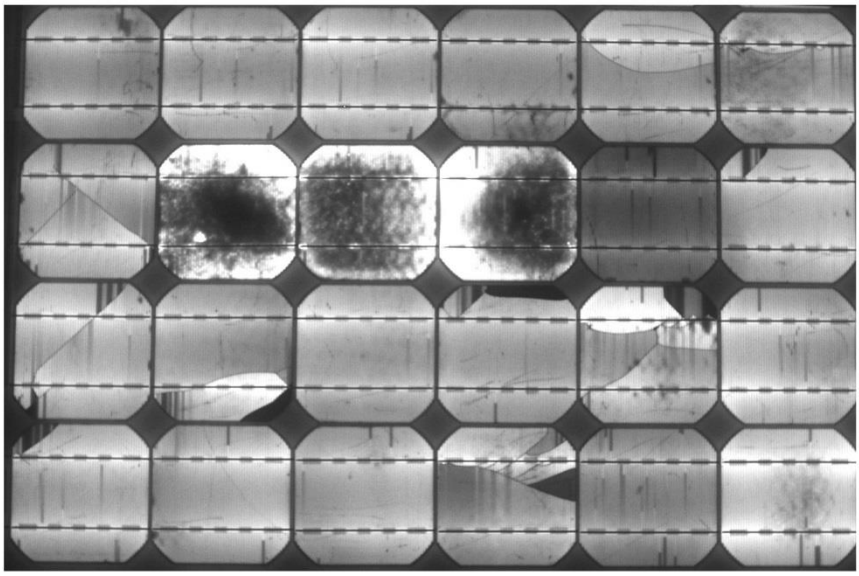

Figure 3-10: EL image of a monocrystalline PV module with various defects (from [60]*).*

In some cases, it is possible to recognize crack patterns induced by impacts. To understand if it is due to an accidental localized pressure applied during installation or by hail impacts, a visual inspection of the module is required. In such cases, branching cracks originate from few centres of impact (Figure 3-11) and have the same pattern as from simulated impact tests performed in the laboratory [81].

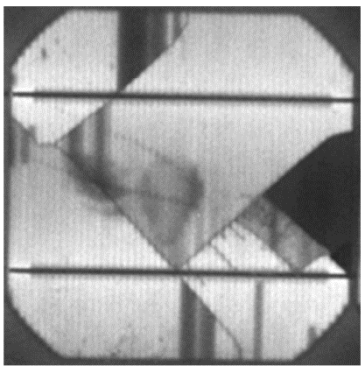

Figure 3-11: EL image of a solar cell with a typical crack pattern due to impacts (from [60]*).*

An example of a wide crack pattern in polycrystalline silicon PV modules is shown in Figure 3-12, with large portions of solar cells electrically inactive. In the case of potential induced degradation (PID), on the other hand, EL images show the appearance of dark solar cells at the boundaries of the PV module, see Figure 3-13.

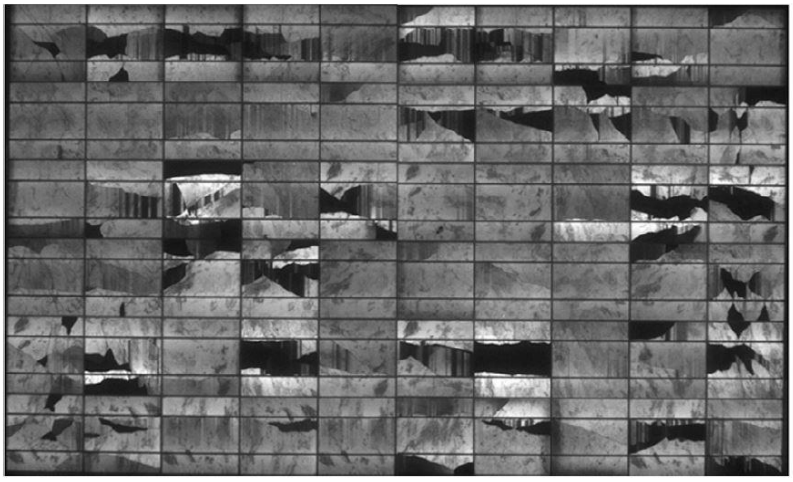

Figure 3-12: EL image of a polycrystalline PV module with cracked cells (from [60]*).*

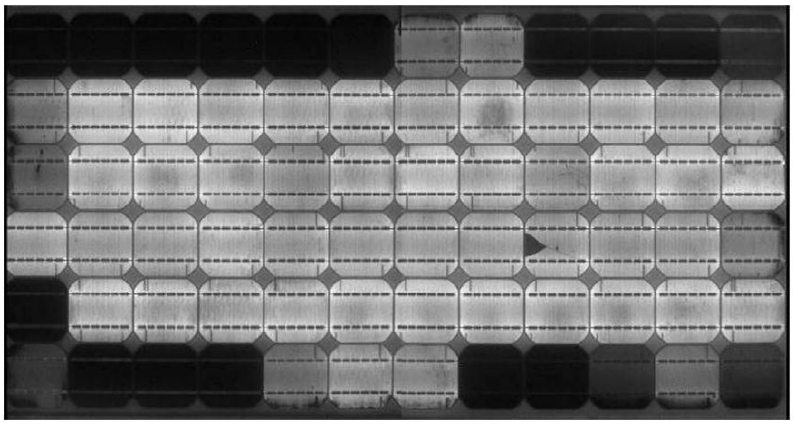

Figure 3-13: EL image of a monocrystalline PV module with potential induced degradation (from [60]*).*

Night-time EL imaging of PID affected modules installed in the field, in a black-white-red colour scheme and using an exposure time of about four minutes, shows current passing through the decreased parallel resistance instead of the PN-junction for the cells near the edges, see Figure 3-14. On the other hand, daylight outdoor lock-In thermography of the same modules affected by PID (whose night-time EL image is shown in Figure 3-14) shows that modules are repeatedly toggled between short and open circuit with a period time of 50 seconds, while a thermography camera observes transient temperature waves at the glass surface. The amplitude of the waves is plotted, white being no thermal change in time, black indicating heat-up of 0.1 K at short circuit, while red indicates heat-up of 0.1 K at open circuit.

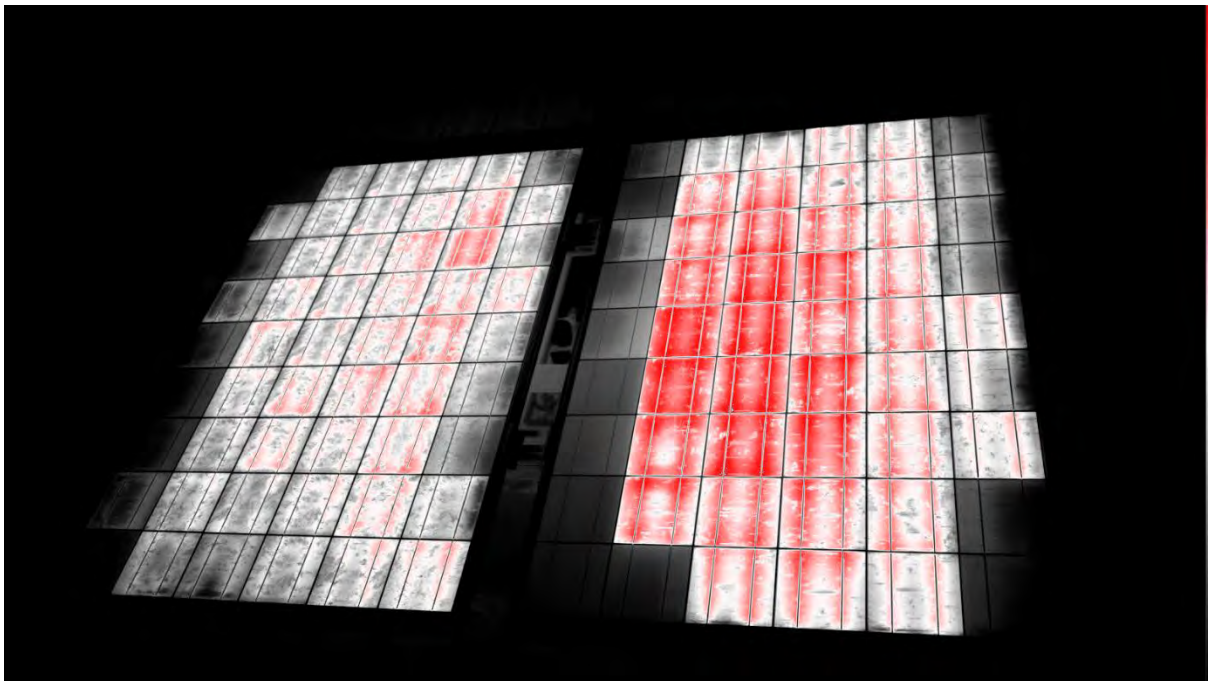

Figure 3-14: Night-time EL using a Consumer DSLR of PID affected modules, in a black-white-red colour scheme. The accumulated exposure time was around four minutes. The darkening of cell edge regions close to the frame can be observed, which is commonly attributed to current passing through the decreased parallel resistance instead of the PN-junction [82].

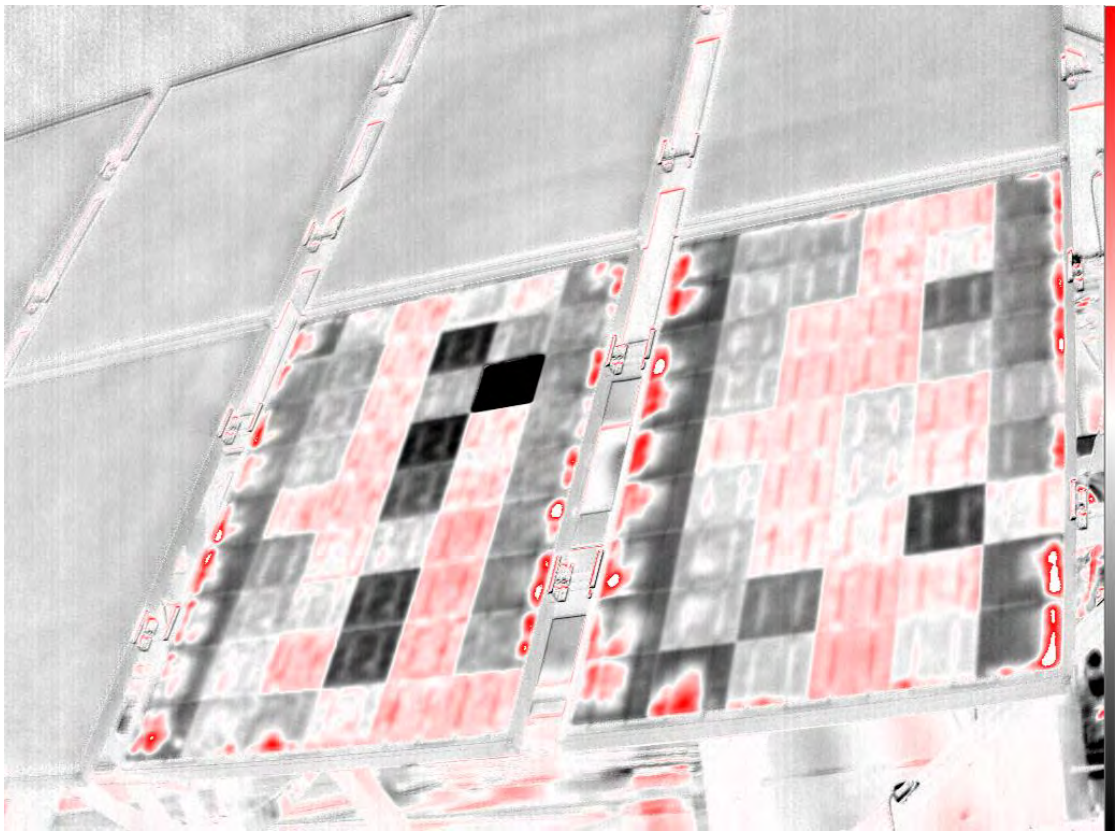

Figure 3-15: Daylight Outdoor Lock-In Thermography of the same modules as in Figure 3-14. The modules are repeatedly toggled between short and open circuit with a period time of 50 seconds, while a thermography camera observes transient temperature waves at the glass surface. The amplitude of the waves is plotted, white being no thermal change in time, black indicating heat-up of 0.1 K at short circuit, while red indicates heat-up of 0.1 K at open circuit [82].

3.3.2 Recommendations for analysis

Electroluminescent (EL) image data provides a rich source of spatially resolvable information pertaining to the health of a PV module. Commonly observed defects and failures contained within these data have been outlined in [3] Sec. 5.4. Using this reference, classification of EL image can be performed by comparison. This qualitative approach has merits for small studies requiring course assessment, however, for large sample quantities or if derived properties are desired, such as electrical properties, techniques for quantitative assessment are needed.

In the present report, Section 3.1.2 describes the types of cameras used for EL imaging and provides a discussion of sensors. Sensors with larger numbers of pixels per unit area typically yield better results for resolving image features, however, depending on the material, noise and quantum efficiency limitations can increase with higher resolution. Though with modern signal processing algorithms and image analysis software it is possible to mitigate a portion of the effects of noise on the resultant images.

Continual development in the areas of signal processing and computer vision have allowed great ease of access to advanced image analysis tools. Freely available open-source versions are available via the Scikit-Image and Opencv projects for the scripting language Python [83], [84]. These softwares provide a full suite of image processing and feature recognition utilities that can be used to perform a variety of EL image analysis tasks [85], [86], [87]. When EL measurements are made in the lab, there is inherently some amount of human induced error in the orientation of the module relative to the camera aperture. Therefore a critical task is to set up a pipeline for processing raw images to uniformly oriented images.

The high-level overview of the algorithm used to perform this task can be seen in Figure 3-16. Using the aforementioned Python packages, an example processing methodology is provided, which has been scaled to process entire libraries of EL image data [88], [89].

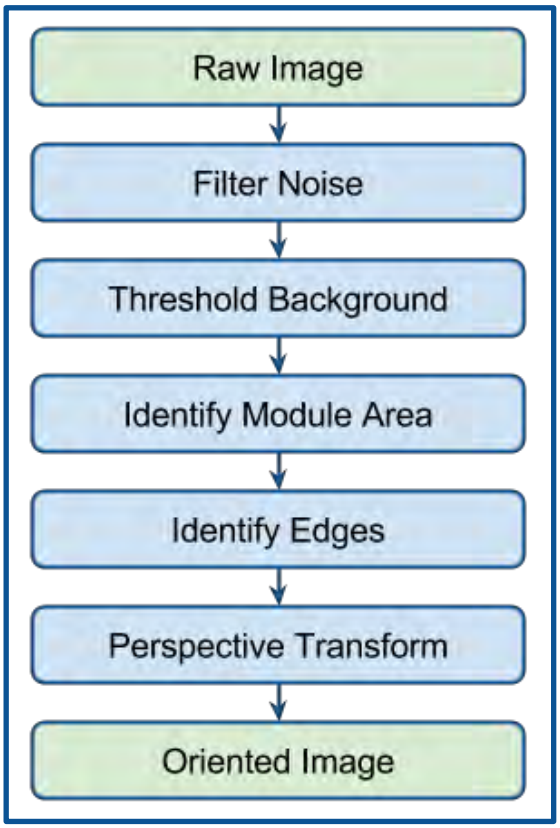

Figure 3-16: A flow diagram for the typical process used to transform raw images to uniformly oriented images.

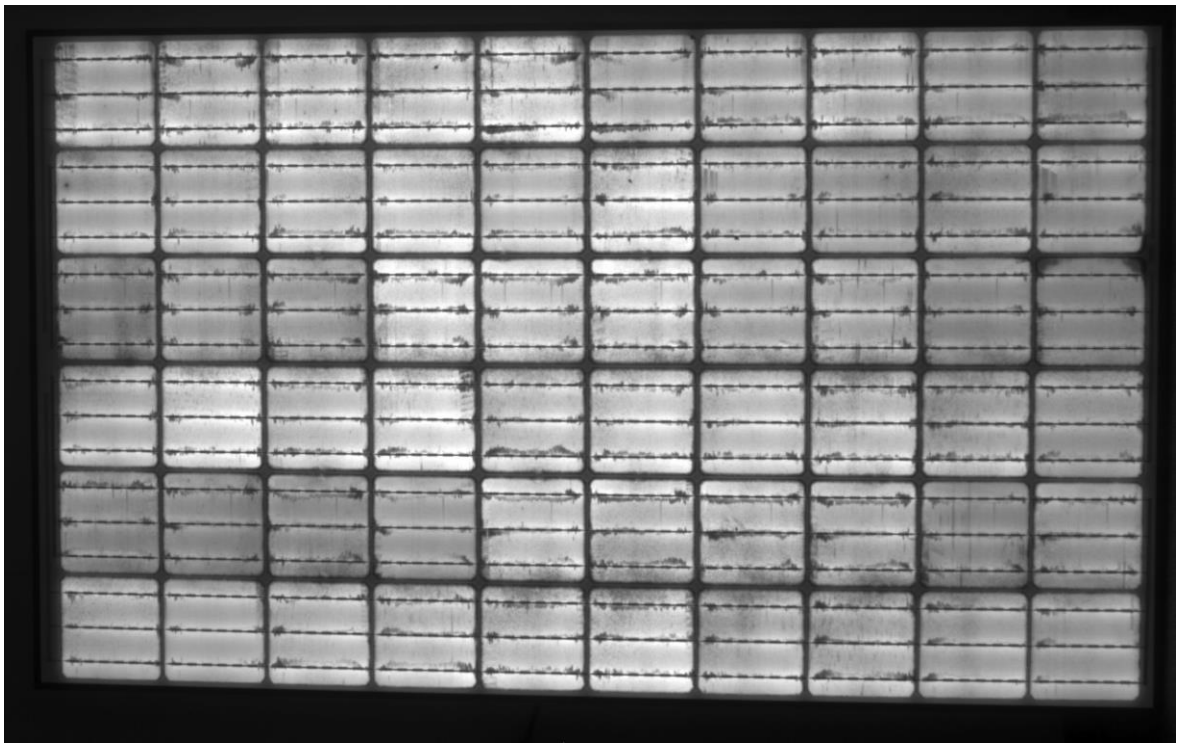

Figure 3-17: A raw grayscale EL image. This particular module has undergone 2500 hours of lab-based accelerated damp-heat exposure [90].

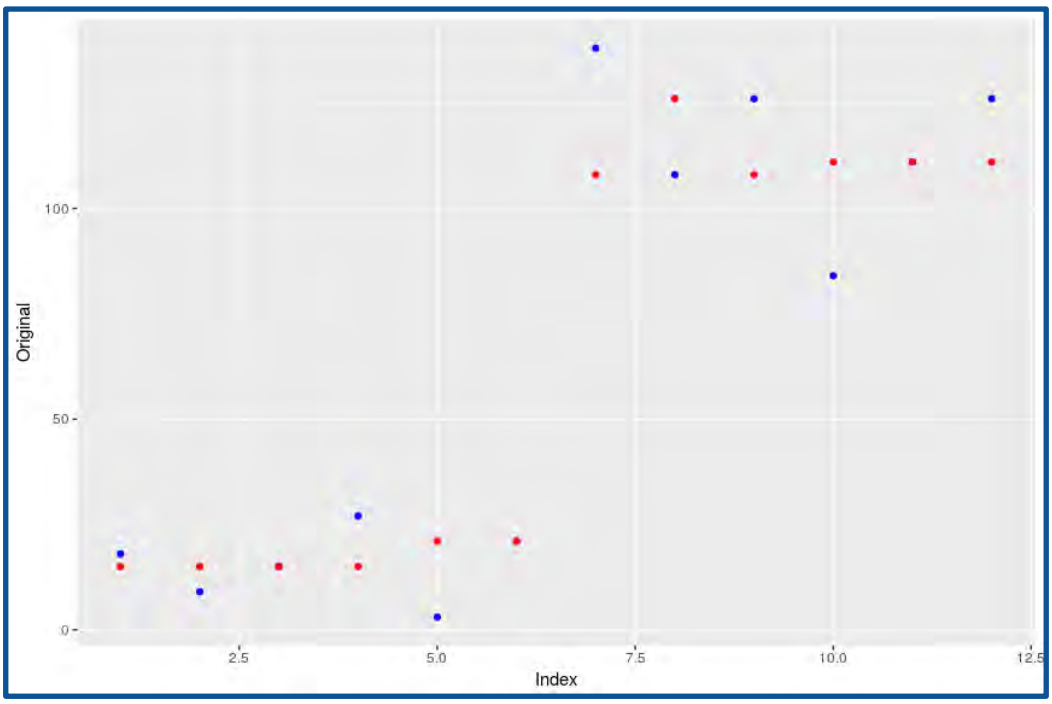

Figure 3-18: A simulated image edge represented as a 1-D vector (blue) and median filter of that vector (red).

The first step is to remove noise in the image. Considering a purpose of identifying features, choosing a filter that retains edges and does perform a global smoothing is appropriate. A commonly used filter for this purpose is the median filter. This is a nonlinear filter, which uses an odd size scanning window to move over the image and assign the middle value contained in that window to the local pixel [83].

With this process visualized it is easy to see that if there was a step in values, such as with an edge, the values on the lower step would be filtered according to the lower values and the higher end of the step filtered according to higher values, thus retaining the edge step, as depicted with simulated data in Fig. 3-18 The usefulness of this filter for edge retention can be seen in Figure 3-18.

This filter is also generally useful to reduce peaks from bright pixels that skew the value range in which the pixel intensities exist. This effect can be seen in Figure 3-19. The size of the scanning window chosen will be a function of the image pixel dimensions.

To identify solely the luminescing cell area, the background, represented by the purple and blue mapping in Figure 3-20, is thresholded to 0 (a black pixel), as seen in Figure 3-21. The value for which to threshold the image will depend on the camera used and the quality of the image. Using a histogram of the pixel values is useful for identifying this cut off. After this threshold value is chosen for images from a particular imaging set-up, it should not need to be adjusted. However, in the case of a severely degraded module, special attention may be needed and this value adjusted.

a). 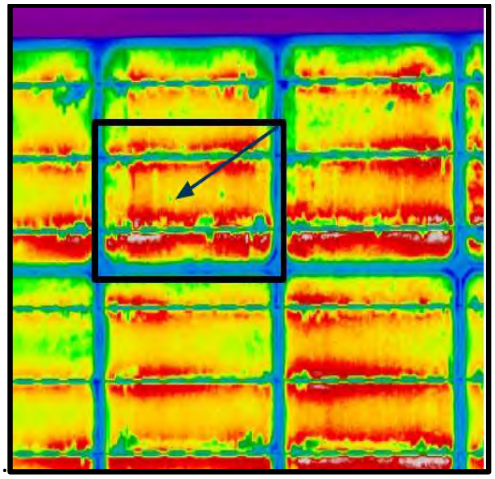 b). 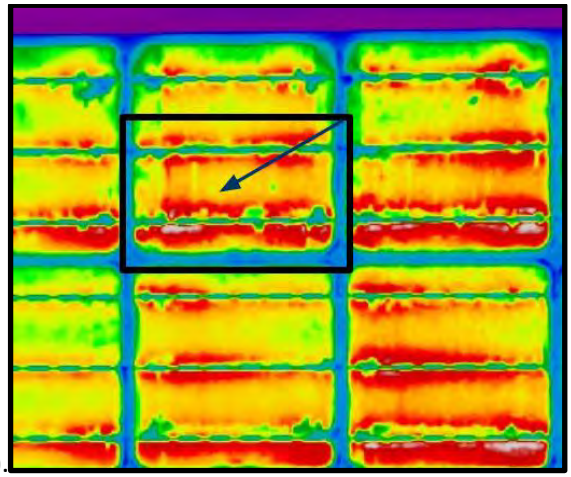

Figure 3-19: An EL image section displayed using a coloured spectral mapping for ease of visualization. The arrow points to a bright pixel value that was reduced by filtering.

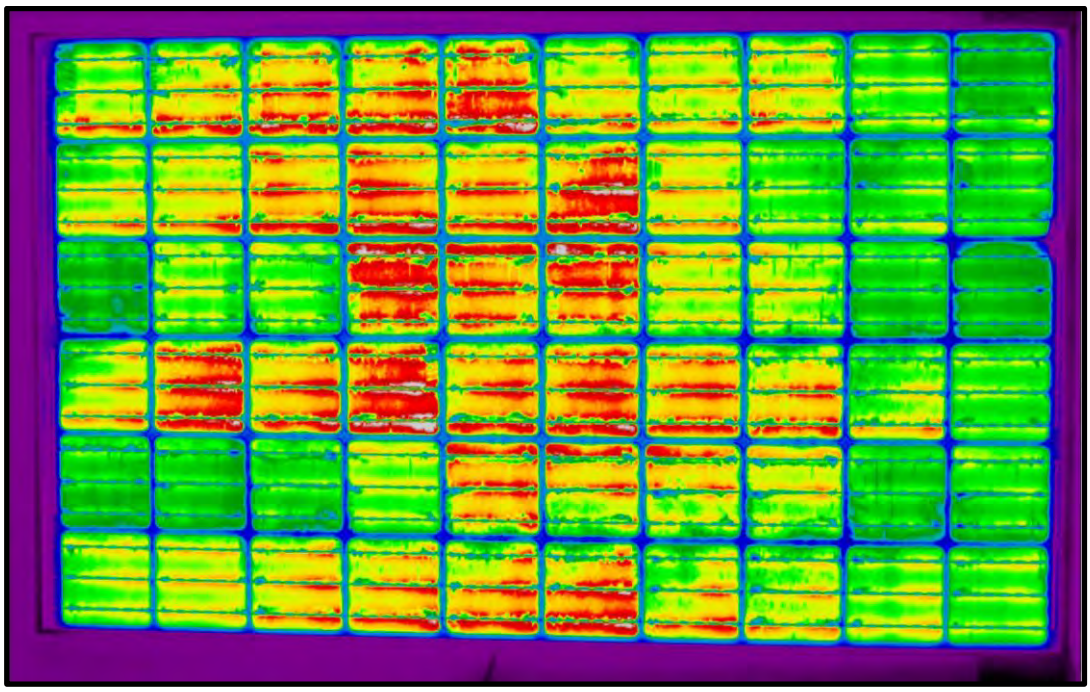

Figure 3-20: A median filtered grayscale EL image. Displayed using a spectral colour mapping.

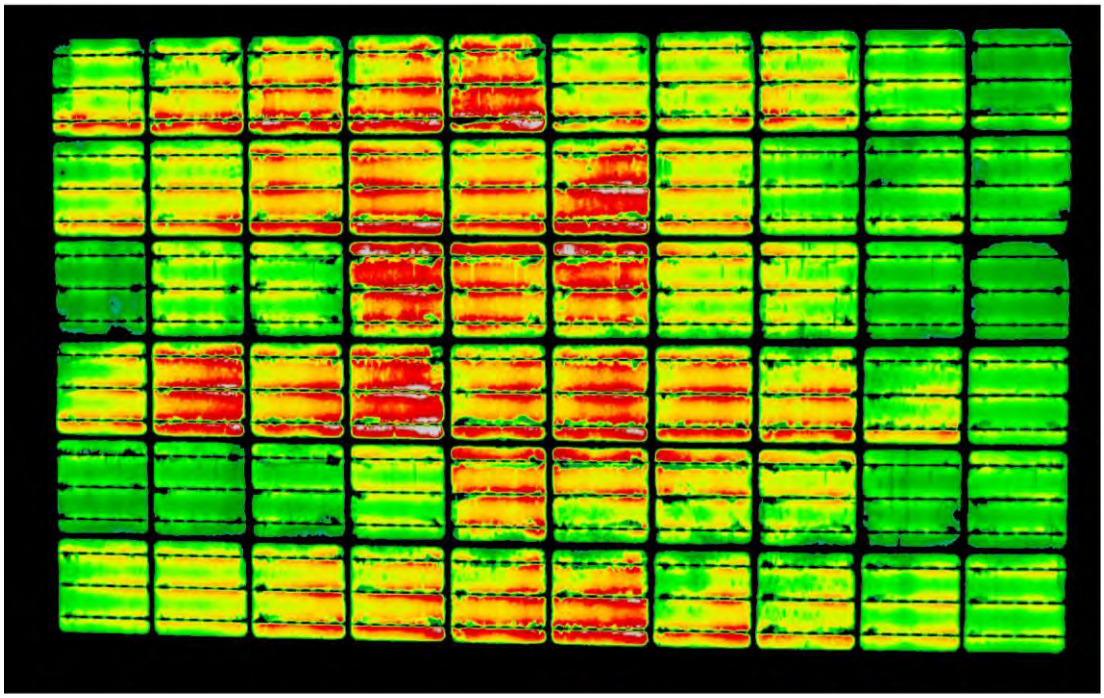

Figure 3-21: A filtered grayscale EL image with the background thresholded to 0 (black). Displayed using a spectral colour mapping.

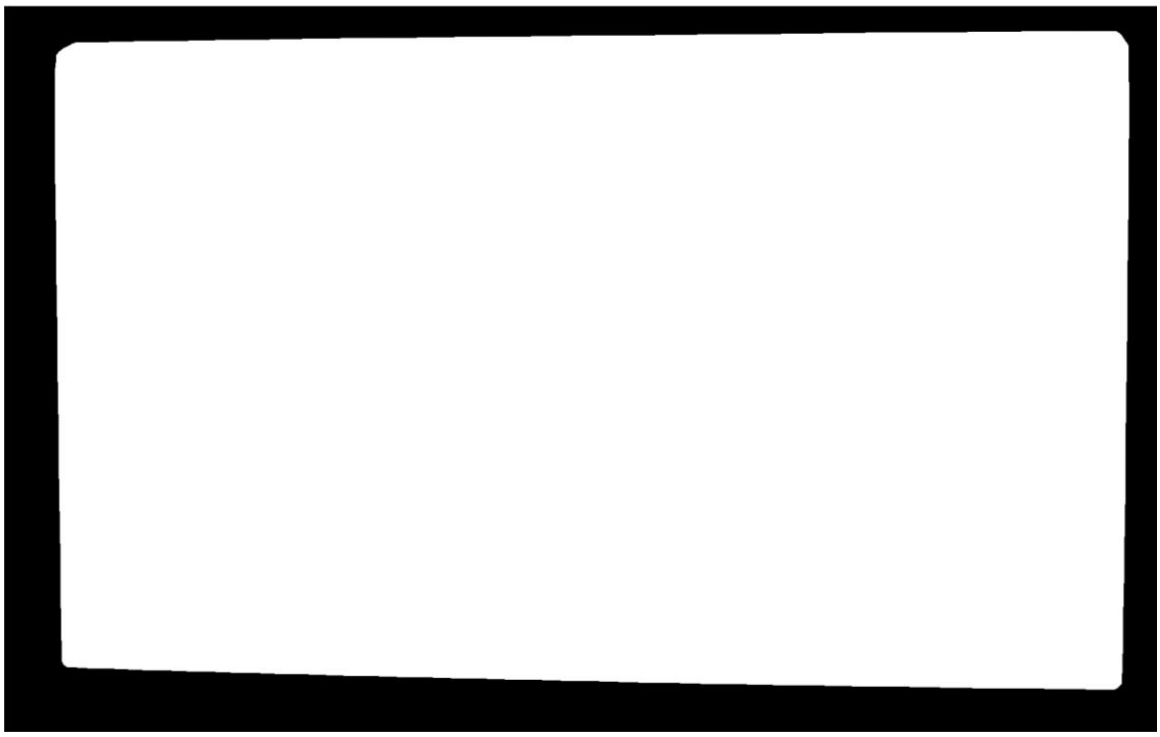

Figure 3-22: Convex Hull algorithm applied to the image in Figure *3-21. This fits the smallest polygon possible to the active cell regions.*

To identify the active cell region, several approaches can be used given the variety of available algorithms. For simplicity of implementation, the convex Hull algorithm can be used to completely encapsulate the active cell regions, as seen in Figure 3-22. This algorithm is designed to find the smallest possible convex set which encloses the non-zero regions of the image. This is additionally advantageous because the algorithm is insensitive to cracked outer cells or between cell gaps.

Now that the misaligned active cell region of the image is identified, the edges can be found by taking periodic vector slices of the image, indicated by the red and blue lines in Figure 3-23, identifying where the vector values change from 0 to 1 or 1 to 0, and fitting a linear regression line to those points, represented by the orange lines in Figure 3-23. Regression fitting allows for some variation along the edge, which could occur due to light scattering through the front side glass causing the cell edge not to be well defined. The linear fit models can be set equal to each other to calculate the four intersection points, represented by the magenta stars in Figure 3-23. These four points are the corners of the active cell region in the raw image.

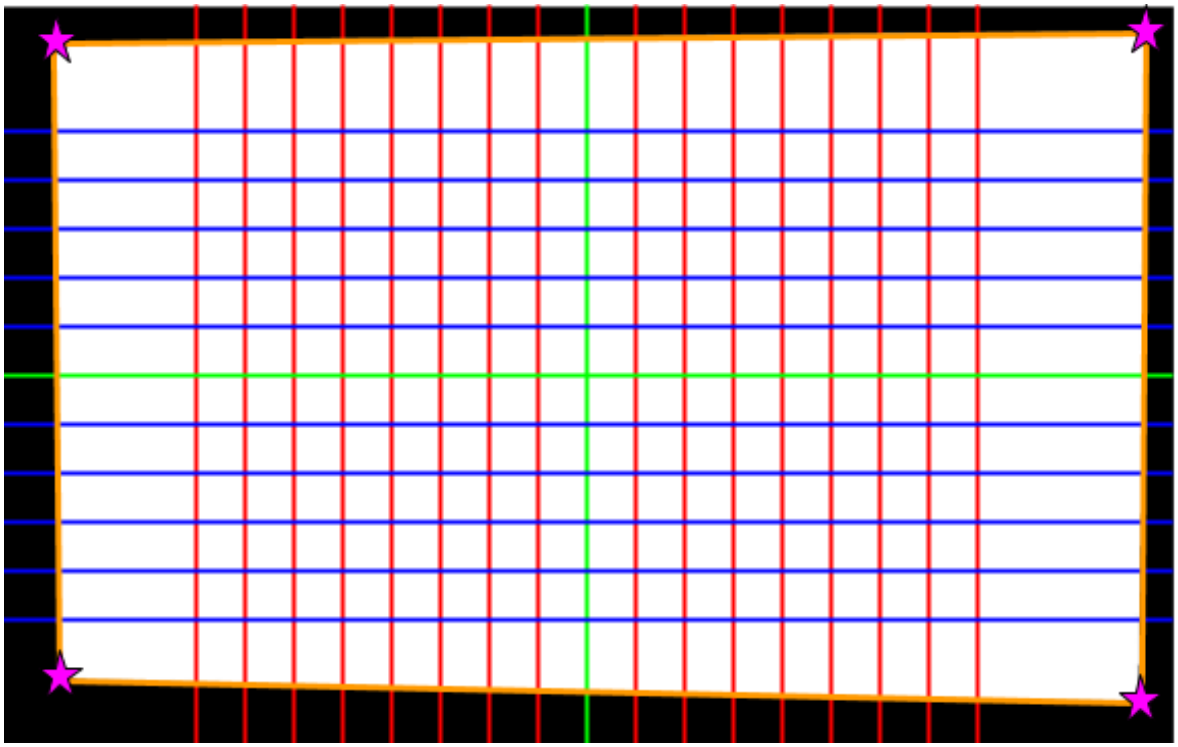

Figure 3-23: Visualization of the steps used to identify the four corners of the active cell region. The green lines are references lines for the mid-points in the x and y dimensions. Blue lines indicate horizontal vector slices. Red lines indicate vertical vector slices. Orange lines represent linear regression fits of the active area edges. Magenta stars represent the four corners of the active cell regions where the linear regression fits intersect.

Lastly, a perspective transformation of these four corner points will result in the final properly oriented image, as seen in Figure 3-24.

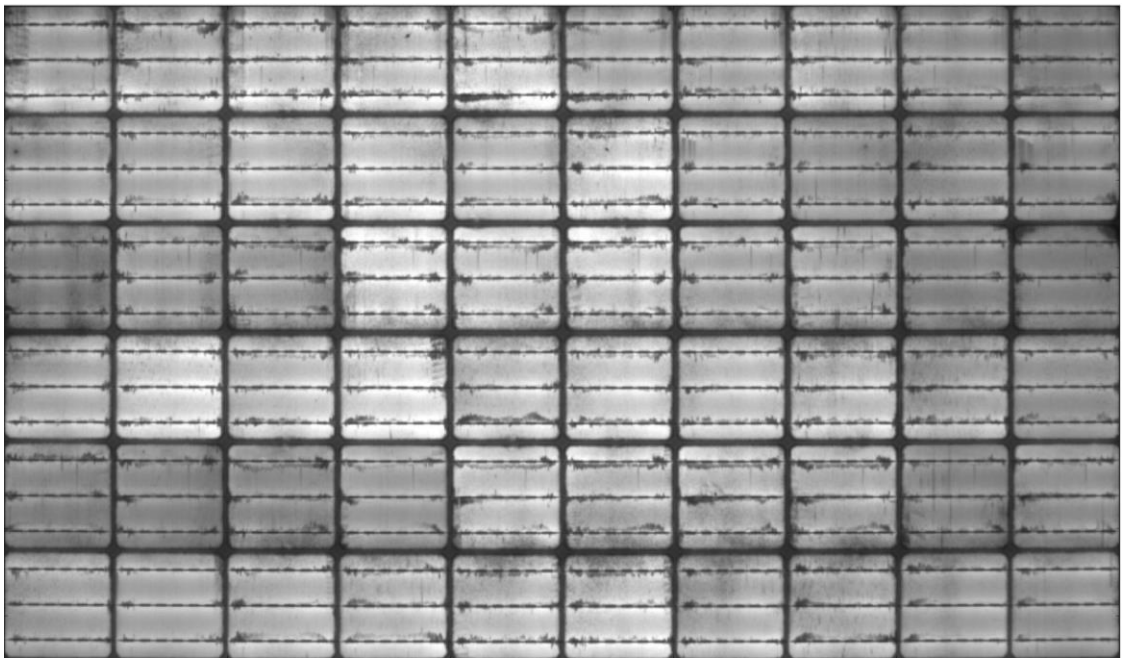

Figure 3-24: A perspective transformed EL image into a uniform orientation using the four corner points represented by the magenta stars in Figure *3-23.*

This image processing method is straight-forward to implement and works well for pipelining entire datasets of images [88]. Similar techniques can be utilized to extract the individual cells and perform feature-level research discussed below. It is important to note that after the corners of the original module are found, the transformation to the final oriented image can be done with any of the images from the intermediary steps. For instance, if the median filtered image used to help identify the module region is not desired in further analysis, the final transformation can be performed on the raw input image, retaining all original pixel values.

Applying the above process to a library of images, the mean substring intensity of three brands of modules is shown in Figure 3-25 through 3000 hours of damp-heat exposure [90]. At each time step (x-axis), three data for three samples are plotted and the standard error shown as a grey shadow behind the data points. This demonstrates one of many possible quantitative analyses that can be performed using EL images properly oriented using the methods outline herein.

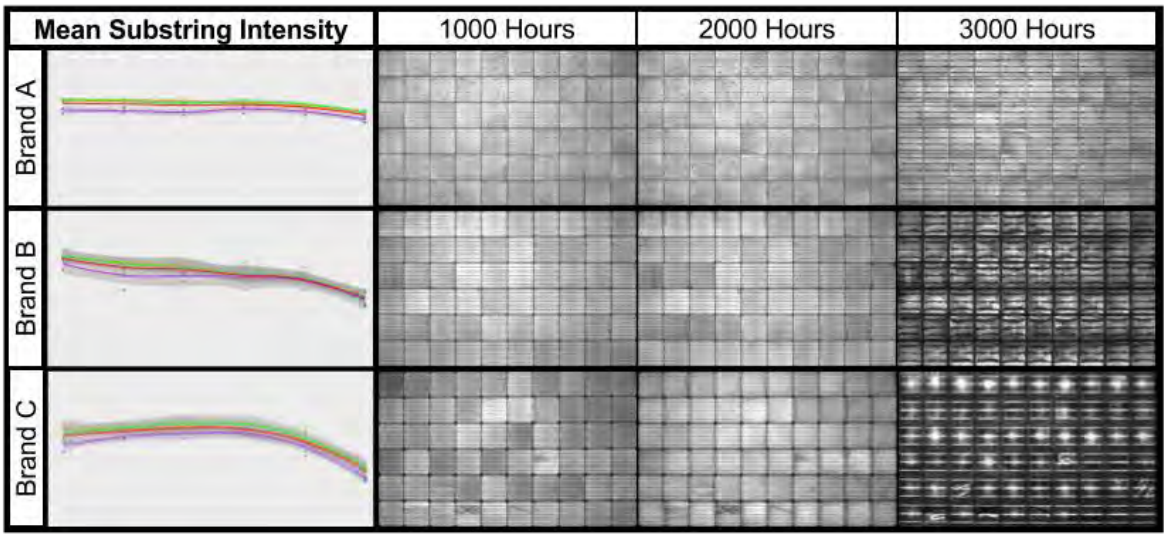

Figure 3-25: Mean substring intensity for three brands of modules over 3000 hours of damp-heat exposure [90]*. The plots show 500, 1000, 1500, 2000, 2500, and 3000 hour steps of exposure along the x-axis, however, for only the corresponding 1000, 2000, and 3000 hour steps are shown as EL images. At each time-step, data points for 3 samples are plotted. The standard error is shown as a gray bounding shadow behind the data points.*

Deriving electrical properties from image data

Electrical properties of PV semiconductor wafers have been deduced from electroluminescent images. Local series resistance at each image pixel has been calculated from the electroluminescent emission and applied voltage [91]. When EL is paired with dark-lock-in thermography, which provides an image of the local heating power, pixel-by-pixel calculation of local series resistance and local series resistance can be performed [92].

Using EL images and the IV-curve of the module, the ideality factors and loss current densities can be determined for each cell in a module image [93].

Machine Learning

Just as with image processing tools, advanced machine and statistical learning codes have become accessible for application to diverse sets of research topics. In PV, recent works have proposed and demonstrated the use of machine learning techniques to aid in research. Fault diagnosis for PV systems using Artificial Neural Networks (ANN) and graph-based semi-supervised learning have been demonstrated successfully using array electrical parameters and environmental data [94], [95]. The feasibility of using supervised statistical and machine learning techniques to analyze massive datasets of time-series I-V curves has been shown to agree well with lab-based experiments and simulations using SPICE circuit models [96]. These techniques can similarly be applied to image data for degradation classification, feature detection, and performance monitoring.

Learning methods fall into two main groups, supervised and unsupervised learning [97], [98]. With supervised modelling, the response of the predictors in the training set are known and therefore the accuracy of the model can be exactly determined. Common supervised models include linear regression, logistic regression, boosting, and Support Vector Machines (SVM). Unsupervised learning algorithms are provided a set of predictors, but not an associated response. Most commonly, cluster analysis is used in the unsupervised domain in an attempt to deduce distinct groups from the input data.

Although many resources are available to implement these methods, open-source code libraries such as Scikit-Learn for Python, provide the opportunity to use these resources without cost [99]. Using this library, we will compare three modern learning algorithms, Support Vector Machines (SVM), Random Forest (RF) and Artificial Neural Networks (ANN) to classify three common EL images: cracked, corroded, and good/clean. The data used consists of 90 60-cell modules containing mono-Si, multi-Si, and PERC cells exposed over 3000 hours of damp heat [90].

For machine learning problems, more data leads to higher accuracies across the classification categories. In the procedure outlined below, we will use 14,200 individual cell image for this problem, however, there is only a few hundred cracked cells present in the data set. This causes the classification accuracy to be low for this category because the model was not able to train on many images in the cracked state. This may not be as much of an issue for data that is relatively consistent, such as the good/clean cells, however, most crack patterns are unique, making a larger dataset advantageous for accurate learning [100], [101].

With a dataset of properly oriented module images, such as the module in Figure 3-24, the cell images are extracted to individual files. Since the module is well aligned, a computationally efficient way of doing this is to simply take the number of X pixels and Y

pixels and divide by the number of cells in that corresponding dimension, effectively slicing the image into individual cells. Due to manufacturing and lifetime exposure conditions, it is possible for the cells to be slightly ajar in the encapsulant and therefore, this could be noticeable using this simple slicing method, as seen in Figure 3-26. However, this misorientation of cells is minor and does not cause the cell area to fall outside the boundary of each slice. Additionally, if more advanced algorithms like the aforementioned convex Hull were used at the cell-level, useful information about the degradation of the cells could be lost. If a convex Hull algorithm or similar method was used to extract a cell such as the one in Figure 3-26c from a module image, valuable information about the edge corrosion would be lost. Additionally, this border is also not significant for machine learning, as it is a random variation of each cell image. However, if a more precise extraction is desired for a specific purpose, the above image processing techniques can be adapted for this purpose, albeit with a larger computational expense.

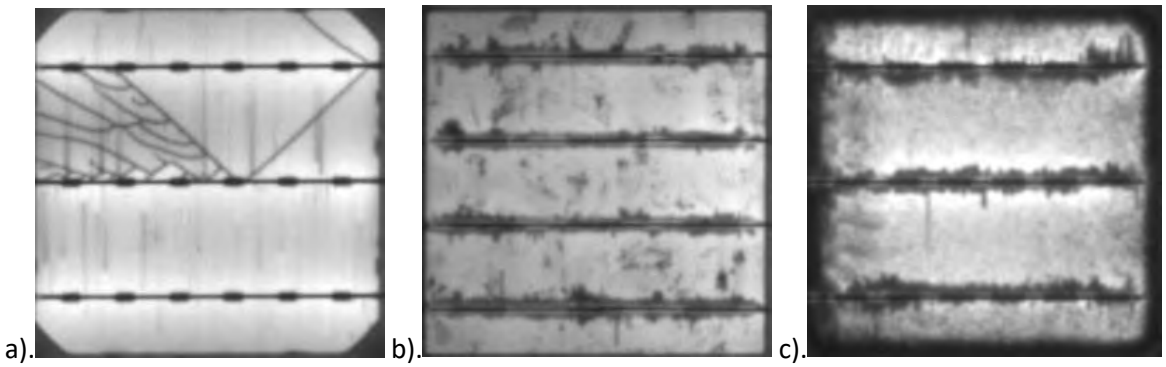

Figure 3-26: An assortment of extracted cells using simple slicing of uniformly oriented module images.

For a supervised learning approach, each cell needs to be classified manually. This is a tedious task and will inherently have some error associated with human judgement. However, with care this task will only need completed once, because after the classification model is created all future cell images can be classified via pipeline automatically. Characteristic cells used for classification can be seen in Figure 3-27 for each of the three categories.

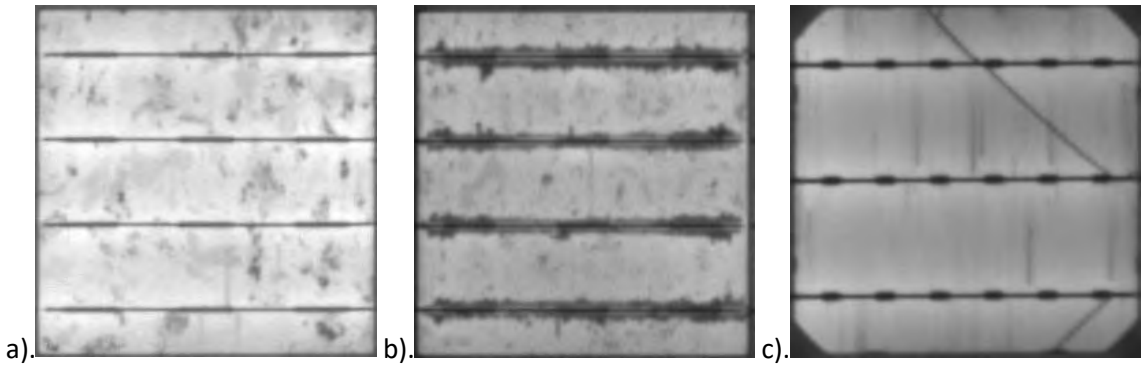

Figure 3-27: Characteristic cells for each of the 3 cell types classified a). Good/clean, b). Busbar corroded and c). Cracked.

At this point it is possible to use the method of data augmentation to increase or data set by a factor of four. For classification purposes, it is not important whether a crack propagates from left to right or right to left. Similarly, it is not important if a crack propagates from an upper edge or a bottom edge. Therefore, we take each image and rotate it 180°, flip it about the x-axis, and flip it about its y-axis, as seen in Figure 3-28. These three augmentations keep the busbars oriented in the same direction.

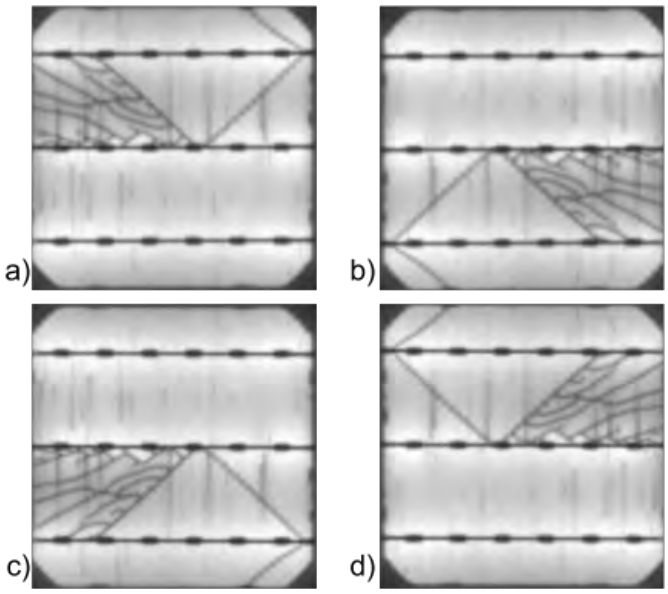

Figure 3-28: a) Original, b) Rotate 180°, c) Flip about x-axis, d) Flip about y-axis.

Each of these categories will have a different number of corresponding images. To ensure that the model does not overfit and prioritize one category over another, equal numbers will be used from each set for model training. A common rule of thumb to choose this number is 80% of the smallest representative data set category. In this example, the cracked images had the smallest sample size. To mitigate this issue, algorithms have been developed for working with unbalanced data sets such as this [102]. For increased accuracy, cross-validation methods, such as k-fold or bootstrapping can be used to resample the dataset to evaluate models for many combinations of training and testing data, to reduce error.

The results of these machine learning models are provided in [Table 3.3.1] and [Table 3.3.2].

Table 3.3.1: Table of classification accuracies as a function of machine learning model.

	SVM	**RF**	**ANN**
Accuracy (%)	98.77	96.90	98.13
Training Time (s)	85.52	90.12	2250

Table 3.3.2: Table of classification accuracies as a function of machine learning model and degradation type.

	Good/Clean	**Cracked**	**Corroded**
SVM	99.92	66.32	100
RF	99.87	19.38	99.12
ANN	100	47.96	99.71

For this task, SVM performed the best for overall accuracy, training time, and highest accuracy per category. As was mentioned above, due to the small sample set and variability of cracked cell images, the classification accuracy was poor for this simple model. To increase accuracy without acquiring new data, more complex models can be used. Ensemble models can be used as a way to benefit from many different models in the same analysis [103], [104].

4 Pros and Cons

Electroluminescence and infrared imaging are non-destructive measurement techniques. These types of optical measurements provide fast, real-time and high resolution images with a two-dimensional distribution of the characteristic features of PV modules [105]. In previous works, a combination of EL and IR measurements was proposed in order to quickly detect the most common defects in a PV module with high accuracy [106].

Using IR thermography by means of IR measurements of the thermal behaviour of cells in a PV module, a number of defects (e.g. short circuits in solar cells, shunts, inactive cell parts etc.) can be clearly identified. Several defects can be distinguished by varying the electrical load corresponding to certain states of the current voltage characteristics [106]. Concerning IR thermography measurements it turned out that illuminated thermography is more suited for crystalline modules and dark thermography is a better tool for thin-film modules. Compared to the dark thermography images the illuminated thermography images of crystalline modules supply more details and a better defect resolution. For thin-film modules the opposite is true [107].

However, not all the failures of PV modules lead to an increase in temperature. Taking this into consideration, the IR measurements cannot identify all the types of failures. On the other hand, PV modules with clear EL images sometimes provide IR images with hot areas. A combination of both techniques can identify the maximum number of failures in a PV module.

EL measurements take advantage of the radiative inter-band recombination of excited charge carriers in solar cells. The solar cells are supplied with a defined external excitation current while the camera takes an image of the emitted photons. Damaged areas of a solar module appear dark or radiate less than areas without defects. The high resolution of the EL images enables resolving some defects more precisely than in IR images. In a study by [107], it was shown very clearly that electroluminescence is a good method to detect micro cracks, interrupted contacts or a number of process failures (e.g. shunts or defects in the antireflection layer), but it was not possible to determine the impact of these defects on the module power output.

Both IR and EL-based methods have their own strengths and weaknesses. The appropriate method depends on the specific technological problem to be studied. While EL is superior for lifetime mapping, bulk defect imaging, series resistance imaging and exact junction breakdown site imaging, IR-based techniques are superior for all tasks requiring quantitative current measurements [108]. As the origin of a defect is not always located in the identified high temperature area or the remarkable dark EL areas, a combination of EL and IR techniques is necessary in order to identify as many defects as possible [107].

Table 4.1.1: Comparison of the IR and EL imaging methods [105].

Comparison of Methods			
Electroluminescence		Infrared	
Advantages	Disadvantages	Advantages	Disadvantages
1. High resolution	1. Origin of a defect is not identifiable	1. Contactless	1. Not all defects (EL) lead to a temperature increase
2. Identifiable	2. Difficult to determine influence of defects on cell/module performance	2. Identifiable	2. High temperature area: not always the origin of defects
a. Faulty laser scribing	3. Unremarkable EL images sometimes supply IR images with hot areas	a. Different thermal behavior	3. Difficult to determine exact position of defects or large number of small spots
b. Short circuited bypass diodes, disconnected cell regions, shunts, short circuited cells, cell cracks, layer defects etc.	4. Electrical contact necessary	b. Shunts, hot spots, Moisture, Shading, Mismatches, Installation Failures etc.	4. Not distinguishable between low shunt and high series resistance

Table 4.1.1 shows and compares the advantages and disadvantages of the two methods.

5 Conclusions

Investigations of PV modules benefit from infrared and electroluminescence imaging techniques, and both are widely used for indoor and outdoor measurements. Currently there are no international standards existing within the IEC for IR, and EL measurements, however, draft versions are under development. The Technical Specification IEC/TS 62446-3 describes investigations of PV modules and the entire plant under operation in natural sunlight. This document has outlined guidance for preventive maintenance and fault diagnostics of PV plants operating under natural sunlight by means of infrared imaging techniques.. The subjects of the investigation included PV modules, as part of the array, as well as balance of system (BOS) components such as cables, fuses, switches and inverters.

There is a broad variety of infrared cameras with a range of specifications on the market. The most suitable type of camera will depend on the application at hand. For example, handheld cameras are suitable for field inspection of PV modules, however, there are recommendations on the minimum resolution required as described in section 2.2. However, the same range of specifications may not be available for other applications such as airborne (UAV) surveys of PV plants due to the different lenses and distances in use. As to provide a useful guidance in an appropriate selection of a specific IR camera product, four different IR cameras classes are defined: Lower, medium, professional, upper professional. The professional class is recommended over the medium class, however, for several IR inspection applications, medium class cameras are fully sufficient. This is an important note due to the relative costs of the camera systems.

It is recommended to take IR images at high solar irradiance (> 600 W/m²) and constant ambient conditions, i.e. no clouds, low wind speeds, stable ambient temperatures. Stable environmental conditions are crucial for high quality outdoor IR imaging of PV modules and arrays. Weather fluctuations must be much slower than the thermal time constant of the PV module. Typically, a PV module takes 5 to 15 minutes to thermally stabilize for new environmental conditions such as change of global irradiation intensity, temperature, or wind speed. Clouds also can produce thermal reflections on the PV modules which may distort the evaluation of the IR image. For this reason, thermal reflections of clouds, buildings, trees, or other objects should be avoided or minimized. This is usually done by either waiting for more stable conditions or moving the position of the IR camera to avoid specific reflections.

All IRT recordings, either terrestrial or aerial should be performed in compliance with recommended specifications. In most cases, a scaling of the relevant colours of around 20-30 K temperature difference (span) for a module efficiency of 15 % at 1000 W/m² is useful. For a module efficiency of 10 % at 750 W/m², a span of about 10-15 K is suggested. It is highly recommended to obtain so-called "IR overviews" of a PV installation, even under lower image resolution, for a good orientation and visualization of large extended defects on string level, which might otherwise be undetected. The IRT personal should have detailed knowledge of thermal imaging technique as well as of PV module design and PV system behaviour. For warranty claims of the supplied modules, it is recommended to conduct the first IRT during the commissioning of the PV plant.

Using IRT on PV modules, strings and arrays, typical PV module defects can clearly be identified such as e.g. short circuits in solar cells, shunts, inactive cell parts etc. The correlation between failure types, thermal signatures and power loss of PV modules showed that by the combination of several IRT measurement methods, typical defects in crystalline silicon (c-Si) PV modules and their impact on the I-V curve can be explained. The main thermal abnormalities, which can be detected by IR imaging in PV power plants are: Hot spots due to breakage of front glazing, external shading or internal cell problems; heated bypass diodes inside the PV module junction box; heated string fuses in combiner box, and heated DC and AC cables and connections points. IRT imaging can also efficiently be employed to investigate the degree of PID degradation by shunts (PID-s).

Detected thermal abnormalities should lead to close observation in regular thermographic inspections or even immediate replacement of the component depending on the degree of severity and safety relevance of the detected failure.

The International Technical Specification [59] specifies methods to capture electroluminescence images of photovoltaic modules, process images to obtain quantitative descriptors, and provide guidance to qualitatively interpret the EL images.

There are a number of cameras and products available on the market that are suitable for EL measurements of PV modules ranging from modified DSLR or the closely related “mirrorless” MILC cameras through to dedicated EL systems with a corresponding broad range of specifications. It has been shown by [73] that a relative simple modification enables consumer DSLRs to perform EL imaging and more recently [74] non-reflex, mirrorless interchangeable lens cameras with large sensors can also be modified for EL application. The choice of the type of EL camera that is used when imaging PV modules is dependent on a range of factors. As with many types of camera equipment, there is trade-off between cost, resolution and sensitivity.

A good rule of thumb is that proper EL exposures start at a brightness where reading a book gets difficult (approximately 50 mW/m^2). These conditions are often met one hour after typical sunset. The EL technique can be profitably applied to detect and distinguish between different failures modes. The relevance for this type of non-destructive inspection regards the possibility to ascertain the reason of power losses and tries to attribute it to the different stages of the PV module lifetime.

IR and EL based imaging methods are complementary imaging techniques used in identifying problems with PV plants. As discussed in Chapter 4, each have their own strengths and weaknesses and can identify different problems with PV modules. The appropriate method depends on the specific technological problem to be studied.

6 References

[1] "IEC TS 62446-3 Ed.1: Photovoltaic (PV) systems - Requirements for testing, documentation and maintenance - Part 3: Photovoltaic modules and plants - Outdoor infrared thermography." 2017.

[2] "Draft IEC/TS 60904-12 Ed.1: Photovoltaic devices -Part 12: Infrared thermograhpy of photovoltaic modules." 2016.

[3] M. Köntges *et al.*, *Review of Failures of Photovoltaic Modules*. 2014.

[4] O. Breitenstein *et al.*, "LOCK-IN THERMOGRAPHY - A UNIVERSAL TOOL FOR LOCAL ANALYSIS OF SOLAR CELLS," in *20th European Photovoltaic Solar Energy Conference*, 2005.

[5] D. S. Tezcan, S. Eminoglu, and T. Akin, "A low-cost uncooled infrared microbolometer detector in standard CMOS technology," *IEEE Trans. Electron Devices*, vol. 50, no. 2, pp. 494–502, Feb. 2003.

[6] G. J. Zissis and W. . Wolfe, *The Infrared Handbook*, Revised ed. General Dynamics, 1978.

[7] J. Chynoweth, "Infrared detector resolution: How important is it?" .

[8] A. Redjimi, D. Knežević, K. Savić, N. Jovanović, M. Simović, and D. Vasiljević, "Noise Equivalent Temperature Difference Model for Thermal Imagers," *Sci. Tech. Rev.*, vol. 64, no. 2, pp. 42–49, 2014.

[9] J. A. Tsanakas, L. Ha, and C. Buerhop, "Faults and infrared thermographic diagnosis in operating c-Si photovoltaic modules: A review of research and future challenges," *Renew. Sustain. Energy Rev.*, vol. 62, pp. 695–709, Sep. 2016.

[10] C. Buerhop, U. Jahn, U. Hoyer, B. Lerche, and S. Wittmann, "Abschlußbericht der Machbarkeitsstudie zur Überprüfung der Qualität von Photovoltaik-Modulen mittels Infrarot-Aufnahmen," Bayern, Erlangen, 2007.

[11] A. Moropoulou, J. Palyvos, M. Karoglou, and V. Panagopoulos, "Using IR thermography for photovoltaic array performance assessment," in *Proc. 4th International Conference on NDT - Hellenic Society for NDT*, 2007, pp. 1804–1806.

[12] G. Makrides, B. Zinsser, M. Norton, G. E. Georghiou, M. Schubert, and J. H. Werner, "Error Sources in Outdoor Performance Evaluation of Photovoltaic Systems," in *Proc. 24th EU-PVSEC*, 2009, pp. 3904–3909.

[13] A. Krenzinger and A. C. de Andrade, "Accurate outdoor glass thermographic thermometry applied to solar energy devices," *Sol. Energy*, vol. 81, no. 8, pp. 1025–1034, Aug. 2007.

[14] C. Buerhop-Lutz, D. Schlegel, C. Vodermayer, and M. Nieß, "Quality control of PV-modules in the field using infrared-thermography," in *Proc. 26th EUPVSEC*, 2011, pp. 3894–3897.

[15] C. Buerhop, H. Scheuerpflug, and R. Weißmann, "The role of infrared emissivity of glass on IR-imaging of PV-plants," in *Proc. 26th EUPVSEC*, 2011, pp. 3413–3416.

[16] U. Hoyer *et al.*, "Analysis of PV modules by electroluminescence and IR thermography," in *Proc. 24th EUPVSEC*, 2009, pp. 3262–3266.

[17] C. Vodermayer *et al.*, "First results – Correlation between IR images and electrical behavior and energy yield of PV modules," in *Proc. 23rd EUPVSEC*, 2008, pp. 3134–3137.

[18] S. Wendlandt, A. Drobisch, T. Buseth, S. Krauter, and P. Grunow, “Hot spot risk analysis on silicon cell modules,” in *Proc. 25th EUPVSEC/ 5th World Conference on Photovoltaic Energy Conversion*, 2010, pp. 4002–4006.

[19] P. N. Botsaris and J. A. Tsanakas, “Infrared thermography as an estimator technique of a photovoltaic module performance via operating temperature measurements,” in *Proc. 10th European Conference on NDT*, 2010.

[20] G. Acciani, G. B. Simione, and S. Vergura, “Thermographic analysis of photovoltaic panels,” in *Proc. ICREPQ*, 2010.

[21] F. Ancuta and C. Cepisca, “Failure analysis capabilities for PV systems,” in *Proc. International Conference of Recent Researches in Energy, Environment, Entrepreneurship, Innovation*, 2011, pp. 109–115.

[22] J. A. Tsanakas and P. N. Botsaris, “On the detection of hot spots in operating photovoltaic arrays through thermal image analysis and a simulation model,” *Mater. Eval.*, vol. 71, no. 4, pp. 457–465, 2013.

[23] J. A. Tsanakas and P. N. Botsaris, “Passive and Active Thermographic Assessment as a Tool for Condition-Based Performance Monitoring of Photovoltaic Modules,” *J. Sol. Energy Eng.*, vol. 133, no. 2, p. 21012, 2011.

[24] P. Sánchez-Friera, M. Piliougine, J. Peláez, J. Carretero, and M. Sidrach de Cardona, “Analysis of degradation mechanisms of crystalline silicon PV modules after 12 years of operation in Southern Europe,” *Prog. Photovoltaics Res. Appl.*, vol. 19, no. 6, pp. 658–666, Sep. 2011.

[25] E. Kaplani, “Degradation effects in sc-si PV modules subjected to natural and induced ageing after several years of field operation,” *J. Eng. Sci. Technol. Rev.*, vol. 5, no. 4, pp. 18–23, 2012.

[26] E. Kaplani, “Detection of Degradation Effects in Field-Aged c-Si Solar Cells through IR Thermography and Digital Image Processing,” *Int. J. Photoenergy*, vol. 2012, pp. 1–11, 2012.

[27] J. A. Tsanakas, M. Karoglou, E. T. Delegou, P. N. Botsaris, A. Bakolas, and A. Moropoulou, “Assessment of the performance and defect investigation of PV modules after accelerated ageing tests,” in *Proc. ICREPQ’13*, 2013.

[28] R. Moreton Villagrá, E. Lorenzo, J. Leloux, and J. M. Carrillo, “Dealing in practice with hot-spots,” in *Proc. 29th EUPVSEC*, 2014, pp. 2722–2727.

[29] Y. Hu, W. Cao, J. Ma, S. J. Finney, and D. Li, “Identifying PV Module Mismatch Faults by a Thermography-Based Temperature Distribution Analysis,” *IEEE Trans. Device Mater. Reliab.*, vol. 14, no. 4, pp. 951–960, Dec. 2014.

[30] C. Buerhop, D. Schlegel, M. Niess, C. Vodermayer, R. Weißmann, and C. J. Brabec, “Reliability of IR-imaging of PV-plants under operating conditions,” *Sol. Energy Mater. Sol. Cells*, vol. 107, pp. 154–164, Dec. 2012.

[31] C. Buerhop-Lutz and H. Scheuerpflug, “Characterization of defects in PV-modules by their temperature development using IR-thermography,” in *Proc. 31st EUPVSEC*, 2015, pp. 1789–1792.

[32] C. Buerhop-Lutz, H. Scheuerpflug, and T. Pickel, “Defect analysis of installed PV-modules – IR-thermography and in-string power measurement,” in *Proc. 31st EUPVSEC*, 2015, pp. 1692–1697.

[33] J. A. Tsanakas, G. Vannier, A. Plissonnier, D. L. Ha, and F. Barruel, “Fault diagnosis and classification of large-scale photovoltaic plants through aerial orthophoto thermal

mapping," in *Proc. 31st EUPVSEC*, 2015, pp. 1783–1788.

[34] H. Denio, "Aerial solar Thermography and condition monitoring of photovoltaic systems," in *Proc. 38th IEEE Photovoltaic Specialists Conference*, 2012, pp. 000613–000618.

[35] C. Buerhop-Lutz, R. Weißmann, H. Scheuerpflug, R. Auer, and C. J. Brabec, "Quality control of PV-modules in the field using a remote-controlled drone with an infrared camera," in *Proc. 27th EUPVSEC*, 2012.

[36] P. B. Quater, F. Grimaccia, S. Leva, M. Mussetta, and M. Aghaei, "Light Unmanned Aerial Vehicles (UAVs) for Cooperative Inspection of PV Plants," *IEEE J. Photovoltaics*, vol. 4, no. 4, pp. 1107–1113, Jul. 2014.

[37] M. Dalsass, H. Scheuerpflug, M. Maier, and C. J. Brabec, "Correlation between the monitoring data of a photovoltaic power plant and module defects detected by drone-mounted thermography," in *Proc. 31st EUPVSEC*, 2015, pp. 1793–1798.

[38] U. Muntwyler, E. Schüpbach, and M. Lanz, "Infrared (IR) drone for quick and cheap PV inspection," in *Proc. 31st EUPVSEC*, 2015, pp. 1804–1806.

[39] E. Schubert, U. Siegfriedt, R. Haselhuhn, B. Weinreich, B. Schauer, and R. Haas, "Standardization of infrared imaging of photovoltaic plants in operation," in *Proc. 31st EUPVSEC*, 2015, pp. 1780–1782.

[40] Z. Zou, Y. Hu, B. Gao, W. L. Woo, and X. Zhao, "Temperature recovery from degenerated infrared image based on the principle for temperature measurement using infrared sensor," *J. Appl. Phys.*, vol. 115, no. 4, p. 43522, Jan. 2014.

[41] S. Armstrong and W. G. Hurley, "A thermal model for photovoltaic panels under varying atmospheric conditions," *Appl. Therm. Eng.*, vol. 30, no. 11–12, pp. 1488–1495, Aug. 2010.

[42] E. Skoplaki and J. A. Palyvos, "Operating temperature of photovoltaic modules: A survey of pertinent correlations," *Renew. Energy*, vol. 34, no. 1, pp. 23–29, Jan. 2009.

[43] M. Fuentes, "A simplified thermal model for flat-plate photovoltaic arrays," 1987.

[44] B. Herteleer, "Outdoor thermal and electrical characterisation of photovoltaic modules and systems," KU Leuven, 2016.

[45] J. Leloux, L. Narvarte, A. Luna, and A. Desportes, "Automatic detection of PV systems failures from monitoring validated on 10,000 BiPV systems in Europe," in *Proc. 28th EUPVSEC*, 2014, pp. 4013–4016.

[46] F. Martinez-Moreno, E. Lorenzo, J. Munoz, R. Parra, and T. Espino, "On site tests for the detection of potential induced degradation in modules," in *Proc. 28th EUPVSEC*, 2013, pp. 3313–3317.

[47] N. Tyutyundzhiev, K.Lovchinov, F. M. Moreno, J. Leloux, and L. Narvarte, "Advanced PV modules inspection using multirotor UAV," in *Proc. 31st EUPVSEC*, 2015, pp. 2077–2081.

[48] M. Aghaei, P. B. Quater, F. Grimaccia, S. Leva, and M. Mussetta, "Unmanned Aerial Vehicles in Photovoltaic Systems Monitoring Applications," in *Proc. 29th EUPVSEC*, 2014, pp. 2734–2739.

[49] R. Gini, D. Pagliari, D. Passoni, L. Pinto, G. Sona, and P. Dosso, "UAV PHOTOGRAMMETRY: BLOCK TRIANGULATION COMPARISONS," *ISPRS - Int. Arch. Photogramm. Remote Sens. Spat. Inf. Sci.*, vol. XL-1/W2, pp. 157–162, Aug. 2013.

[50] J. A. Tsanakas, L. D. Ha, and F. Al Shakarchi, “Advanced inspection of photovoltaic installations by aerial triangulation and terrestrial georeferencing of thermal/visual imagery,” *Renew. Energy*, vol. 102, pp. 224–233, Mar. 2017.

[51] Optris, “Lens Calculator.” [Online]. Available: http://www.optris.com/optics-calculator. [Accessed: 13-Feb-2017].

[52] InfraTec GmbH, “Field of view calculator,” 2017. [Online]. Available: http://www.infratec.eu/thermography/infrared-camera/variocamr-high-definition.html. [Accessed: 13-Feb-2017].

[53] G. Mathiak, S. Kämmer, M. Schweiger, and W. Herrmann, “Potential Induced Degradation (PID) – Comparison of Different Test Methods. Shunt Resistance Measurements of Individual Cells Inside a Module and Infrared Imaging of PV Modules,” in *Proc. 28th EUPVSEC*, 2013, pp. 3332–3335.

[54] P. Hacke and S. Johnston, “All about PID – testing and avoidance in the field PV Tech Power,” *PV Tech Power*, vol. 8.

[55] C. Buerhop *et al.*, “IR-images of PV-modules with potential induced degradation (PID) correlated to monitored string power output,” in *Proc. SPIE 9938*, 2016, p. 99380J.

[56] T. Kaden, K. Lammers, and H. J. Möller, “Power loss prognosis from thermographic images of PID affected silicon solar modules,” *Sol. Energy Mater. Sol. Cells*, vol. 142, pp. 24–28, Nov. 2015.

[57] B. Weinreich, “Fehlererkennung an Modulen im Feld mittels Thermographie,” in *Proc. 13th Workshop “Photovoltaik-Modultechnik,”* 2016.

[58] M. Diehl, “Methoden zur Erkennung von PID,” 2015. [Online]. Available: http://www.photovoltaikbuero.de/pv-know-how-blog/pid-erkennung-diagnose-methoden/. [Accessed: 22-Dec-2016].

[59] “Draft IEC/TS 60904-13: Photovoltaic Devices - Part 13: Electroluminescence of photovoltaic modules.” 2017.

[60] F. Spertino *et al.*, “A power and energy procedure in operating photovoltaic systems to quantify the losses according to the causes,” *Sol. Energy*, vol. 118, pp. 313–326, Aug. 2015.

[61] I. Berardone, J. L. Garcia, and M. Paggi, “Quantitative analysis of electroluminescence and infrared thermal images for aged monocrystalline silicon photovoltaic modules,” in *IEEE 44th Photovoltaic Specialists Conference (PVSC)*, 2017.

[62] T. Fuyuki, H. Kondo, Y. Kaji, A. Ogane, and Y. Takahashi, “Analytic findings in the electroluminescence characterization of crystalline silicon solar cells,” *J. Appl. Phys.*, vol. 101, no. 2, p. 23711, 2007.

[63] I. Berardone, M. Corrado, and M. Paggi, “A Generalized Electric Model for Mono and Polycrystalline Silicon in the Presence of Cracks and Random Defects,” *Energy Procedia*, vol. 55, pp. 22–29, 2014.

[64] M. Paggi, M. Corrado, and I. Berardone, “A global/local approach for the prediction of the electric response of cracked solar cells in photovoltaic modules under the action of mechanical loads,” *Eng. Fract. Mech.*, vol. 168, pp. 40–57, Dec. 2016.

[65] T. Fuyuki, H. Kondo, T. Yamazaki, Y. Takahashi, and Y. Uraoka, “Photographic surveying of minority carrier diffusion length in polycrystalline silicon solar cells by electroluminescence,” *Appl. Phys. Lett.*, vol. 86, no. 26, p. 262108, Jun. 2005.

[66] T. Potthoff, K. Bothe, U. Eitner, D. Hinken, and M. Köntges, “Detection of the voltage distribution in photovoltaic modules by electroluminescence imaging,” *Prog. Photovoltaics Res. Appl.*, vol. 18, no. 2, pp. 100–106, Mar. 2010.

[67] UTC-Aerospace-Systems, “1024-LDM Linesan Camera.” [Online]. Available: http://www.sensorsinc.com/products/detail/1024-ldm-linescan-camera. [Accessed: 22-Dec-2016].

[68] U. Hoyer *et al.*, “Electroluminescence imaging of organic photovoltaic modules,” *Appl. Phys. Lett.*, vol. 97, no. 23, p. 233303, 2010.

[69] T. Weber, A. Albert, M. Roericht, S. Krauter, and P. Grunow, “Electroluminescence investigation on thin film modules,” in *Proc. 26th EUPVSEC*, 2011.

[70] ANDOR, “Photovoltaic EL Imaging.” [Online]. Available: http://www.andor.com/learning-academy/photovoltaic-el-imaging-an-overview-of-andor%27s-solutions-for-pv-el. [Accessed: 22-Dec-2016].

[71] T. Fuyuki and A. Kitiyanan, “Photographic diagnosis of crystalline silicon solar cells utilizing electroluminescence,” *Appl. Phys. A*, vol. 96, no. 1, pp. 189–196, Jul. 2009.

[72] D. Hinken, C. Schinke, S. Herlufsen, A. Schmidt, K. Bothe, and R. Brendel, “Experimental setup for camera-based measurements of electrically and optically stimulated luminescence of silicon solar cells and wafers,” *Rev. Sci. Instrum.*, vol. 82, no. 3, p. 33706, 2011.

[73] K. Mertens and Th. Stegemann, and T. Stöppel, “LowCost EL: Erstellung von Elektrolumineszenzbildern mit einer modifizierten Standard-Spiegelreflexkamera,” in *Proc. OTTI -Symposium Photovoltaische Solarenergie*, 2012, pp. 214–219.

[74] J. S. Fada, N. R. Wheeler, D. Zabiyaka, N. Goel, T. J. Peshek, and R. H. French, “Democratizing an electroluminescence imaging apparatus and analytics project for widespread data acquisition in photovoltaic materials,” *Rev. Sci. Instrum.*, vol. 87, no. 8, p. 85109, 2016.

[75] D. R. Falk, D. R. Brill, and D. G. Storkt, *Seeing the Light: Optics in Nature, Photography, Color, Vision, an Harmony*. 1986.

[76] W. Kester, “Oversampling Interpolating DACs,” 2009.

[77] S. Schwartz, *Visual Perception: A Clinical Orientation, Fourth Edition (Optometry)*, Fourth. 2009.

[78] Greateyes, “Inspection Systems.” [Online]. Available: http://www.greateyes.de/en/systems.html. [Accessed: 22-Dec-2016].

[79] S. Koch, “OUTDOOR ELECTROLUMINESCENCE IMAGING OF CRYSTALLINE PHOTOVOLTAIC MODULES: COMPARATIVE STUDY BETWEEN MANUAL GROUND - LEVEL INSPECTIONS AND DRONE - BASED AERIAL SURVEYS,” in *32nd EU PVSEC*, 2016.

[80] M. Köntges, I. Kunze, S. Kajari-Schröder, X. Breitenmoser, and B. Bjørneklett, “The risk of power loss in crystalline silicon based photovoltaic modules due to micro-cracks,” *Sol. Energy Mater. Sol. Cells*, vol. 95, no. 4, pp. 1131–1137, Apr. 2011.

[81] M. Paggi, I. Berardone, A. Infuso, and M. Corrado, “Fatigue degradation and electric recovery in Silicon solar cells embedded in photovoltaic modules,” *Sci. Rep.*, vol. 4, no. 4506 (2014), Mar. 2014.

[82] B. Kubicek, T. Schlager, and M. Halwachs, “Outdoor Lock-In Thermographie von PID-Modulen,” in *31. Symposium Photovoltaishce Solarenergien*, 2017.

[83] S. van der Walt *et al.*, “scikit-image: image processing in Python,” *PeerJ*, vol. 2, p. e453, 2014.

[84] G. Bradski, “The OpenCV Library,” 2000. [Online]. Available: http://www.drdobbs.com/open-source/the-opencv-library/184404319.

[85] M. Beyeler, P. Joshi, and J. Howse, *OpenCV: Computer Vision Projects with Python*. Birmingham: Packt Publishing, 2016.

[86] G. Bradski, *Learning OpenCv 3*. O’Reilly Media, 2016.

[87] G. B. . Enano, O. D. Suarez, J. L. E. Aranda, J. S. Tercero, I. S. Gracia, and N. Vallez, *Learning Image Processing with OpenCV*. Birmingham: Packt Publishing, 2015.

[88] J. S. Fada, M. A. Hossain, J. L. Braid, S. Yang, T. J. Peshek, and R. H. French, “Electroluminescent Image Processing and Cell Degradation Type Classification via Computer Vision and Statistical Learning Methodologies,” in *Area 9: PV and System Reliability, Proceedings of the IEEE PVSC 44th*, 2017, pp. 1–3.

[89] J. S. Fada *et al.*, “Correlation of I-V Curve Parameters with Module-Level Electroluminescent Image Data Over 3000 Hours Damp-Heat Exposure,” in *Area 9: PV and System Reliability, Proceedings of the IEEE PVSC 44th*, 2017.

[90] “IEC 61215 Terrestrial photovoltaic (PV) modules - Design qualification and type approval.” 2016.

[91] D. Hinken, K. Ramspeck, K. Bothe, B. Fischer, and R. Brendel, “Series resistancenimaging of solar cells by voltage dependent electroluminescense,” *Appl. Phys. A*, vol. 91, no. 18, p. 182104, 2007.

[92] D. Hinken, K. Ramspeck, K. Bothe, B. Fischer, and R. Brendel, “Series resistance imaging of solar cells by voltage dependent electroluminescence,” *Appl. Phys. Lett.*, vol. 91, no. 18, pp. 1–3, 2007.

[93] F. Fruehauf and M. Turek, “Quantification of Electroluminescence Measurements on Modules,” *Energy Procedia*, vol. 77, pp. 63–68, 2015.

[94] W. Chine, A. Mellit, V. Lughi, A. Malek, G. Sulligoi, and A. Massi Pavan, “A novel fault diagnosis technique for photovoltaic systems based on artificial neural networks,” *Renew. Energy*, vol. 90, pp. 501–512, 2016.

[95] Y. Zhao, R. Ball, J. Mosesian, J.-F. de Palma, and B. Lehman, “Graph-Based Semi-supervised Learning for Fault Detection and Classification in Solar Photovoltaic Arrays,” *IEEE Trans. Power Electron.*, vol. 30, no. 5, pp. 2848–2858, 2015.

[96] T. J. Peshek *et al.*, “Insights into metastability of photovoltaic materials at the mesoscale through massive I-V analytics,” *J. Vac. Sci. Technol. B, Nanotechnol. Microelectron. Mater. Process. Meas. Phenom.*, vol. 34, no. 5, p. 50801, 2016.

[97] G. James, D. Witten, T. Hastie, and R. Tibshirani, *An Introduction to Statistical Learning*. New York, 2015.

[98] T. Hastie, R. Tibshirani, and J. Friedman, *The Elements of Statistical Learning*. New York: Springer New York, 2009.

[99] G. Hackeling, *Mastering Machine Learning with scikit-learn*. Birmingham: Packt Publishing, 2014.

[100] V. Gade, N. Shiradkar, M. Paggi, and J. Opalewski, “Predicting the long term power loss from

cell cracks in PV modules," in *2015 IEEE 42nd Photovoltaic Specialist Conference, PVSC 2015*, 2015, pp. 1–6.

[101] S. Kajari-Schröder, I. Kunze, U. Eitner, and M. Köntges, "Spatial and orientational distribution of cracks in crystalline photovoltaic modules generated by mechanical load tests," *Sol. Energy Mater. Sol. Cells*, vol. 95, no. 11, pp. 3054–3059, 2011.

[102] S. K. Thompson, *Sampling, 3rd edition*. Wiley, 2012.

[103] Y. Ren, P. N. Suganthan, and N. Srikanth, "Ensemble methods for wind and solar power forecasting- A state-of-th-art review," *Renew. Sustain. Energy Rev.*, vol. 50, pp. 82–91, 2015.

[104] L. Berliner and J. Brynjarsdottir, "A Framework for Multi-Model Ensembling," *SIAM/ASA J. Uncertain. Quantif.*, vol. 4, no. 1, pp. 902–923, 2016.

[105] R. Ebner, B. Kubicek, G. Újvári, S. Novalin, M. Rennhofer, and M. Halwachs, "Optical Characterization of Different Thin Film Module Technologies," *Int. J. Photoenergy*, vol. 2015, pp. 1–12, 2015.

[106] R. Ebner, B. Kubicek, and G. Ujvari, "Non-destructive techniques for quality control of PV modules: Infrared thermography, electro- and photoluminescence imaging," in *IECON 2013 - 39th Annual Conference of the IEEE Industrial Electronics Society*, 2013, pp. 8104–8109.

[107] R. Ebner, S. Zamini, and G. Újvári, "Defect Analysis in Different Photovoltaic Modules Using Electroluminescence (EL) and Infrared (IR)-Thermography," in *Proc. 25th EUPVSEC*, 2010, pp. 333–336.

[108] O. Breitenstein *et al.*, ""Luminescence imaging versus thermography on solar cells and wafers," in *26th EUPVSEC*, 2011, pp. 1031–1038.

For further information about the IEA Photovoltaic Power Systems Programme and Task 13 publications, please visit www.iea-pvps.org.

ISBN 978-3-906042-53-4